A DROPLET-BASED PLATFORM FOR HIGH THROUGHPUT SCREENING OF DRUG ADMINISTERED CELLS

by

Müge Kasım

B.S., Chemical Engineering, Boğaziçi University, 2017

Submitted to the Institute for Graduate Studies in
Science and Engineering in partial fulfillment of
the requirements for the degree of
Master of Science

Graduate Program in Chemical Engineering

Boğaziçi University

2019

ACKNOWLEDGEMENTS

I would like to express my sincere thanks to my thesis supervisor, Prof. Kutlu O. Ülgen, for her endless support and encourage throughout my study. Her high motivation and immense knowledge helped me to improve myself and my study. Her guidance made me stay in the right direction while I was on my way.

Also, I am grateful to my defense jury member Prof. Berna Sarıyar Akbulut and Prof. Şenol Mutlu for the time devoted on my thesis and valuable recommendations.

I would like to express my gratitude to my family, my mother, my father and my sister for providing me their continuous support. They always proud of me and encouraged even when I was in doubt. I could not achieve this success without them. So I thank them for giving me this opportunities and experiences that have made me who I am.

There are several special people that I want to especially thank to. First, I thank to my dear friends Elif Esvap, Selin Baç, Özlem Özbek, Begüm Yağcı and Dilara Göreke who made this journey full of joy and friendship. I am grateful to to you for giving me unforgettable memories in and out of the labs. I also would like to thank to Özge Selçuk, Merve Yüce, Feyza Öner, İlke Kaykanat and Ayşegül Karakuş for the motivation and encouragement they gave.

I would thank to thank members of the KB440, Ulgen Research Group, which I have shared lots of great moments. I especially thank to Elif Gençtürk for her endless support and friendship. I learned a lot from her and she was really patient during this process. Also, I thank Şafak Kılıç, Selma Başıbüyük, Mustafa Sertbaş and Ekin Yurdakul for the entertaining environment they create in the lab.

I would like to deeply thanks to my closest friend Çağrı Kıraç for his endless support and encouragement during this process. He was always there for me and made me believe I can achieve anything I want.

Finally, I acknowledge, this thesis has been financially supported by Boğaziçi Research Fund through the project 14261R.

ABSTRACT

A DROPLET-BASED PLATFORM FOR HIGH THROUGHPUT SCREENING OF DRUG ADMINISTERED CELLS

Droplet-based microfluidic systems move forward since 2000s having benefits compared to the conventional methods like improved sensitivity, automated and high throughput operation. This thesis involves a combined approach of the engineering and biological principles and analyses within the droplet-based microfluidic system. The performances of different microfluidic bioreactor designs were tested, and the surfactant concentration against the toxicity to cells and the flow rates were optimized. Diploid BY4743 strain with GFP tagged Rpl5 protein and haploid EY0987 strain with Nop56 protein were treated with hydroxyurea (HU) and temsirolimus drugs to understand the functions of these proteins in ribosome biogenesis. The responses of the cells were measured based on the cell area and the amount of protein expressions. SOM analysis was performed, and several clustering approaches gather the over- and underexpressed genes together. GO analysis was applied to these clusters to understand the cumulative functions of the genes in the clusters. The experimental and computational results on the response of the cells were interpreted within the context of ribosome biogenesis. HU inhibits cell growth, decreases cell dimension and protein expression of Nop56 and Rpl5, which function in ribosome biogenesis. Temsirolimus, inhibits EY0987 yeast cell growth, decreases cell dimension and protein expression of Nop56, whereas the drug effects on diploid BY4743 strain and Rpl5 protein are unclear. SOM analysis reveals that the clusters, in which NOP56, NOP58 and RPL5 are involved, are related to ribosome biogenesis, rRNA processing and nucleolus, and the genes in these clusters are suppressed after 10 to 14 minutes of rapamycin treatment. This study elucidates the role of nucleolar components, snoRNP proteins, in ribosome biogenesis and confidently lead to novel therapeutic strategies for ribosomal protein related diseases.

ÖZET

DAMLACIK TABANLI PLATFORMDA İLACA MARUZ BIRAKILMIŞ HÜCRELERİN HIZLI ÇIKTI GÖRÜNTÜLEMESİ

2000li yıllardan beri sürekli gelişmekte olan damlacık tabanlı mikro-akışkan sistemler, gelişmiş hassasiyette olmaları, otomatize edilebilmeleri ve yüksek çıktı alınabilmesi itibariyle geleneksel yöntemlere kıyasla daha faydalıdır. Bu tezde, mühendislik ve biyoloji, damlacık tabanlı mikroakışkan sistemde birleştirilmiş; farklı mikroakışkan biyoreaktör tasarımları test edilmiş, sürfaktan konsantrasyonu hücrelere olan toksisitesine karşı belirlenmiş ve akış oranları ayarlanmıştır. Deneysel çalışmalarda, RPL5 proteini yeşil floresan etiketli BY4743 ve NOP56 proteini kırmızı floresan etiketli EY0987 suşlarına hidroksiüre ve temsirolimus ilaçları uygulanmasıyla, bu proteinlerin ribozom biyojenezindeki işlevleri açıklanmaya çalışılmıştır. Hücrelerin tepkileri hücre alanlarına ve protein ifadelerine bakılarak ölçülmüştür. SOM analiz ile elde edilen çeşitli kümeleme yaklaşımları, aşırı/az ifade edilmiş genleri bir araya getirmiştir. Bu kümelerdeki genlerin genel fonksiyonlarını anlamak için bu kümelere gen zenginleştirme analizi uygulanmıştır. Hem deneysel hem de hesaplamalı elde edilen sonuçlar, ribozom biyojenezi kapsamında yorumlanmıştır. HU'nun hücre büyümesini engellediği ve NOP56 ve RPL5 genlerinin protein ifadesini azalttığı açıkça görülmüştür. Temsirolimus'un EY0987 suşu üzerinde hücre büyümesini engellemek ve Nop56 protein ifadesini azaltmak gibi etkileri varken, BY4743 suşu üzerindeki hücre büyümesi ve Rpl5 protein ifadesine etkisi açık değildir. SOM analizi, NOP56, NOP58 ve RPL5 genlerinin dahil olduğu kümelerin, ribozom biyojenezi, rRNA işleme ve nükleolus ile ilişkili olduğunu göstermektedir ve bu kümelerdeki genlerin 10-14 dakikalık rapamisin tedavisinden sonra bastırıldığını ortaya koymaktadır. Bu çalışma, nükleolar bileşenlerin ribozom biyojenezindeki rollerini açıklamaktadır ve ribozomal proteinlerle alakalı hastalıklara karşı yeni terapötik stratejilerin gelişmesine liderlik edeceği düşünülmektedir.

TABLE OF CONTENTS

LIST OF FIGURES

LIST OF TABLES

LIST OF SYMBOLS

d	Characteristic length
D	Molecular diffusion
m	Mass
M	Molar
n	Mole
t	Time
u	Characteristic velocity
V	Volume
γ	Interfacial tension
η	Dynamic viscosity
λ	Average number of the cells in the volume of a droplet
υ	kinematic viscosity
X	Probability of number of cells in a droplet

LIST OF ACRONYMS/ABBREVIATIONS

Ca	Capillary number
DLD	Deterministic lateral displacement
DMSO	Dimethyl sulfoxide
FADS	Fast activity screening module
FITC	Fluorescein isıthiocyanate
Fo	Fourier number
GFP	Green fluorescence protein
HU	Hydroxurea
LoC	Lab on a chip
LSU	Large suburnit of ribosome
MW	Molecular weight
Pe	Peclet number
Re	Reynolds number
PMT	Photomultiplier tube
RFP	Red fluorescence protein
RP	Ribosomal proteins
RNP	Ribonucleo protein
SCA	Spineceerebral ataxia
snoRNP	Small nucleolar ribonucleoprotein
SSU	Small subunit of ribosome
YNB	Yeast nitrogen base
YPD	Yeast extract-peptone-dextrose

1. INTRODUCTION

Microfluidic system technologies have become widespread since 2000s and have improved sensitivity and application in processing and analytical techniques compared to conventional methods. Thanks to these systems, studies have been carried out in picoliter and nanoliter volumes, and there has been a significant reduction in the amount of materials and energy consumed. This technology also creates an ideal environment for the fluid in process to be precise, controlled and fast. Hence, this technology is not only about getting fast output, but also about running efficient, controlled, automated and more economical processes.

Microfluidics systems have rapid heat and mass transfer due to its microscale nature that has high surface area to volume ratio. This ratio makes the system efficient and safe for chemical reactions. Microfluidics systems is used in many fields, biological analysis, chemical synthesis, and optics and information technology [1]. These systems have many advantages because the system is characterized by laminar flow which prevents a back mixing caused by turbulence. In the biological field, cell research, polymerase reaction (PCR), diagnostic tools and simulation of entire organ systems are developed by using microfluidic systems [2, 3].

The main advantages of using microfluidic systems are [4]:

- Small reagent volumes, microreactors and footprint
- Selectivity of microreactors
- Rapid and safe reactions in microreactors
- Scale up and scale out potential of microreactors
- Green chemistry with microreactors

The main disadvantages of using microfluidic systems are [4]:

- an enabling technology rather than a replacing technology

- Hard to manage multi-phase reactions
- Complexity of fabrication of chip materials
- Physical limitations of amounts

In this thesis, microfluidic chips are used to investigate the yeast growth against different drugs. A droplet generator chip is used for encapsulating yeast cells. The generated droplets behave as a bioreactor. The aim is to encapsulate one cell per bioreactor and obtain high throughput results. Up to 200 droplets per second are desired to be generated in this thesis work. Consequently, hundred thousands of bioreactors are generated, and the response of each cell to the drugs (hydroxyurea and temsirolimus) are investigated. Then, a computational study is conducted to get further insight on the time period that the experiments cannot cover.

In the following chapters of this thesis, the theoretical background (second chapter) is given by explaining the droplet based microfluidic systems. A brief explanation about ribosomopathies is also given in the Theoretical Background part. In the third chapter, the experimental and computational methods that are used in this study are explained. In the fourth chapter, the results are given and discussed. Finally, in the Conclusion part, the achievements obtained from both experimental and computational studies are summarized and the different ideas for further exploration of the subject are given in the Recommendations section.

2. THEORETICAL BACKGROUND

The fundamental behavior of the fluids at the micro scale is complex. This is why dimensionless numbers are used to describe the microfluidic behavior with respect to everyday experience. Reynold number is the most discussed one which quantifies the relative importance of inertial forces and viscous forces. It is given in the following equation where u is characteristic velocity, d is characteristic length and υ is the kinematic viscosity of the fluid.

$$Re = \frac{du}{\upsilon} \tag{2.1}$$

When the *Reynolds* number is smaller than 2000, the flow becomes laminar while it is turbulent as the *Reynolds* number is larger than 2000. For a microfluidic system, flow must be laminar, so *Reynolds* number becomes smaller than 2000 [1]. For the mixing behavior of the fluid, a system is described by using *Peclet (Pe)* and *Fourier (Fo)* dimensionless numbers. *Pe* number describes the relative rate of convective transport to mass transport where D is the molecular diffusion constant. *Fo* number defines the diffusive mixing efficiency where t is time.

$$Pe = \frac{du}{D} \tag{2.2}$$

$$Fo = \frac{Dt}{d^2} \tag{2.3}$$

Also, *capillary number (Ca)* is defined as the relative magnitude of viscous and surface tension forces where γ is the interfacial tension and η is the dynamic viscosity of the fluid.

$$Ca = \frac{\eta u}{\gamma} \tag{2.4}$$

There are three microfluidic platforms to study the biological issues. These can be named as continuous-flow, batch and droplet-based microfluidics [5]. The basic characteristics of continuous-flow microfluidic systems are uniphasic flow and continuous manipulation to the flow in the microchannel. This system has a handicap because it causes precipitation, fouling and contamination due to the contact of molecules to the walls. Batch systems are conducted by using mixing area after a series of continuous flow channels. Droplet-based microfluidic systems are conducted by using two different phases. The reagent phase is surrounded by an immiscible carrier phase, which can prevent precipitation, fouling or contamination of the reagent to the walls. This system helps to create several discrete nL to pL volumes of reactors. The main reason of encapsulating cells is to create small volumes of micro bioreactors. Compartmentalization of cells or biomolecules in these droplets helps to investigate the protein expression of a cell at molecule level. Also, screening at high resolution can be possible with such a system.

2.1. Droplet Generation

Droplet generation within chip can be made by many methods, such as, electric field, pneumatic pressure, thermal control etc. However, these methods have low efficiency. Most widely used method is to employ two immiscible fluids [5]. For such systems of droplet-based microfluidics, there are three main types of droplet generation methods. These are co-flowing method, flow focusing method and T-junction method [6]. The common part of these methods is the liquid with the higher affinity to the channel wall forms the continuous phase and the lower affinity fluid splits to form the droplets.

- In a T-junction method, continuous phase is connected to the channel perpendicularly.
- In a flow focusing method, discrete flow is pumped through an orifice and continuous phase surrounds the central stream with two reciprocal streams [5].
- In a co-flowing method, dispersed phase channel is in the middle of the continuous phase channel. In this method, dispersed phase becomes unstable and breaks up

into droplets according to the Rayleigh-Plateau principles. Following Figure 2.1 can help to visualize these methods.

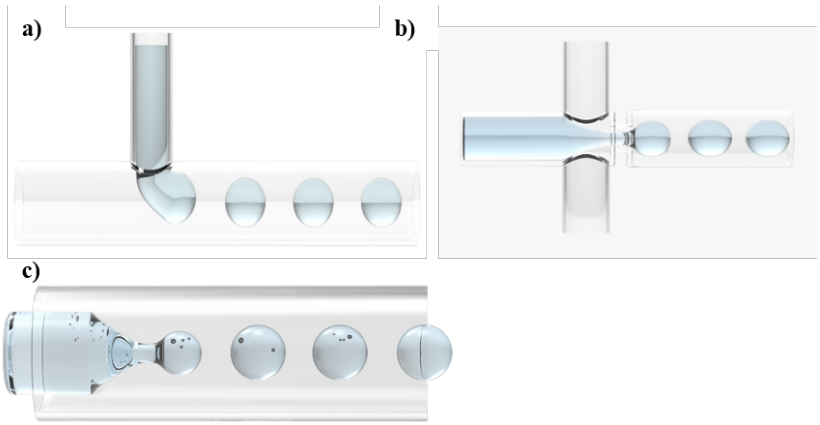

Figure 2.1. a) T-junction, b) Flow-focusing, c) Co-flowing [4].

In the chip system, continuous phase is generally made from oil, which has high affinity to channel walls and is immiscible with water contains cells and cell medium which is discrete phase. With this system, up to 2000 droplets can be produced within a second. The aim is to put a single cell in a droplet; however, cells are theoretically distributed to the droplets based on the Poisson distribution [7]. The probability of finding x cells per droplet can be found from the given equation:

$$P(X = x) = e^{-\lambda}\frac{\lambda^x}{x!} \tag{2.5}$$

where λ represents the average number of cells in the volume of each droplet [8]. For instance, to encapsulate $\lambda = 0.3$ cells in 50-pl droplets, cells should be prepared at a density of 6×10^6 cells per ml. Considering that the cell encapsulation process is completely random, this choice of cell density will result in 74.08% of the droplets containing no cells, 22.22% containing a single cell, 3.3% containing two cells and 0.38% containing more than two cells. Following the same approach, we can estimate the number of cells per droplet. If we aim to have a higher average number of cells per droplet, for example, an average of one cell per 50-pl droplet ($\lambda = 1.0$), we need to prepare a mixture containing 5×10^7 cells per ml.

2.2. Picoinjection

Picoinjection is an alternatively used part of the droplet-based microfluidic sorting mechanism to fill the drop with a reagent especially with a fluorogenic substrate, continuously. In this part, fluorogenic substrate is injected to droplet after incubation is allowed for growth of cell [9]. AC field is applied to the channel so, the controlled volume of reagent is triggered and merged with the droplet [10]. Since it is hard to synchronize the droplets, picoinjection is a difficult process.

Basic working principle of the picoinjector unit is to unstabilize the water-oil interphase of the droplet by the electric field. As the electric field is applied, the stability of the thin film of water oil interphase is ruptured; thus, the reagent can enter to the drop.

Droplet velocity and the injection pressure are the essential parameters to control the volume of reagent. Also the electrode voltage is a parameter; however, as the electrodes are switched on, reagent is injected to the droplet no matter what the magnitude of the voltage is. On the other hand, as the droplet velocity increases, the volume of the injected reactant decreases and, as the injection pressure increases, the volume of injected reagent increases [10]. The effects of these parameters are shown in Figure 2.2.

2.3. Droplet Screening and Sorting

Most of the techniques require tags or labels for droplets where some new methods do not require biological label. These methods separate droplets by using physical properties of the droplets and they are identified as passive separation methods. However, labelled cells are sorted by applying AC field pulses.

One of the passive sorting methods is to separate droplets by their size. After droplet generation, droplets are incubated, and they may coalesce with each other. When the droplets enter to the sorting unit, center of the droplets are aligned differ-

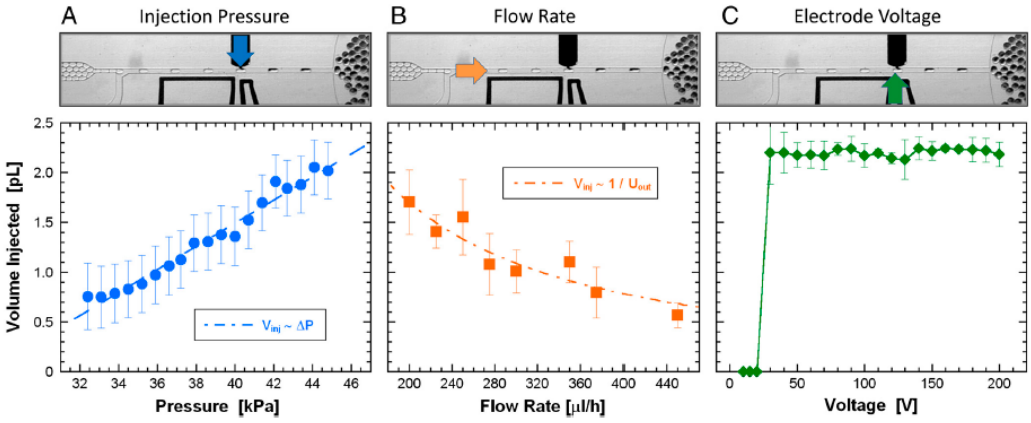

Figure 2.2. a) Injection pressure effect, b) Flow rate effect, c) Electrode voltage effect [10].

ently, and according to their size larger droplets are separated in the y-direction as it can be seen in Figure 2.3 [11]. Another passive sorting method is deterministic lateral

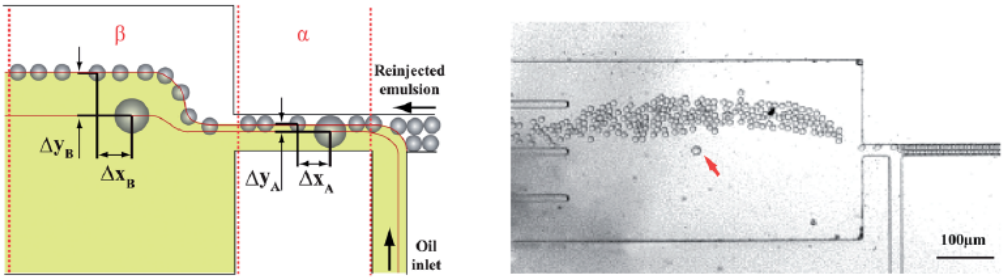

Figure 2.3. Sorting by droplet size [11].

displacement (DLD) technique. DLD is also a size-based sorting method, however, laminar fluid flow companies the large and small size droplets. Droplets below a critical size follow streamlines through the array gaps with no net displacement from the original streamline while droplets above the critical size are displaced laterally to cross sequential streamlines. Figure 2.4 shows the DLD technique of sorting [12].

In another sorting technique, gravitational force is used perpendicular to the channel flow and droplets are separated according to the velocity on their radius, the

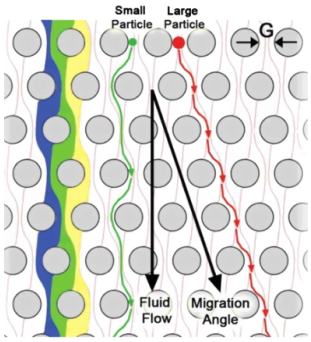

Figure 2.4. DLD technique [12].

acceleration of gravity, the difference between the density of the droplets and the density of the fluid, and the viscosity of the fluid (Figure 2.5) [13].

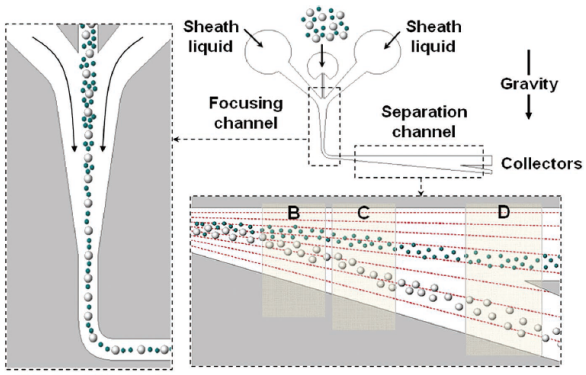

Figure 2.5. Separation by gravity [13].

Alternative to the passive sorting methods, fluorescence activated droplet sorting method can be used to separate the droplets (Figure 2.6). In this method, electrodes are placed in the microfluidic chip to create electric field. With this way, droplets are separated according to activities of the cells. For this aim, fluorogenic substrate is injected to the droplets and the droplets are screened by an optical setup. Incubated cells will be transferred to fast activity screening module (FADS). In this system, cells, that fluoresce or not, will be observed by reverse fluorescence microscopy (inverted fluorescence microscope, Nikon Eclipse Ti). The filter block (FITC) with stimulus and emission filters is also used to reduce the optical background to the minimum. If necessary, another focusing lens is used to focus on the photomultiplier tube by means

of a fluorescent light spatial filter (100 mm) emanating from the droplet [14]. The signal from the detector is collected by the photon counting header and the counting unit. It is saved to a computer via the data collection card. Here, the high pulse corresponds to the high intensity value collected by the PMT. Through the LabView and MATLAB software, beat values from the PMT are acquired as a function and saved automatically. The drop peak obtained here will determine the negative and positive dropouts [14, 15]. Activation is identified by emitting light from fluorescing droplets and the emitted light is separated into two by photomultiplier tube (PMT) to send to the LabView program to analyze the data. According to the data, if the droplet fluoresces, electric field is turned on and the fluorescent droplets are separated through the positive channel [9].

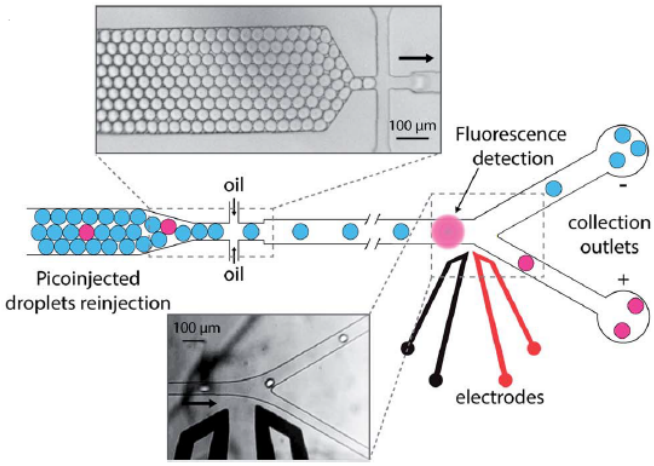

Figure 2.6. Fluorescence-activated droplet separation [9].

The positioning of the electrodes used to separate the droplets is effective on the correct separation of the droplets. The study by Beneyton *et al.* in 2016 shows that the positions of the electrodes used for separation change the false positive and false negative rates in the separation results. Again, according to the same study, the effect of the positioning varies according to the volume of the droplets. When the droplets larger than 158 pL are desired to be separated, positioning on the same side; when the droplets smaller than 158pL are desired to be separated, positioning on the opposite side provides maximum separation [9].

2.4. Applications of Droplet-based Microfluidics Platforms

Several studies have been conducted on droplet-based micro-fluids. Chou *et al.* wrote a revision of all the studies made after 2013, stating that droplet-based microfluidics can be used in other applications such as molecular detection, imaging, drug release, diagnosis, cell biology and food products [16].

In 2004, Srinivasan and his colleagues used the micro-fluid lab-on-a-chip (LoC) platform to calculate glucose for clinical diagnostic applications. The droplets were used as reaction chambers and are manipulated by electrolysis. Glucose was observed by the color change in the droplets and the absorption measurement system with light emitting diodes and photodiodes [17].

In another study, Baroud *et al.* examined 3 different aspects of microfluidic dynamics of droplets. The formation and geometric shapes of droplets, the transport of droplets depending on velocity and pressure, and the combination of droplets with a liquid film were investigated. At the end of this research, a standard for microfluidic droplet operations was found and guided results for the future research were obtained [18]. Tang and her research group investigated the disintegration of droplets depending on the flow stress of the droplets in the channels, the viscosity ratio of the solution, the size of the channels and the amount of flow applied [19]. Solvas and deMello have worked on high-throughput monitoring and synthesis applications for high-output droplet-based micro-fluidized platforms, as well as high information content detection-integration methods, long-term droplet stabilization and large and viable biological trials [20].

The droplet-based microfluidic system is also used in mass production using yeast cells. Sjostrom and his colleagues have conducted a study aiming at separating the droplets with less than ten thousandths of false positive results [21]. In this study, mutated yeast cells, which are improved in α-amylase production, are separated from the standard strain of yeast. This study shows that this system has a throughput in in α-amylase production more than 300 times than the industry used, which is microtiter

plate robot. Lombardi and Dittrich tested drug screening to benefit from micro conditions, saving time and expense and increasing the efficiency of reactions. They have also introduced innovative micro-fluid platforms by working with new chemical reactions, cell and tissue engineering, and small volumes. These platforms, continuous, semi-continuous and intermittent operation modes have worked well [22]. When combined with a large number of protein library technologies with the introduction of cheap DNA synthesis, the use of high output technologies has become necessary to monitor and analyze proteins. Developments in the field of protein engineering and synthetic biology will help further depending on the rapid output and monitoring systems [23].

2.5. Ribosomes and the Disorders Related with Small Nucleolar RNPs

Ribosomes are the machines that translates the mRNA codes and synthesize proteins which are crucial for cellular growth and proliferation. Two ribosomal subunits, which are 40S (small ribosomal subunit, SSU) and 60S (large ribosomal subunits, LSU), create 80S ribosome. 40S is the small subunit and consists of 18S ribosomal RNA (rRNA) and 33 ribosomal proteins (RPs). This unit is responsible for bringing mRNAs and tRNAs together. 60S is the large subunit and consists of 28S, 5S and 5.8S rRNA and 47 ribosomal proteins [24]. This unit is responsible for catalyzing the peptide bonds, that form protein chains. RNA polymerase enzymes work during ribosome biogenesis to produce ribosomal proteins (RPs) and rRNAs. Polymerase I is required to produce 18S, 5.8S and 28S by cleaving the pre-RNA (35) while 5S is produced by Polymerase III seperately. Ribosomal proteins are produced by Polymerase II. Ribosome biogenesis and protein synthesis is the most energy requiring process in a cell. More than 2000 ribosomes are assembled each minute in a growing cell (Figure 2.7) [24, 25].

2.5.1. Mechanism of Action of C/D Box proteins (Nop1p, Nop56p, Nop58p, Snu13p)

Small ribosomal subunit processome is required for ribosome assembly and it mediates the cleavage of the pre-RNA in the external transcribed spacer (ETS) or in

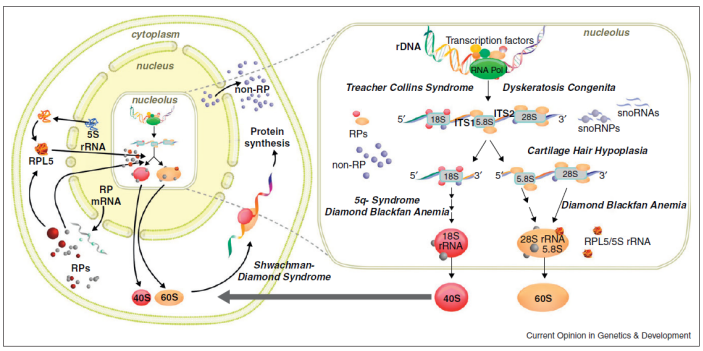

Figure 2.7. Ribosome synthesis [26].

the internal transcribed spacer (ITS). SSU processome is created by SSU processome assembly factors (SPAFs) [27]. A subset of the SPAFs comes together and creates the subcomplexes of the SSU processome called UtpA, UtpB, UtpC, Mpp10 and U3 snoRNP. SPAFs of the UtpA are Utp4, Utp5, Utp8, Utp9, Utp10, Utp15, Utp17, while SPAFs of the U3 snoRNP are Nop1, Nop56, Nop58, Snu13 and Rrp9 [24]. Thus, the protein-protein interaction between the Nop56 and Utp8 via Nop58, mentioned in Section 4.4.1, can be explained. They both have a role on creating SSU processome which leads creating 18S small nucleolar ribosome.

Small nucleolar RNAs (snoRNAs) are subunits of small nucleolar ribonucleoprotein (snoRNPs) and they play role in posttranscriptional maturation of ribosomal RNAs (rRNA) [28]. They are divided into two parts as box C/D snoRNAs and box H/ACA, which are responsible for 2'-O-methylation of pre-RNA and pseudouridinylation, respectively [29]. Box C/D snoRNP complex consists of box C/D snoRNA, Nop1, Nop56, Nop58 and Snu13. rRNA and snoRNA create a RNA:RNA duplex and the catalytic site of Snu13 binds to the D boxes of the RNA. Then, Nop56, Nop58 and Nop1 (FBL) bind to the complex, creating k-motif as shown in the Figure 2.8 [30].

2.5.2. Ribosomopathies

Ribosomopathies arise from deficiency of either rRNA or the various ribosomal proteins during ribosome biogenesis. Because ribosome and its products have role in

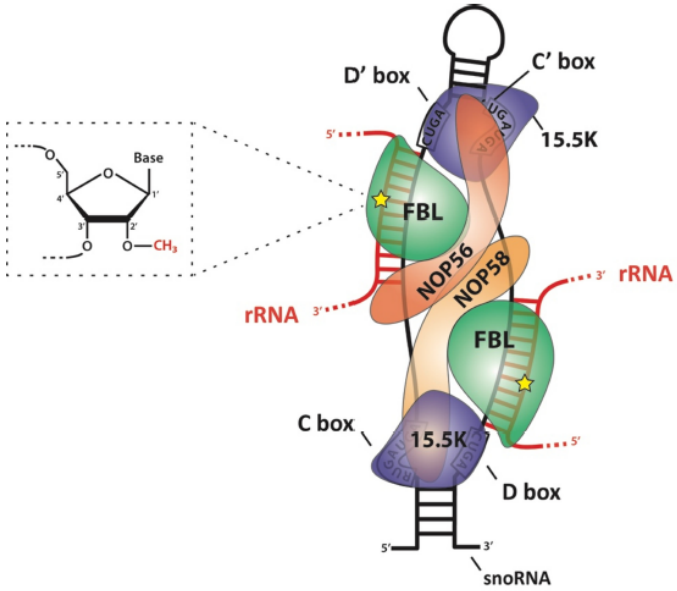

Figure 2.8. Box C/D snoRNP [30].

the regulation of mRNA translation, cell cycle control and signaling pathways, this deficiency affects cell proliferation and may cause cancer. Some of the ribosomopathies are Diamond Blackfan Anemia (DBA), Treacher Collins syndrome (TCS), isolated congenital asplenia, Shwachman Diamonds Syndrome (SDS), Cartilage hair hypoplasia (CHH), X-linked dyskeratosis congenital and 5q- syndrome. Of these diseases, DBS, TCS and isolated congenital asplenia are the autosomal dominant diseases where SDS and CHH are autosomal recessive diseases [25]. Moreover, DBA and 5q- syndrome can be classified as ribosomal protein affected diseases while SDS, CHH and TCS can be classified as non-RP ribosomopathies [26].

Diamond Blackfan Anemia, DBA, is a bone marrow failure syndrome. This disease is basically characterized by macrocytic anemia and insufficiency of erythroid precursors, and caused by deletion or mutation of RPS19, RPS 24, RPL35A, RPS17, RPL5, RPL11, RPS7, RPS10 and RPS24 genes [25].

5q- syndrome is myelodysplastic syndrome, and its effects are refractory macrocytic anemia and thrombocytosis. It is caused by specific deletions or mutations in

chromosome 5 which share common deleted region (CDR). However, only RPS14 deletion is known as it causes macrocytic anemia, so this could link the deficiency in ribosome biogenesis to the failure of erythropoiesis [26].

Cartilage hair hypoplasia, CHH, is an autosomal disease that causes short stature, defects in cellular immunity and predisposition of cancer, especially lymphoma cancer. This disease occurs when RMRP gene has a mutation. This gene is responsible for encoding the RNase MRP which is also responsible for ribosome biogenesis and cell cycle regulation [25].

X-linked dyskeratosis causes bone marrow failure, predisposition cancer and short stature. This disease occurs when DKC1 gene has a mutation. This gene is responsible for pseudouridine synthesis.

p53 is a tumor suppressor protein which is a strong checkpoint to verify whether ribosome biogenesis is correct before it allows cell division. In a healthy cell, p53 level is low. Because it is rapidly degraded by MDM2 (murine Double Minute 2) and HDM2 in human, this protein is short lived protein. HDM2 is an E3 ubiquitin ligase, and it facilitates p53 ribosomal degradation. When there is a deficiency in RPs, RPL5 and RPL11 proteins form a complex with 5S rRNA and this complex inactivates HDM2 activity (Figure 2.9). When the inhibitory function of HDM2 protein is deactivated, p53 level increases [31].

S. cerevisiae has been an important model cell for the study of ribosomopathies, Studies in yeast have revealed important aspects of the underlying pathophysiology of two human genetic diseases of ribosome biogenesis: Diamond–Blackfan anemia (DBA) and Shwachman–Diamond syndrome (SDS). In case of DBA, the haploinsufficiency of the affected r-protein results in autosomal dominant genetic transmission. There is an increased risk of cancer over time [24]. On the other hand, SBDS is primarily caused by defects in cytoplasmic steps in ribosome biogenesis. Literature reportfs indicated that these disorders affected cell growth and caused defective ribosome biogenesis [24, 25].

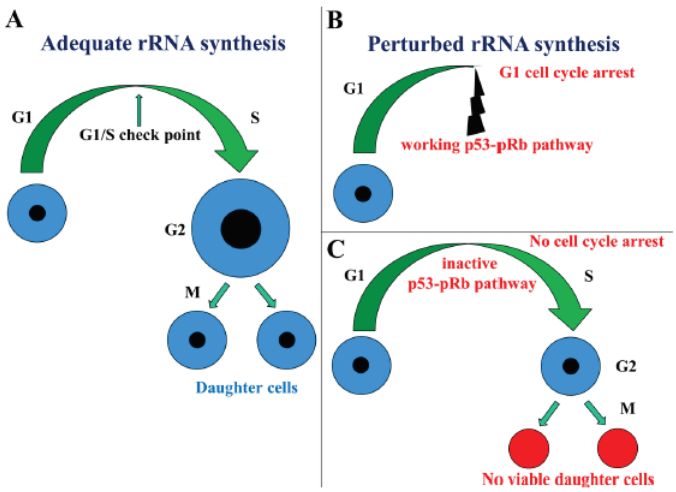

Figure 2.9. p53-pRb pathway [31].

2.5.3. Spino cerebellar ataxia (SCA) and Nop56 protein

Yeast cells are used as a model system for eukaryotic cells. The small nucleolar RNP Nop56 protein, which has a homologue in humans, functions in protein biogenesis. Normally, when the NOP56 gene is mutated, it has been shown to cause Spino cerebellar ataxia (SCA) [32]. NOP56 gene mutations causing SCA36 include six DNA construct block sequences (nucleotides) that are located in an area of the gene known as intron 1. In healthy individuals, this sequence is repeated 3 to 14 times. For people with SCA36, this sequence is repeated at least 650 times [33]. Spino cerebellar ataxia (SCA) is a disease in which the balance of the cerebellum and spinal cord is lost due to loss of cells or failure to work properly. SCA disease has 30 subtypes expressed by numbers (eg SCA1, SCA2, SCA3, etc.). SCA36 is associated with the Nop56 gene and the protein it encodes. Most SCAs are hereditary. Rarely, this disease can occur in children without SCA in family members. Since SCAs are genetic diseases, there is no definitive treatment today. Patients are given symptom-reducing treatments for epilepsy, involuntary movements and tremor. Any drug used to inhibit this gene / protein, when expressed too much, is not given in the literature [34].

3. MATERIALS AND METHODS

3.1. Yeast Experiments

3.1.1. Yeast Strain

Wild type EY0987 haploid strain (EY0987 ATCC 201389: *MATα his3Δ1 leu2Δ0 lys2Δ0 ura3Δ0* (S288C)) is used in the experiments. This strain contains RFP tagged NOP56 protein (YLR197W), which means the cells are fluorescing when this protein is expressed. Nop56p is a yeast nucleolar protein Nop56p (Ribonucleoprotein), and it is required for assembly of the 60S ribosomal subunit and is involved in pre-rRNA processing.

Wild type BY4743 diploid strain, which has URA3 resistance, is also used in the experiments. This particular strain contains GFP tagged RPL5 protein (YPL131W). The RPL5 gene encodes a member of the L18P family of ribosomal proteins and component of the 60S subunit. Rpl5p is Ribosomal 60S subunit protein L5 (Ribosomal Protein of the Large subunit). The RPL5:GFP strain is knocked out one copy of the protein coding gene: YAL067C (SEO1, putative permease, Suppressor of sulfoxyde EthiOnine resistance).

3.1.2. Sterilization of Materials

Materials that will be used in the experiments such as pipette tips, beakers, Erlenmeyer flasks, graduated cylinders, schott bottles are sterilized in the autoclave. The tip of the beakers and graduated cylinders are covered with the aluminum foil while erlenmeyer flasks are plugged with gauze and then covered with aluminum foil. The caps of schott bottles are semi-closed to get rid of excessive pressure in bottles during sterilization in the autoclave. After all the materials are covered, they are put in an autoclave and sterilized at 121°C for 15 minutes. Also, the laminar flow hood is

sterilized with ethyl alcohol and all the sterilized materials are put in the hood. Finally, the hood is left in working condition to avoid contamination from air.

3.1.3. Yeast Culturing in Liquid Medium

RPL5 tagged and NOP56 tagged yeast strains are grown in different YNB medium. In order to prepare 2% YNB medium for RPL5 tagged yeast cells, 1.7 g/L YNB (yeast nitrogen base), 5 g/L ammonium sulfate, 0.02 g/L histidine, 0.1 g/L leucine, 0.02 g/L methionine, 0.03 g/L lysine and 2% glucose are used. 200 mL YNB medium is prepared with 0.34 g YNB, 1 g ammonium sulfate, 0.04 g histidine, 0.02 g leucine, 0.004 g methionine, 0.006 g lysine and 4 g glucose.

In order to prepare 2% YNB medium for NOP56 tagged yeast cell, 1.7 g/L YNB (yeast nitrogen base), 5 g/L ammonium sulfate, 0.02 g/L histidine, 0.1 g/L leucine, 0.02 g/L uracile, 0.03 g/L lysine and 2% glucose are used. 200 mL YNB medium is prepared with 0.34 g YNB, 1 g ammonium sulfate, 0.04 g histidine, 0.02 g leucine, 0.004 g uracile, 0.006 g lysine and 4 g glucose. The rest of steps are same for both NOP56 and RPL5 tagged strains. 4 g glucose is mixed with 40 mL of distilled water in a schott bottle and sterilized at 121°C for 3 minutes while the rest is mixed with 160 mL of distilled water in a different schott bottle and sterilized at 121°C for 15 minutes. After sterilization, both schott bottles are kept in the hood for cooling before they are mixed.

200 mL of YNB medium is separated into two 100 mL flasks, each containing 20 mL of YNB medium. Then, 0.5 mL of frozen stock cells is added to each flask and both flasks are placed into the shaker for incubation. The incubator shaker is run at 180 rpm and 28°C temperature for 1 day.

YPD medium is also used especially in optimization experiments. In order to prepare 2% YPD medium, 2% yeast extract, 2% glucose and 1% peptone is used. 500 mL YPD medium is prepared with 10 g yeast extract, 5 g peptone and 10 g glucose. 10 g yeast extract and 5 g peptone are dissolved in 350 mL water and sterilized at

121°C for 15 minutes at autoclave. Also, 10 mg glucose is dissolved in 150 mL water and sterilized at 121°C. Finally, 500 mL YPD medium is prepared after the cooled solutions are mixed in a 1000 mL schott bottle.

3.1.4. Estimation of Yeast Density in Inoculum

Yeast density in the inoculum is calculated by cell counting. 2 μL of sample is put on a glass slide, which covers 5.25 cm^2 area, and the number of cells in 11 different regions are counted. These areas on 40X zoom are 1636 px $\times$1088 px (1 px=0.21 μm, 0.000782 cm^2) and average number of the cells in these areas is 21. Proportional to this value, there are roughly 1.4 $\times 10^5$ cells covered on the glass slide (2 μL of sample). In a 5 mL, there should be roughly 3.52×10^8 cells. Yeast density in culture for each experiment is tabulated and given in Appendix A.1.

3.1.5. Surfactant Preparation

Oil phase for droplet generation is prepared by mixing Krytox 157-FSH (DuPont) surfactant. 2% or 3% of Krytox is mixed with HFE-7500 (3M (TM) Novec (TM)) Engineered fluid oil, i.e. 150 μL Krytox is mixed with 4850 μL Novec7500 for 3% solution. 5 mL of oil phase is prepared in a syringe.

3.1.6. Yeast (Aqueous Phase) Solution with Jeffamine Preparation

0.75% w/w Jeffamine is added to the total mass of the yeast solution. Krytox, that have an anionic head, is dissolved in oil [35]. This anionic group and the Jeffamine additive in aqueous phase bind together at the water oil interface (Figure 2.8). Thus, the droplets are generated that bio-compatible and resistant to coalesce with each other.

For the experiments, yeast culture is diluted with YNB medium at ratio of 1 to 1. Because the density of Jeffamine (1.065 g/mL) is close to density of water (1 g/mL),

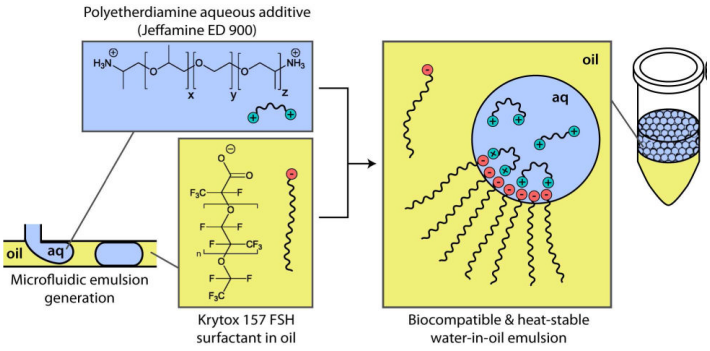

Figure 3.1. Structure of Jeffamine [35].

0.75% v/v Jeffamine is used. As the industrial Jeffamine bought is 50% v/v [36], 1.5% is used, i.e. 75 μL of Jeffamine is added to 4925 μL of diluted yeast solution.

3.1.7. Drug Preparation

Drug phase is prepared by dissolving the drug in the nutrient medium. For HU experiments [37], 200mM or 400 mM HU solution is prepared, i.e. 0.1521 g HU is dissolved in 10 mL YNB medium for 200 mM HU solution. The drug amount is doubled since the drug phase is diluted with the aqueous phase during the flow into the microfluidic device. Mass of the drug used is calculated from the Equations 3.1 and 3.2.

$$M = \frac{n}{V} \tag{3.1}$$

$$M = \frac{m}{MW} \tag{3.2}$$

For temsirolumus experiments, 0.4 μg/mL solution is prepared [38–41]. For that aim, 0.2 mg of temsirolumus is dissolved in 10 mL DMSO. Then, 200 μL of this solution is added to 10 mL of yeast medium. The reason of preparing 10 mL of drug solution is to facilitate the measurement of the tiny amount of drug on the balance.

3.1.8. Flow Rate and Droplet Size

The flow rate is set to 800 μL/h for oil phase and 60 μL/h for yeast aqueous phase at the beginning of the experiment. For 10-15 minutes, only oil phase and yeast solution are sent to the chip to get rid of the bulk yeast cells, which come up from the syringe initially. By doing this, lots of bulk cells are encapsulated in the first droplets formed and they are not counted when the analysis is done. After 10-15 minutes, accumulation of the cells decreases. Then, the drug solution is sent to the chip, and its flowrate is initially set to 60 μL/h. However, the drug solution has insufficient pressure to reach to the mixing junction, so the flow rate is increased to 100 μL/h; thus, it can mix with the aqueous (yeast) phase.When the drug phase is entered into the microfluidic system, the molarity of the drug is assumed to be half due to the mixing with the yeast cells, which entered to the chip system in the aqueous phase.

Droplet diameters vary between 100-200 μm. In the first three chambers, there are coalescence between the droplets due to the instability of the generated droplets.

3.1.9. Flow Rate and Droplet Size

To make the single cell analysis, the most important point is that there should be very few cells in each droplet, i.e. only one cell, or at most three, in each droplet. Taking this into consideration, specific cells were identified in every chamber and the same cells were observed for 6-24 hours of drug treatment. Since it was a continuous system and it required time for the culture medium to fill all the chambers, the size of the cells before the drug (HU) treatment could not be observed. Thus, when the analysis began, the cells were already facing the HU treatment. The area and integrated fluorescence density of the cells were analyzed by using ImageJ. Up to 45 different cells were examined in each experiment.

3.2. Self-Organized Maps (SOM)

OposSOM package is one of the packages that RStudio supports. This package reduces the large dimension data into metadata. The algorithm of OposSOM makes the data as sample-centered and enables group centered visualizations, sample similarity analysis and functional enrichment analysis. These help the researchers obtain the information content of the data in an effective and intelligent way [42]. First, the expression portraits, which show the expression of the metagenes according to the time at which the samples are taken, are obtained in SOM analysis. Overexpression spots show the strongly expressed metagenes during the drug treatment, whereas underexpression spots show the strongly underexpressed metagenes during the drug treatment. Overrepresented gene sets are identified for each sample set, calculated by using Z-score statistics. Hypergeometric enrichment score is used to find the Gene Set Z-score. Different clustering approaches such as D-clustering, K-clustering, Pearson clustering are used to group the gene expression data and estimate the relationship among the genes of interest and related pathways and finally the crosstalk among these pathways.

3.2.1. Data

The data for the rapamycin treatment were produced by Oliviera *et al.* [40] and downloaded from NCBI Gene Expression Omnibus (GEO) website [43]. Oliviera *et al.* studied the dynamic mRNA gene expression following the rapamycin treatment. For this aim, wildtype YSBN6 yeast strain (MATa mating type with a genotype of FY3 ho:HphMX4 and having antibiotic resistance cassette (Hygromycin B / HphMX4) inserted into HO gene by transformation. URA3 function retrieved by homologous recombination of functional URA3PCR productamplified from S288C parental strain) was exposed to rapamycin with glutamine as the sole nitrogen source. A sample was taken at steady state, i.e. 10 minutes before rapamycin treatment. Then, the samples were taken after 3, 7, 14, 24, 56 and 120 minutes of the drug rapamycin treatment. Biological triplicate gene expression was measured for samples -10, 7 and 24 minutes [40]. For each sample, the data were given as normalized signal intensity in GEO

website; however, SGD reports the data as log2 expression to get rid of the noises of the data. Also, log2 expression data were obtained from SGD [44].

The data for the HU treatment was produced by Krippler *et al.* [45] and downloaded from NCBI Gene Expression Omnibus (GEO) website. Krippler *et al.* studied yeast cells to identify the complement of mRNA targets of P-bodies during replication stress induced by hydroxyurea treatment. The transcript profiling of two wild type strains (BY4741 or BY4742 strains) and one mutant strain (lsm1) were performed. Cells were cultured in YPD medium, and samples were taken before the HU treatment as well as after 1, 2 and 4 hours of 200 mM HU treatment. Also, the replicate gene expression of each sample was taken. The GEO data was given as log2 expression for HU treatment.

4. RESULTS AND DISCUSSION

4.1. Optimization Experiments

4.1.1. Flowrate and Droplet Size

For the optimization of flowrate and the droplet size, wild type yeast strain EY0987, which has RFP tagged NOP56 protein is used. The oil phase includes 2% Krytox. As an aqueous phase, YPD medium is used.

4.1.1.1. Optimization of Flowrate for minimum droplet size. To generate the droplets and optimize the flow rate, droplet generator chips are used as shown in Figure 4.1. As an initial trial, flow rate of oil is set to 600 μL/h total and aqueous phase is set to 150μL/h (1:4 ratio) [46]. After the system becomes steady, it is seen that droplet size is too large, far from the desired volume of droplet (Figure 4.2 and Table 4.1). So, flow rates of the aqueous phase and oil phase are changed. First, protecting the ratio, both flow rates are decreased, and oil phase becomes 200 μL/h for each channel and aqueous phase becomes 100 μL/h. At this ratio, droplet size is still too large. Then, flow rate of aqueous phase is decreased to 40 μL/h (1:10 ratio). At this ratio, droplet diameter becomes 166.5 μm; thus, the volume of the droplet becomes 2421 pL. Because this volume is still too large for a desired droplet, it is decided to increase the flow rate of oil phase to 300 μL/h for each channel and wait for a 10 to 15 minutes to be the system stable. At that ratio, diameter of droplet is calculated as 121.7 μm (Figure 4.3). Then, flow rate of oil phase is increased to 350 for each channel and waited for a while to make the system steady. At that rate, diameter of the droplet is calculated as 91 μm (Figure 4.4). As it is wanted to increase the flow rate of the oil to 400 μL/h, the system becomes steady hardly and the diameter of the droplet doesn't change much, it becomes 100 μm (Figure 4.5). So, it is decided that the optimal flow rate of the oil phase is 400 μL/h for each channel (total 800 μL/h) and 40 μL/h for aqueous phase (1:20 ratio). When this is the case, droplet diameter becomes 100 μm and volume is

roughly 523 pL. Producing smaller volume is hard due to the instability of the flow system.

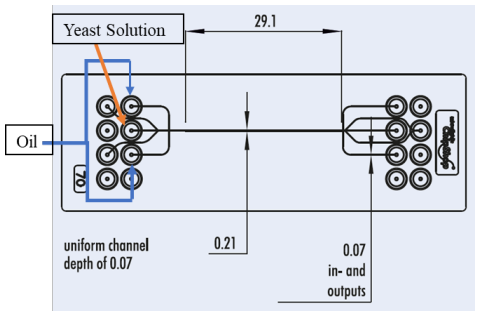

Figure 4.1. Droplet generator chip

Figure 4.2. Oil phase 600 μL/h, aqueous phase 150 μL/h, droplet diameter 250 μm.

Another experiment is done to investigate the droplet sizes in a droplet generation and optimization chip (Figure 4.6). First, to optimize droplet size and flow rate in droplet generation and optimization chip, YPD medium is used as an aqueous phase. Because there is a knowhow about the flow rate from the previous optimization experiment in droplet generation chip, the flow rate of the oil phase is set to 700 μL/h while flow rate of aqueous phase is set to 100 μL/h to make the system steady state. After all the chambers are filled with the oil phase and droplets which have diameter roughly 160 μm, flow rates are changed to 800 μL/h for oil phase and 40 μL/h for aqueous phase as it is optimized at the former experiment. However, due to the different chip design, system is not able to stay at steady state. Thus, the low rate of the aqueous phase is increased to 50 μL/h. At these rates, droplet generation becomes steady and

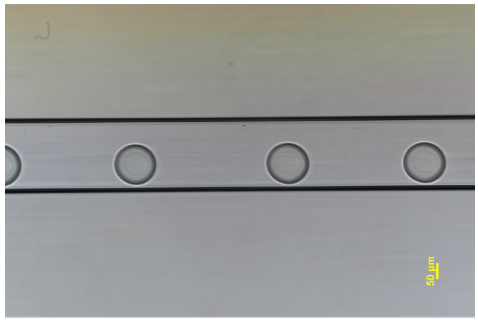

Figure 4.3. Oil phase 600 μL/h, aqueous phase 40 μL/h, droplet diameter 121.7 μm.

Figure 4.4. Oil phase 700 μL/h, aqueous phase 40 μL/h, droplet diameter 91 μm.

Figure 4.5. Oil phase 800 μL/h, aqueous phase 40 μL/h, droplet diameter 100 μm.

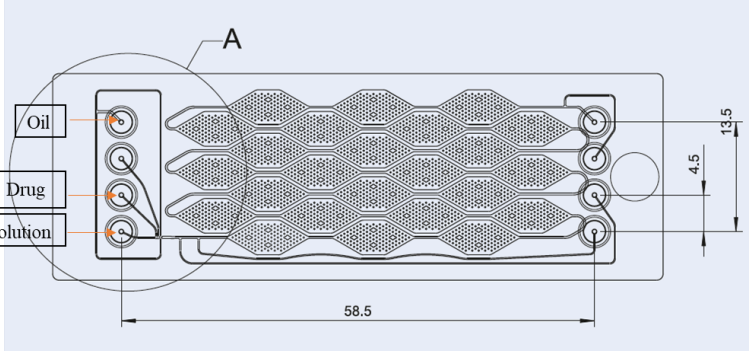

Figure 4.6. Droplet generator and incubator chip.

the droplet diameters vary between 80 to 200 μm. This range occurs because the system is a continuous system and it is hard to generate exactly same size of droplets. According to these diameters, droplet volumes vary between 250 pL to 4200 pL (4.2 nL). This volume range is the smallest droplet volume that can be created with this chip design. Figure 4.7 shows the droplet generation and the droplets in the incubator. All the flowrates tested for the optimization of droplet size are summarized in Table 4.1.

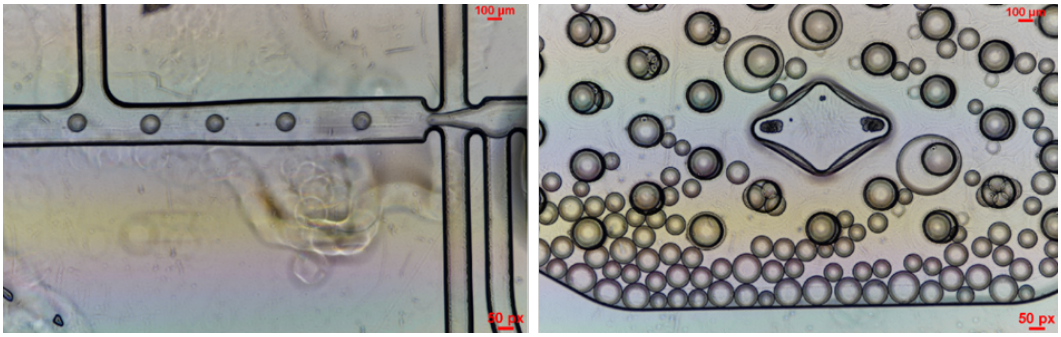

Figure 4.7. Droplet Generation with blank YPD medium.

After 24 hours of incubation, droplets in the chip are analyzed under the microscope. There are 24 chambers in the chip and all of them have droplets of different sizes. 9 chambers are analyzed to investigate the droplets and cells. In general, in the chambers, about 25% of the droplets have diameters larger than 200 μm (Figure 4.8). Almost none of the droplets have diameter smaller than 100 μm. Having big droplets may stem from the large dimensions of the droplet generation channels.

Table 4.1. The flowrates used for the optimization of the droplet sizes in two different chip models.

Chip type	**Oil phase (μL/h)**	**Aqueous phase (μL/h)**	**Droplet diameter (μm)**	**Droplet volume (nL)**	**Faith of droplets**
Droplet generation chip	2x300	150	>200	>4.18	Collected out of the chip
	2x200	100	>200	>4.18	Collected out of the chip
	2x200	40	166.5	2.4	Collected out of the chip
	2x300	40	121.7	0.9	Collected out of the chip
	2x350	40	91	0.39	Collected out of the chip
	2x400	40	100	0.52	Collected out of the chip
Droplet generation and incubation	2x350	100	160	2.14	Collected in chambers inside the chip
	2x400	40	No generation	-	Collected in chambers inside the chip
	2x400	50	80-200	0.26-4.18	Collected in chambers inside the chip

To count and determine the size of the droplets, Matlab program was used. By using image processing tool of the program, large and small droplets are detected and circled with different colors. When the code was run, there were several noises, e.g. lots of small circles that were not droplets (air bubbles) or huge circles which were not droplets. These noises were eliminated first, by decreasing sensitivity from 1 to 0.93; then, remaining ones were eliminated manually. The Matlab code is given in the Appendix A. The Table 4.2 gives the droplet size distribution of each chamber.

Table 4.2. Droplet distribution of each chamber.

	Droplet Diameter (mm)	**Droplet Amount**	**Radius Range (mm)**	**Droplet volume (pL)**	**Droplet size distribution (%)**
Chamber 1	<200	279	38.25-91.75	234-3236	74.6
	>200	95	98.33-387.6	3983-66×10^3	25.4
Chamber 2	<200	209	38.4-91.6	238-3220	70.4
	>200	88	99-254	4065-68×10^3	29.6
Chamber 3	<200	300	36-92	209-3262	76.7
	>200	91	99-224	4174-47×10^3	23.3
Chamber 4	<200	220	37-91	219-3210	74.3
	>200	76	99-271	4142-83×10^3	25.7
Chamber 5	<200	294	49-90	500-3140	78.6
	>200	80	99-216	4075-42×10^3	21.4
Chamber 6	<200	307	50-92	552-3264	77.1
	>200	86	100-232	4250-52×10^3	21.9
Chamber 7	<200	277	50-94	553-3547	79.6
	>200	72	108-207	5284-37×10^3	20.6
Chamber 8	<200	290	50-95	533-3702	83.8
	>200	56	107-200	5223-33×10^3	16.2
Chamber 9	<200	195	39-91	266-3197	76.5
	>200	60	98-215	4010-42×10^3	23.5

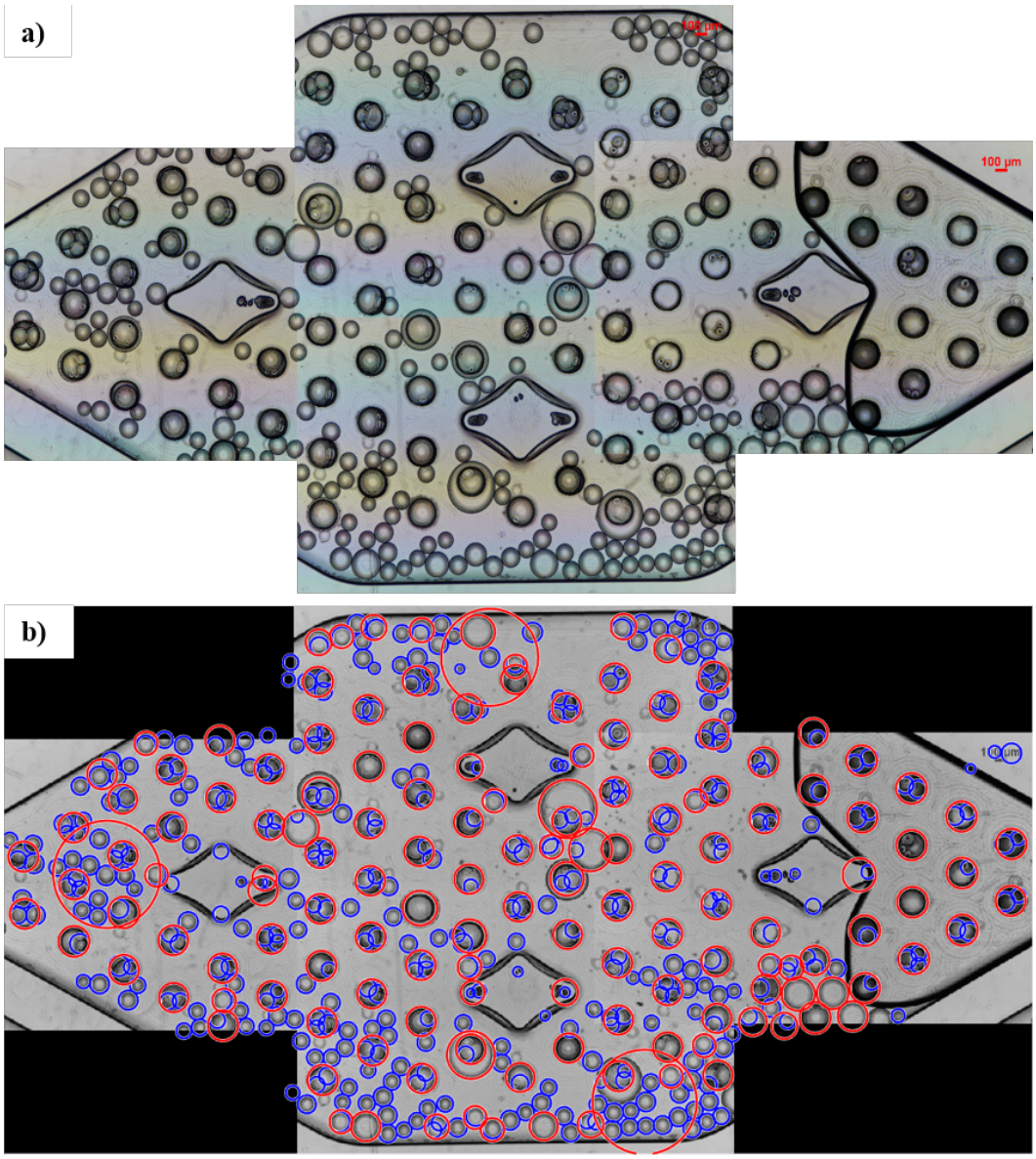

Figure 4.8. a) Droplet analysis after 24 hours b) droplet detection by image processing and Matlab.

4.1.1.2. Droplet Size and Cell Visibility in Droplets After Incubation. A yeast cell solution is sent to this chip system to see the visibility of the cells inside the oil droplet. It is aimed to encapsulate one cell per droplet; therefore the yeast culture is diluted, and after dilution, there are 6.4 $\times 10^6$ cells in a 5 mL syringe to load into the chip system. However, during the experiment, cells couldn't be found in the droplets and after 24-hours incubation, only two droplets contain cells. Even though the bright field images of the droplets show there are cells in it, on the other hand, fluorescence images are not satisfactory. Since YPD medium is fluoresced by itself, it hinders the visibility of the fluorescence of the cells as can be seen in the Figure 4.9 e. So, it is uncertain whether the cells are dead or alive. At the end, it is decided to change the YPD medium to YNB in the experiments. Also, it is decided to use different strain that has more fluorescence, i.e. GFP tagged RPL5 protein. RPL5 is more abundant than NOP56 protein in a cell. Thus, its fluorescence may be more detectable in a droplet.

4.1.1.3. Estimation of Flow Profile in the Chip by COMSOL. *One Aqueous Inlet:* In order to follow the velocity and pressure profiles in the microfluidic platform, the experimental results are also simulated by the computational means using COMSOL Multiphysics Software. Chip design is simplified to reduce the computational burden. The inlet of the chip is drawn with all the real sizes and curvatures. Not identical but adequate distance towards entrance of chamber is drawn. The traps are assumed as full height of the chip and the spacing between them are set as identical with the chip. The slopes of the walls of the chambers are set as identical with the experimental chip. After the specifications such as spacing, wall angles, curvature are identified, COMSOL software is initiated. In the figures, blue part indicates oil phase while the red part indicates aqueous phase. Flow rates of the inlets are set same as the experimental flow rates; oil phase, V_2, is 400 μL/h (1.111×10^{-10} m^3/s, for each side) and aqueous phase, V_1, is 80 μL/h (2.222×10^{-11} m^3/s) (Figure 4.10). Two-Phase Flow includes the setting of interfacial tension (σ) value. It is set as 5 mN/m [47] in this simulation. Wetted wall subsection carries the information about which walls have this condition (it disables no slip) as well as the angle when the fluids are encountered at the wall. First, since the

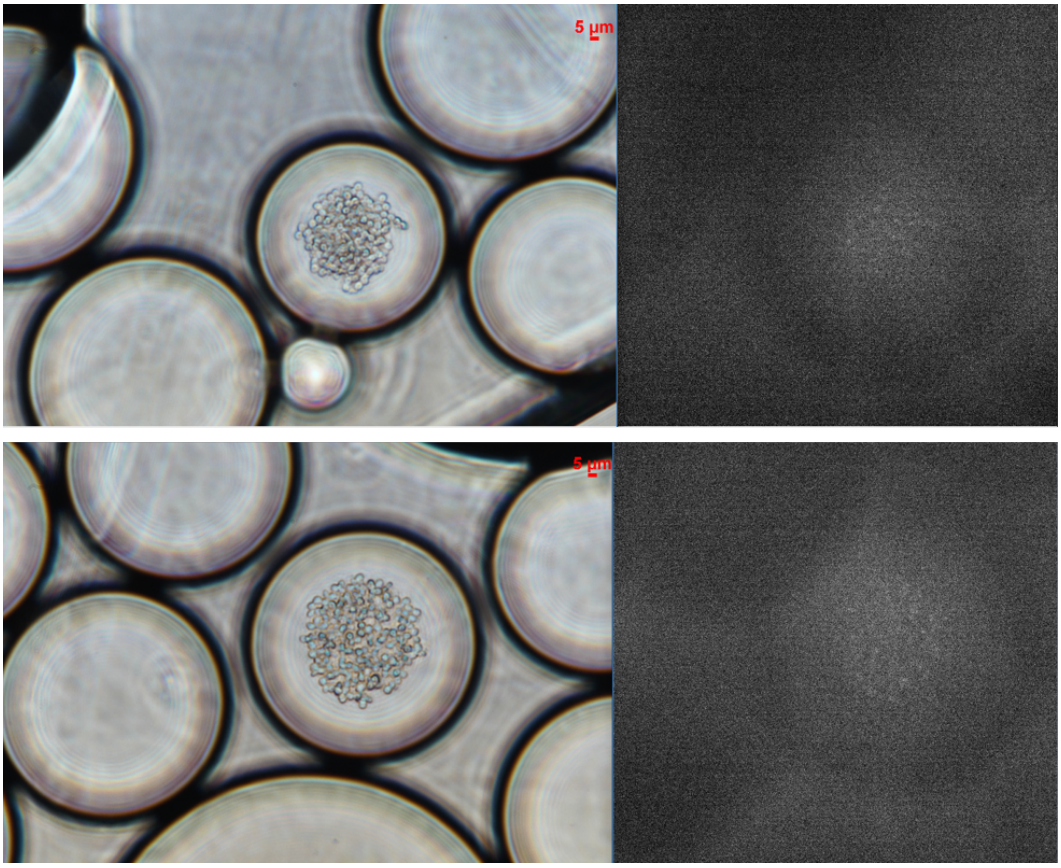

Figure 4.9. Cells in the droplets.

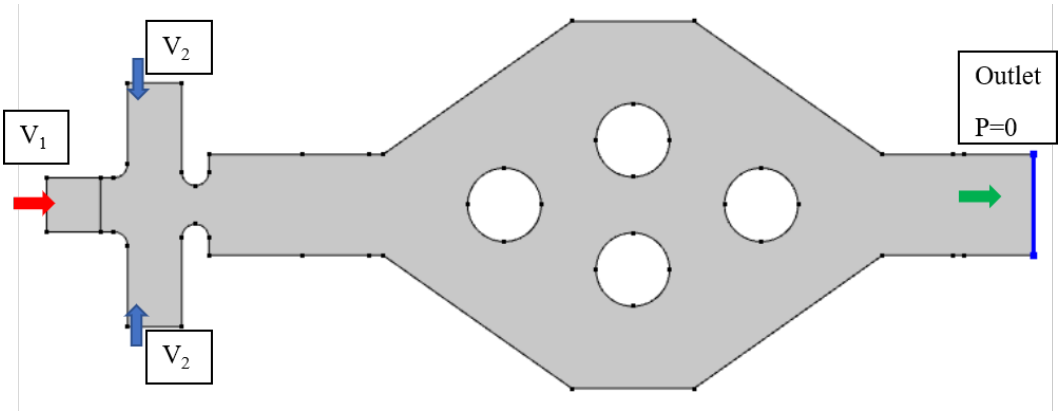

Figure 4.10. Laminar flow assignments.

aqueous phase (shown as red arrow (Figure 4.10) and red fluid (Figure 4.12 and 4.13) in this simulation) does not wet the wall due to its physical background, the angle with the wall (σ_w) for water should be smaller than 90° (Figure 4.11, Fluid 1) This means that oil phase (Fluid 2 in Figure 4.11) is dominant and therefore wets the wall when both liquids are present. The angle is set as 45° in this simulation (Figure 4.12).

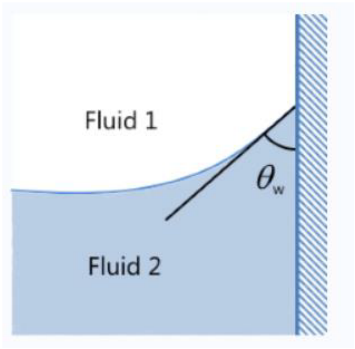

Figure 4.11. Angle with the wall.

When the wetted wall angle is changed from 45° to 135°, which means aqueous phase wets the wall, it is seen that proper droplets are not generated (Figure 4.13).

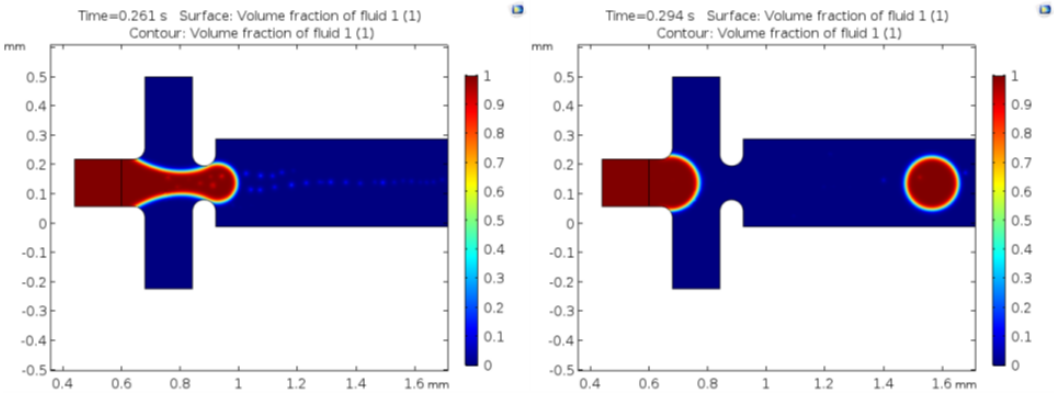

Figure 4.12. Droplet formation when σ_w=45°.

The outcome of these runs is shown in three figures. The simulation is ceased at t=0.969 second and the final composition in the chamber is shown in the Figure 4.14. Simulation shows the merging of the small droplets and creation of bigger droplet, which is a consistent result with the experiment. Also, the random distribution of the droplets in the simulation resemble with the distribution of the droplets in the chip.

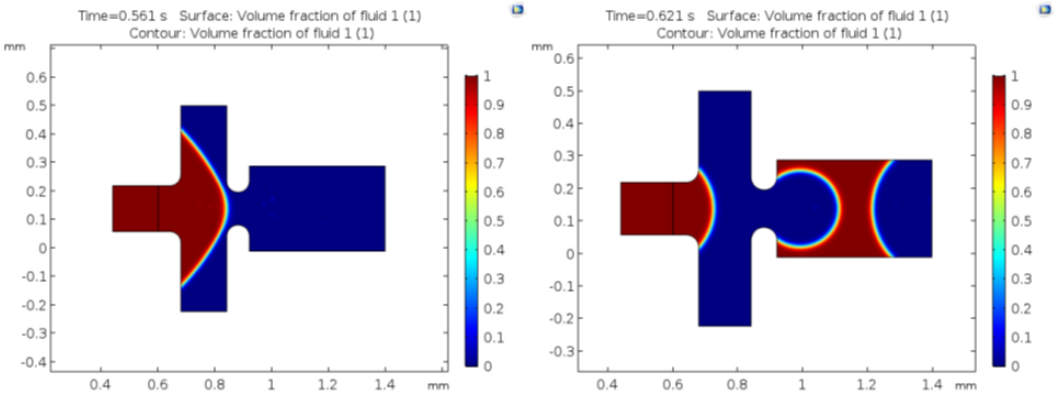

Figure 4.13. Droplet formation when σ_w=135°.

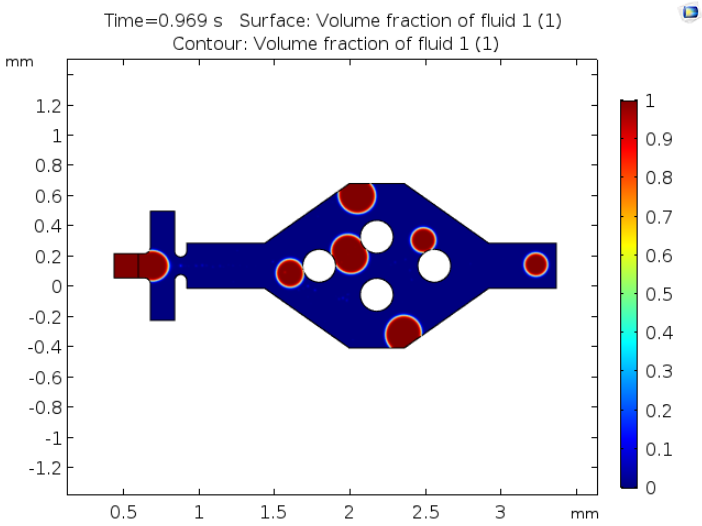

Figure 4.14. Droplet distribution.

Velocity map shows the velocity profile in the chamber (Figure 4.15a). The droplet generation point has the peak velocity since all the inlets sums up there. In the simulation, chamber and aqueous phase inlet seem to be stagnant. Thus, it can be said that, oil phase is the main driving force to keep the droplets moving. Pressure map shows the pressure at the interfaces (Figure 4.15b). As seen in the droplets, pressure gradually decreases toward the interface. This means, droplets are stable and if the pressure at the interface were higher, droplet would burst. Also, the droplet size is calculated when the flow rate of aqueous phase is 80 μL/h, and it is found that the droplets have diameter 0.16 mm (160 μm) as observed in the experiments (Figure 4.15c). Also, flow rate of the aqueous phase is changed to 60 μL/h, and the droplet

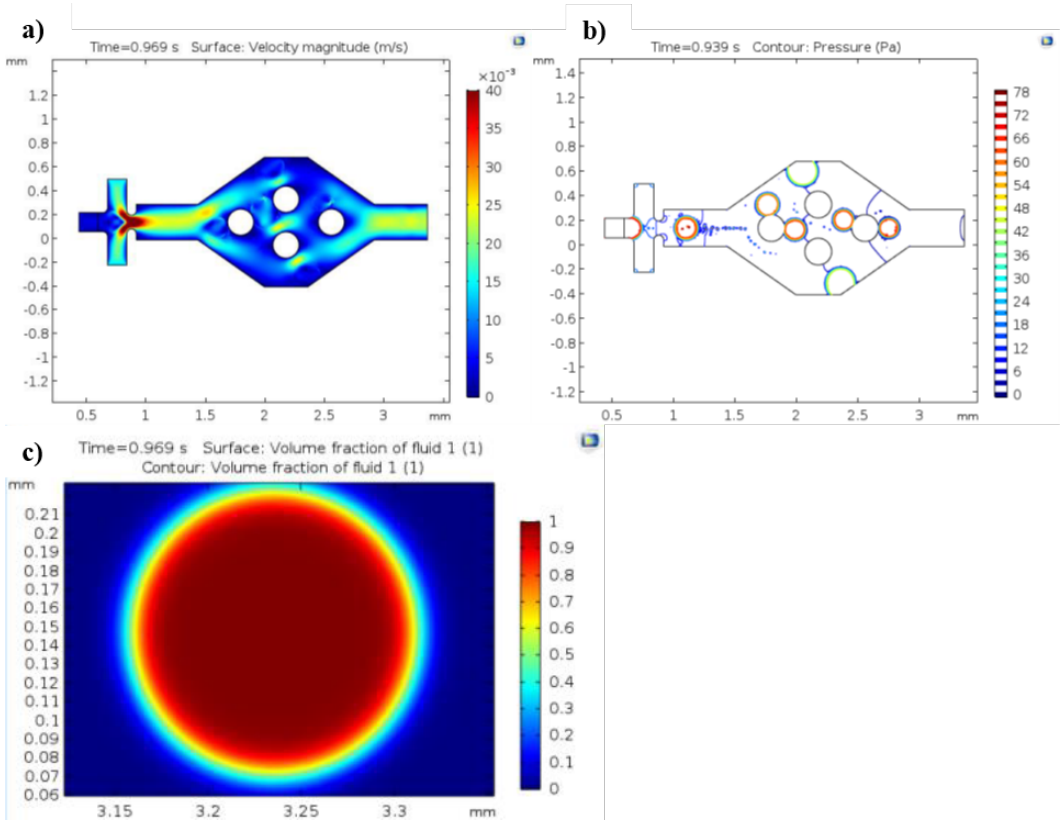

Figure 4.15. a) Velocity profile, b) Pressure profile, c) Droplet size, $Q_{aqueous}$=80 μL/h.

size calculated from the vertical axis. It is seen that the droplet diameter doesn't change much according to the visual observation. The droplet diameter becomes 0.16 mm (Figure 4.16). *All Three Inlets:* The exact inlet of the chip is also simulated by COMSOL. Rather than one aqueous inlet, all three inlets are modelled to investigate

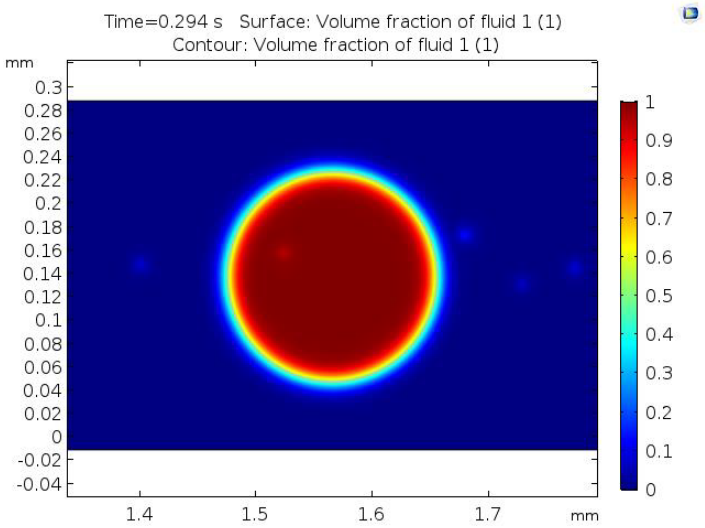

Figure 4.16. Droplet size, $Q_{aqueous}$=60 μL/h.

multiple fluid phase effects in the chip. The desired effect is mixing all the streams uniformly before the droplet generation. Each aqueous stream has 60 μL/h flow rate and oil streams has 400 μL/h, each. Figure 4.17 shows the simulation steps for that aim, and it is seen that, all aqueous phases mix with each other and create a droplet. Since the total flow rate of aqueous phase becomes 180 μL/h, the droplet size increases to roughly 0.25 mm (250 μm) which is also a consistent result with the experimental results. (Figure 4.18).

4.1.2. Surfactant Concentration and Inoculum Size

For these experiments, wild type BY4743strain, which has GFP tagged RPL5 protein, is used. Also, experiment is conducted with oil phase, which includes 2% Krytox. As an aqueous phase, YNB medium is used.

4.1.2.1. 1.5% Krytox. *Yeast Density in Culture and Surfactant Preparation:* The number of cells in 2 μL YNB medium, on the glass slide, is calculated as 3.52 $\times 10^5$. In a 5 mL solution, there should be roughly 881×10^6 cells. As only one cell in each droplet is desired, the yeast solution is diluted roughly 1000 times since the average droplet volume is calculated as 5806×10^{-6} μL.

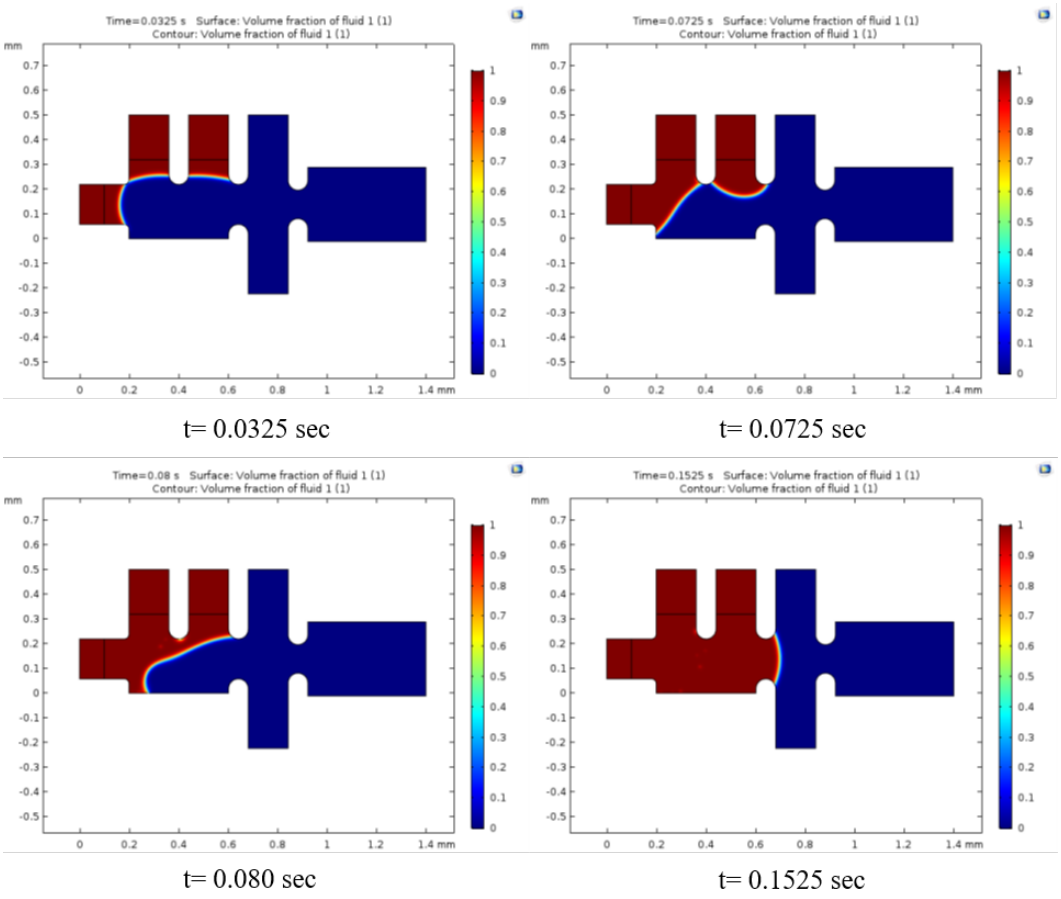

Figure 4.17. Complete inlet simulation of droplet generation and incubation chip.

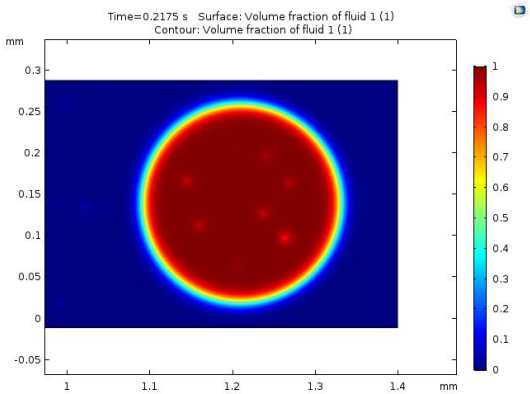

Figure 4.18. Droplet size, $Q_{aqueous}$=180 μL/h.

Oil phase for droplet generation is prepared by mixing it with Krytox surfactant. 1.5% of Krytox is mixed with Novec7500 oil, i.e. 75 μL Krytox is mixed with 4925 μL Novec7500. Total 5 mL of oil phase is sent to the chip system in a syringe.

Flow Rate and Droplet Size: Because there is a knowhow about the flow rate from the optimization experiments, the flow rate of the oil phase is set to 700 μL/h while the flow rate of aqueous phase is set to 100 μL/h to make the system steady. After system reaches steady state, the flow rate of the oil phase is increased to 800 μL/h and the flow rate of the aqueous phase is decreased gradually until the 50 μL/h, referring to the previous experiments. However, at this flow rate, system could not stay in steady state mode, thus, the flow rate of the aqueous phase is increased to 60 μL/h. At this rate, the droplet sizes vary between 180 μm to 250 μm. This range is far away from the desired diameter which is 100 μm; however, it is the closest value to desired value because the depth of the channels is too much. According to these diameters, droplet volumes vary between 3000 pL to 8000 pL.

The reason of these big droplets may be the change of the nutrient medium from YPD to YNB, which may have different cohesion properties. When the cohesion force of the liquid is changed, the flow force of the oil may not be enough to separate the aqueous droplets. Another reason, the syringe pumps may not work correctly as they are set. Although the pump display shows 80 μL/h, the syringe may be pushed with 120 μL/h.

Also, droplets merged with each other just after they are created. The main reason of this merge may be the low concentration of Krytox (1.5%).

Single Cell Analysis: After the loading of each incubation chamber, it is checked whether there is any yeast cell in any droplet. Several droplets are found that contain yeast cells. The detected droplets are analyzed under fluorescence microscopy. Figure 4.19 shows the droplets that contain living yeast cells.

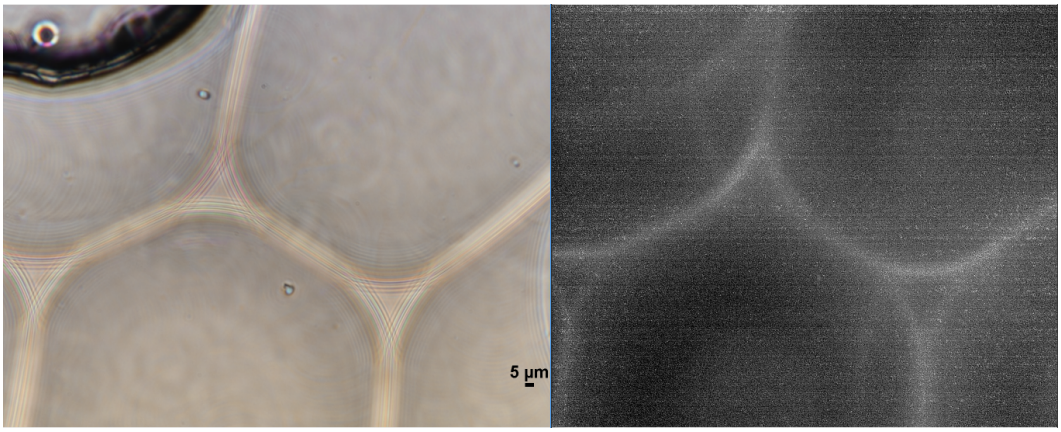

Figure 4.19. Droplets with yeast cells before incubation.

After 24 hours of incubation, droplets in the chip are analyzed again to see the Krytox effects on yeast cells and the stabilization of the droplets. There are 24 chambers and it is seen that all droplets in the chambers are merged and create one big droplet. In the chambers, it is seen that, yeast cells are proliferated, and all the yeast clusters fluoresced (Figure 4.20). It means, this strain, that has GFP tagged RPL5p, does not die under 1.5% Krytox.

As a result, yeast cells can survive against 1.5% Krytox, however, this concentration is not enough to keep the droplets stable and unmerged. Many yeast cells must be encapsulated by a droplet so that, this amount of cell proliferation can occur.

Furthermore, since there are not sufficient number of droplets in the chambers due to the merge, analysis of the droplet size and number cannot be done.

4.1.2.2. 2% Krytox (1 cell/droplet). Aiming to encapsulate 1 cell per droplet, two experiments were done using 2% Krytox and different dilutions of yeast inoculum.

Yeast Density in Culture and Surfactant Preparation: For both experiments, oil phase is prepared by mixing 2% Krytox surfactant to increase the droplet stability for

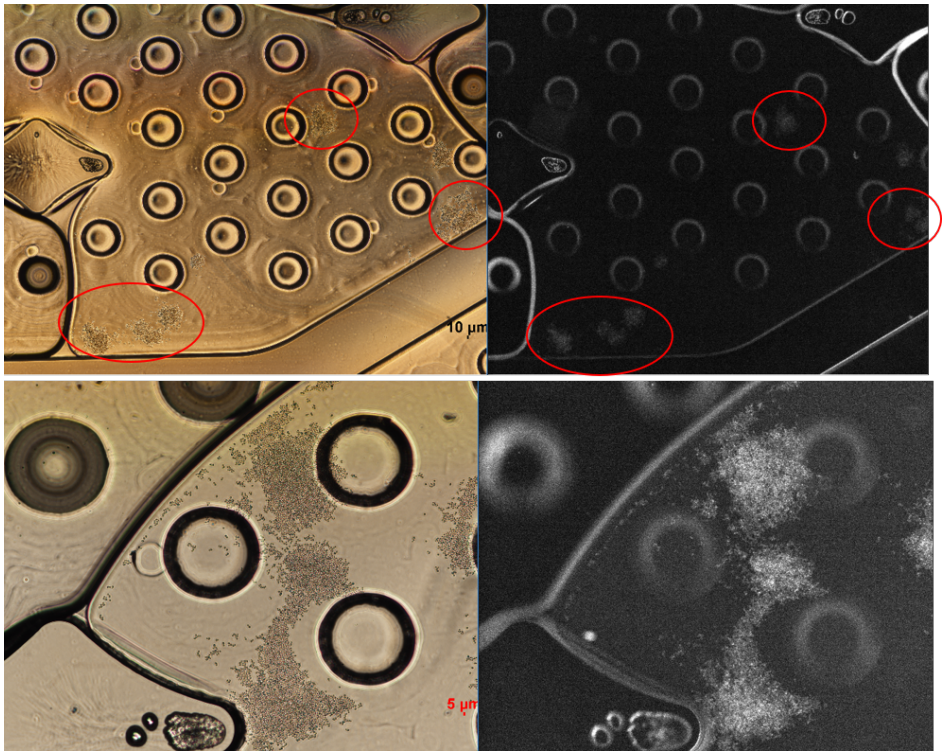

Figure 4.20. Droplets with yeast cells after 24-h of incubation.

the incubation. 100 μL Krytox is mixed with 4900 μL Novec7500. Total 5 mL of oil phase is sent to the chip system in a syringe.

For the first experiment, there are roughly 0.225×10^6 cells covered on the glass slide (2 μL of sample). In a 5 mL, there would be roughly 564×10^6 cells. Also, the average droplet diameter is calculated as 220 μm. It is desired to be one cell in a droplet, so 600 times dilution is done before yeast solution is sent to the chip system.

For the second experiment, there are roughly 1.85×10^6 cells covered on the glass slide (2 μL of sample). In a 5 mL, there would be roughly 4620×10^6 cells. Also, the average droplet diameter is calculated as 220 μm. It is desired to be one cell in a droplet, so 4000 times dilution is done before yeast solution is sent to the chip system.

Flow Rate and Droplet Size: First, only oil phase is sent to the system until all the chambers are full of oil. The flow rate of oil phase is set to 600 μL/h while the flow rate of the aqueous phase is set to 200 μL/h. Then, the flow rate of the oil phase

is increased to 800 μL/h and the flow rate of the aqueous phase is decreased gradually to 50 μL/h to obtain the minimum volume of droplet. At this rate, the droplet sizes vary between 180 μm to 250 μm. This range is far away from the desired diameter, which is 100 μm; however, it is the closest value to the desired value because the depth of the channels is too much. According to these diameters, the droplet volumes vary between 3000 pL to 8000 pL.

Single Cell Analysis: After the yeast cell loading is accomplished is performed, cells are searched in the droplets; however, it could not be found. The reason may be either the cells are not visible in the droplet because of their sizes or none of the cells went in the droplet from the syringe due to the high dilution.

Also, it is seen that stabilization of all the droplets is broken, and they merged with other (Figure 4.21). For this experiment, 2% oil solution is not sufficient to keep the droplets stable during 24-hour incubation.

In the second experiment, after cell loading is performed, it is checked whether there is any yeast cell in any of the droplets. Detecting the cells in the droplets is hard for several reasons. First, the yeast solution sent to the system is too dilute that only a few cells entered the system. Second, most of the droplets merge and create one big droplet, so it is harder to find a yeast cell in a giant droplet. So, only a few small droplets are found that contain yeast cells. The detected droplets are analyzed under fluorescence microscopy. Figure 4.22 shows one of the droplets that contain a living yeast cell.

After 24 hours of incubation, droplets in the chip are analyzed again. It is seen that all the droplets in the chamber are merged and create one big droplet. Also, there are several droplets that maintain small droplet feature and a few of them have yeast cells. In the chambers, it is seen that, the yeast cells are proliferated, and all the yeast clusters fluoresce. It means, this strain, that has GFP tagged RPL5p, can resist to 2% Krytox environment. Figure 4.23 shows the droplets that have 342 μm and 222 μm diameter, respectively.

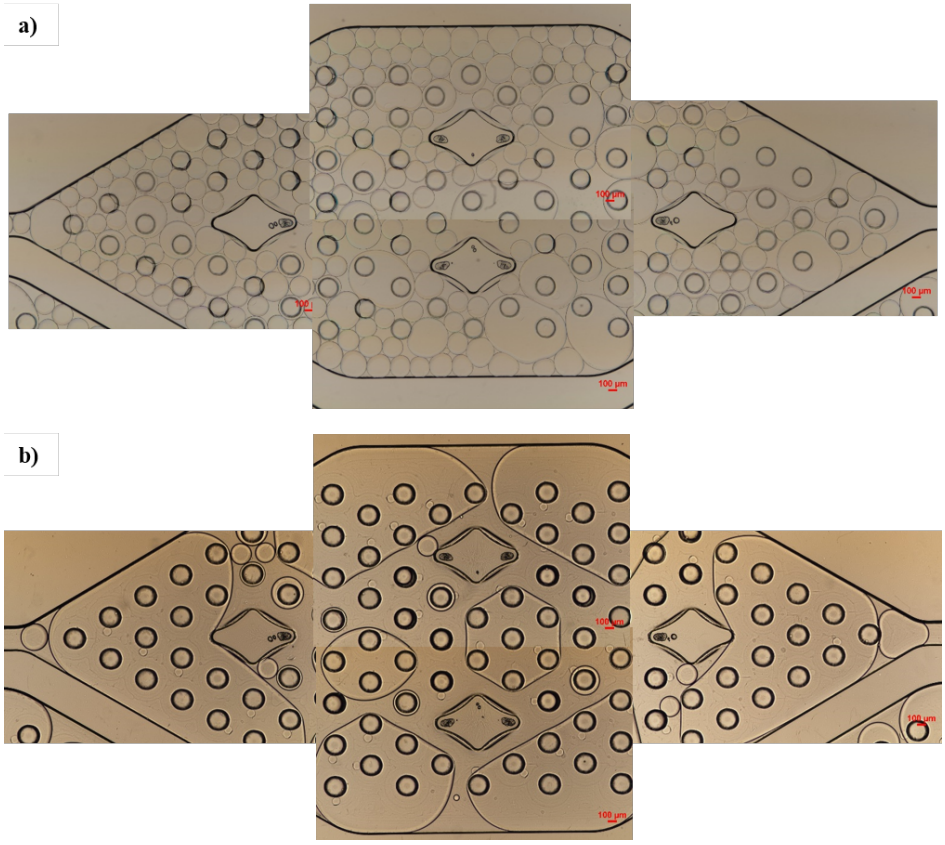

Figure 4.21. a) Chamber before 24-hour incubation, b) Chamber after 24 h of incubation.

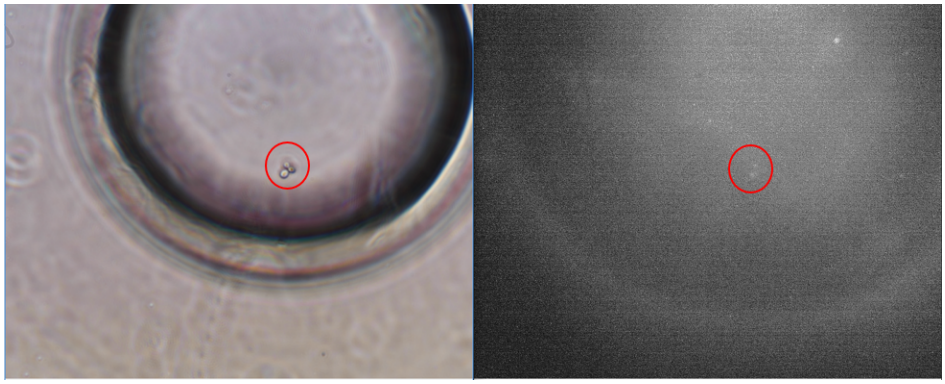

Figure 4.22. Droplet with yeast cells before incubation.

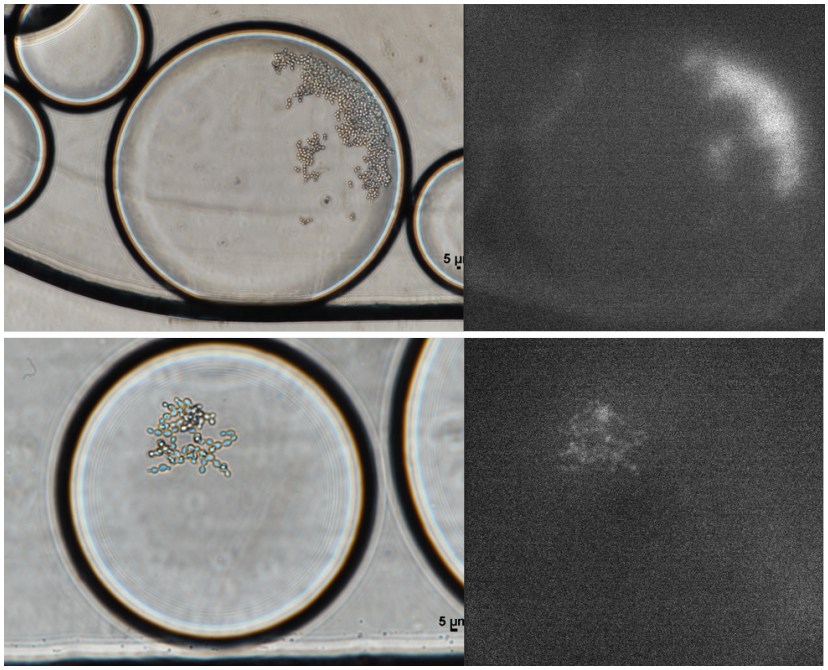

Figure 4.23. Droplet with yeast cells a) before 24-h of incubation, b) after 24-h of incubation.

As a result, yeast cells can survive against 2% Krytox environment. Although 2% Krytox was enough to stabilize 70% of the droplets in the YPD medium, However, in the experiments with YNB medium, 2% Krytox is not enough to keep the droplets stable during the incubation. Even though yeast cells cannot be detected at the end of the yeast cell loading period, they are seen after the 24-hr incubation, i.e. many yeast cells are seen in a droplet.

4.1.2.3. 2% Krytox (10 cell/droplet). *Yeast Density in Culture and Surfactant Preparation:* In this experiment, the aim was to encapsulate 10 cells per droplet. The oil phase is prepared by mixing 2% Krytox surfactant to increase the droplet stability for the incubation. 100 μL Krytox is mixed with 4900 μL Novec7500. Total 5 mL of oil phase is sent to the chip system by a syringe.

Because the dilution for one cell per droplet is not efficient to encapsulate the sufficient number of cells to observe, a dilution aiming for ten cells per droplet was

made. There are roughly 0.2×10^6 cells covered on the glass slide (2 μL of sample). In a 5 mL yeast cells, there would be roughly 569×10^6 cells. Also, the average droplet diameter is calculated as 220 μm. It is desired to be ten cells in a droplet, so 60 times dilution is done before yeast solution is sent to the system.

Single Cell Analysis: After loading the chip with yeast cells, the stabilization of droplets and the encapsulated cells are investigated. After the inlets are closed, many small droplets are formed in the chambers (Figure 4.24a), however, after the droplets are incubated for 24 hours, it is seen that, all the droplets are merged together (Figure 4.24b). Before the incubation, there are not a cell observed in the droplets (Figure 4.24c). After one day of incubation, there was no grown cell population in any of the coalesced droplets. From this experiment, it can be concluded that, 2% oil phase is not sufficient to keep the droplets stable for 24 hours. One of the reasons of yeast cells not entering into the chip may be the precipitation of the cells down in the syringe during cell loading (Figure 4.25). It is decided not to dilute the yeast culture for the next experiment.

4.1.2.4. 2% Krytox (no dilution). *Yeast Density in Culture and Surfactant Preparation:* Oil phase for droplet generation is prepared by mixing Krytox surfactant. 2% of Krytox is mixed with Novec7500 oil, i.e. 100 μL Krytox is mixed with 4900 μL Novec7500. Total 5 mL of oil phase is sent to the system in a syringe. For this experiment, yeast culture is not diluted. There are roughly 560×10^6 in a 5 mL syringe.

Single Cell Analysis: During the experiment, it was again observed that the yeast cells were sedimented down the syringe (Figure 4.25). Also, it was harder to obtain a steady state droplet generation due to the high number of yeast cells. When the chambers were investigated after the cell loading, it was seen that, lots of cells entered the chip. However, droplets have already coalesced and created bigger droplets in the chambers (Figure 4.26a). Nevertheless, there were several smaller droplets containing fluoresced yeast cells (Figure 4.26b).

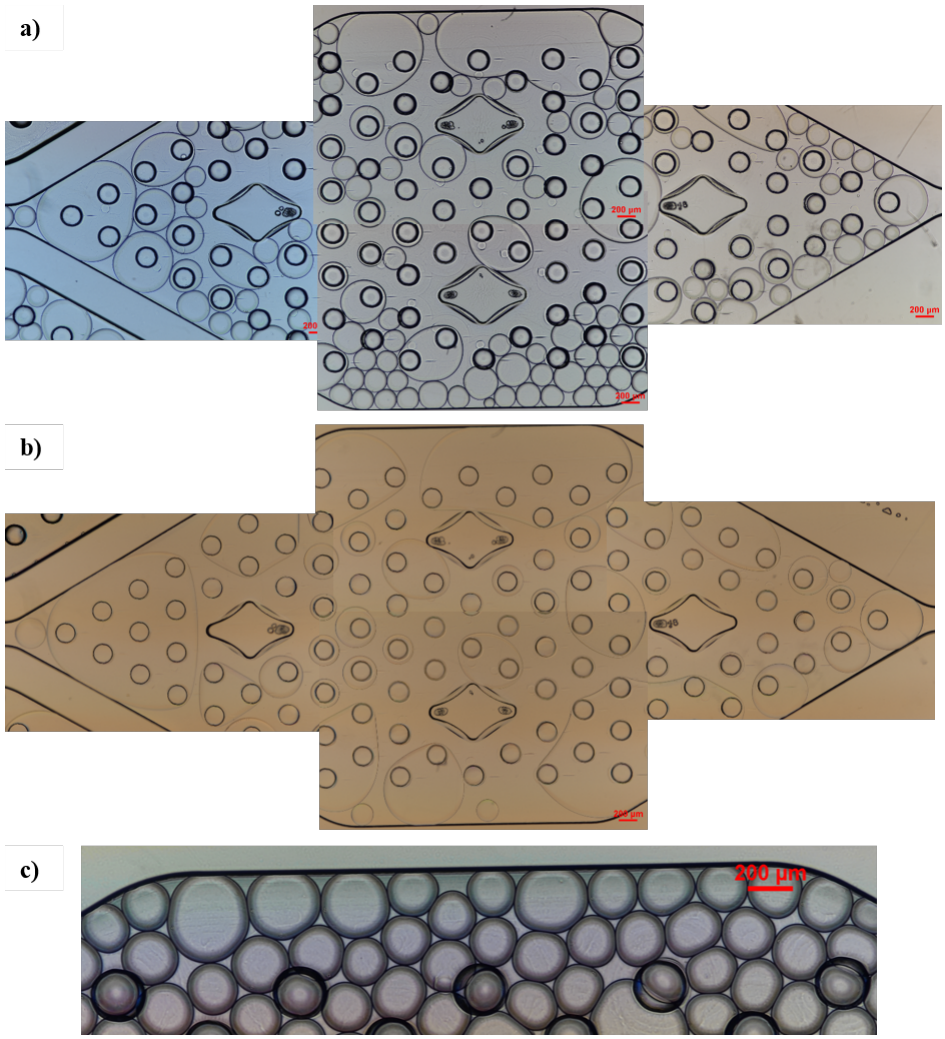

Figure 4.24. a) Chamber before incubation, b) Chamber after 24-h incubation, c) Empty droplets in a chamber.

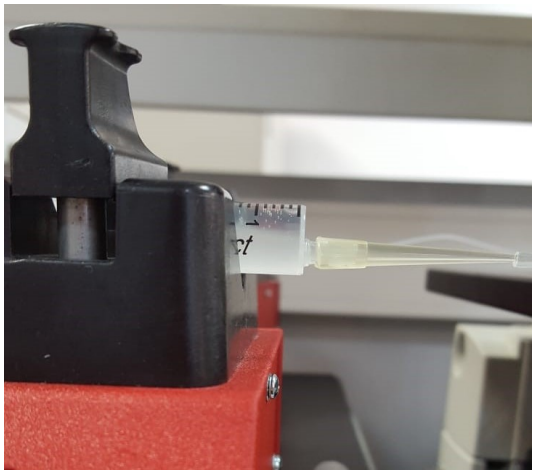

Figure 4.25. Precipitation of the cells in a syringe.

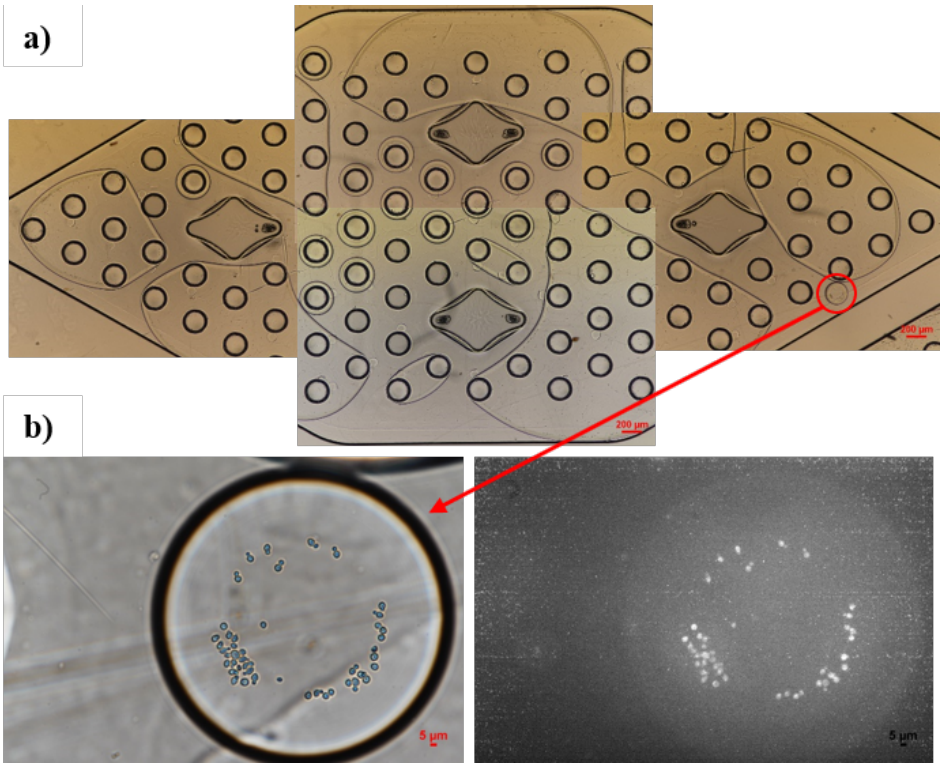

Figure 4.26. a) Coalesced droplets, b) Fluoresced droplets.

After one day of incubation, the cells were grown in the droplets and they were fluorescing. Figure 4.27 shows the particular droplets before and after 1-day of incubation. Since most of the droplets are merged together, it can be concluded again, 2% Krytox in oil phase is not sufficient to keep the droplets stable for 24 hours.

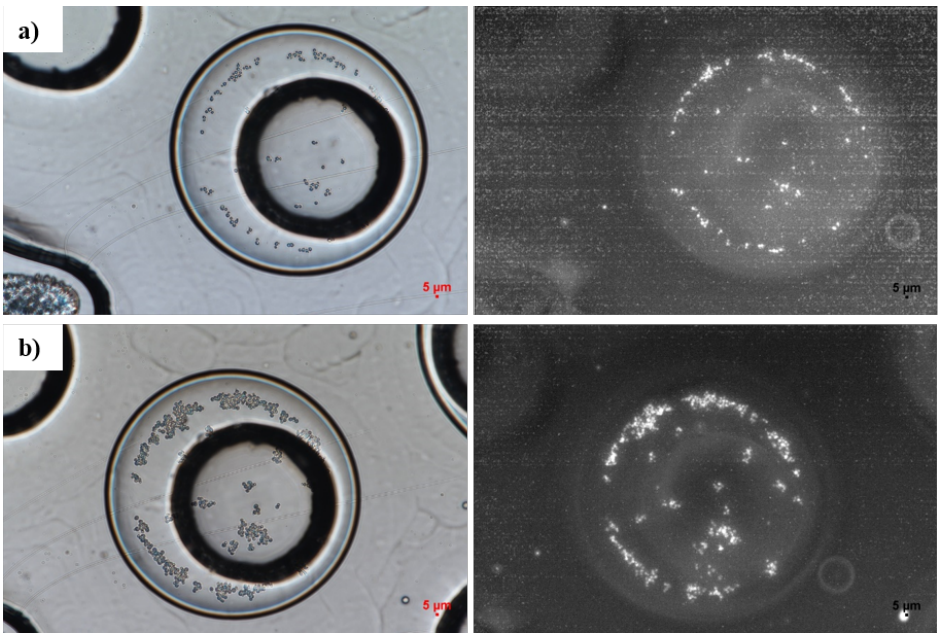

Figure 4.27. a) Fluoresced droplets before incubation, b) Fluoresced droplets after 24-h incubation.

4.1.2.5. 3% Krytox (1 to 1 dilution and Jeffamine). *Yeast Density in Culture and Surfactant Preparation:* Oil phase for droplet generation is prepared by mixing Krytox surfactant. 3% of Krytox is mixed with Novec7500 oil, i.e. 150 μL Krytox is mixed with 4850 μL Novec7500. Total 5 mL of oil phase is sent to the chip system by a syringe.

Since no dilution of inoculum caused instability in droplets, 1 to 1 dilution is used to trap the cells in the droplets. There are roughly 0.3×10^6 cells covered on the glass slide (2 μL of sample). In a 5 mL, there would be roughly 775×10^6 cells. When 1 to 1 dilution is made, there should be roughly 387×10^6 cells in a 5 mL syringe.

Also, to keep the droplets stable, an aqueous phase surfactant called Jeffamine is used. As explained in the Methods part, 0.075% Jeffamine is added into aqueous phase.

Single Cell Analysis: After the cell loading is done, droplets and cells are investigated. It is seen that, until the 6th chamber, droplets stability is not maintained, and the droplets merge with each other (Figure 4.28). On the other hand, small droplets keep their stability in the latter chambers. Also, in a droplet, one or more cells are observed as can be seen in the Figure 4.29.

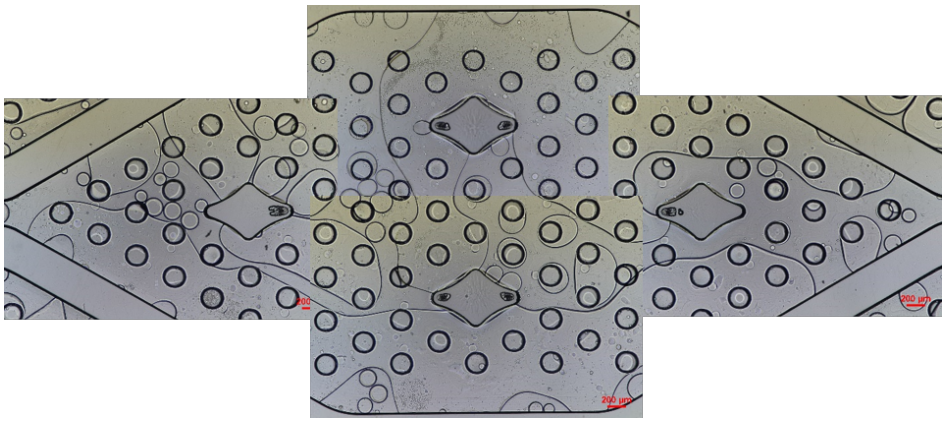

Figure 4.28. Chamber 6 – unstable droplets.

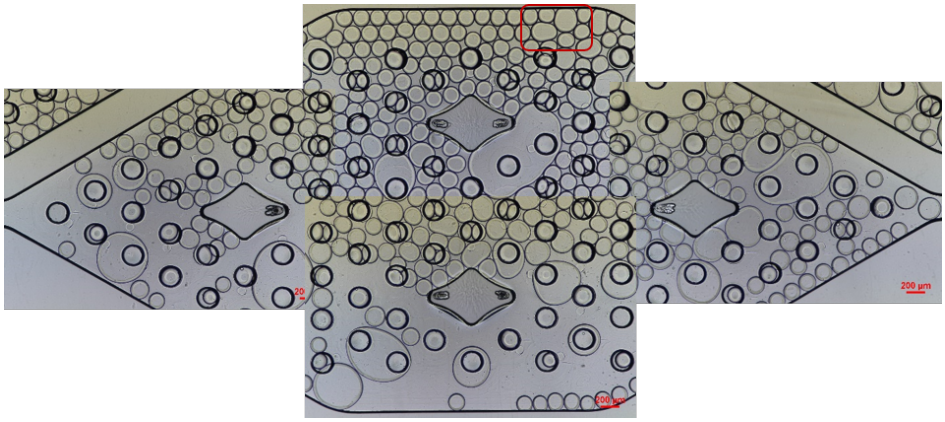

Figure 4.29. Chamber 22 – Stable droplets.

When the red area is zoomed in (Figure 4.30), it can be seen that single cells are encapsulated in the droplets that have diameters between 70 μm and 200 μm. Also, 24-hours incubated cells are observed, and it is seen that cells are alive. Thus, it can be concluded that 3% Krytox containing oil phase and Jeffamine are not toxic to cells and 3% surfactant is enough to stabilize the droplets for 24 hours.

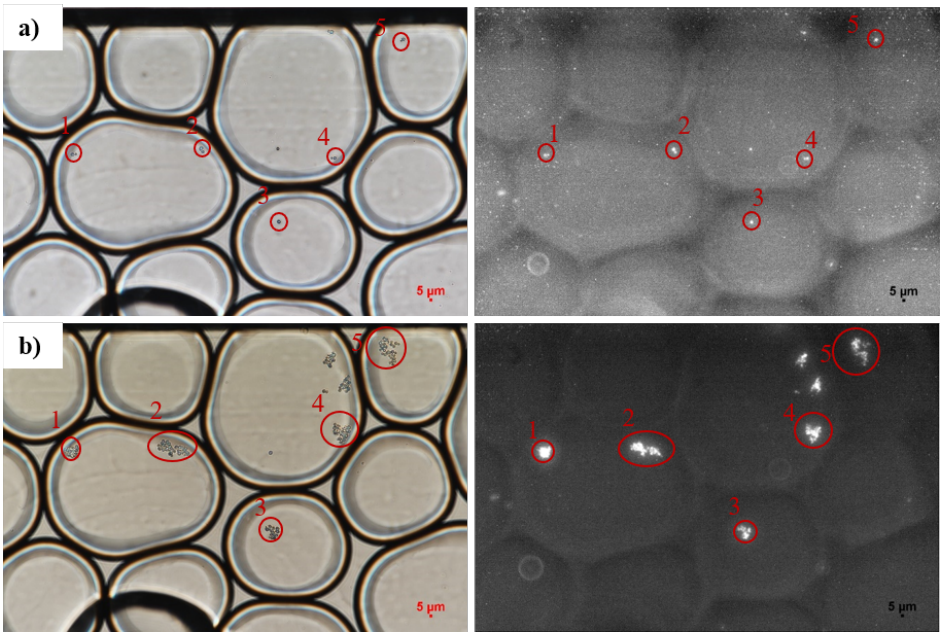

Figure 4.30. Chamber 22 a) Before incubation, b) After 24-hour of incubation.

4.1.3. Control Experiment with RPL5 tagged Strain

This experiment is done with GFP tagged RPL5 protein to investigate the growth and proliferation of a yeast cell when there is not ant treatment. The experimental conditions are set as 3% Krytox surfactant in oil phase and 0.075% w/w Jeffamine in aqueous phase.

Yeast Density in Culture and Surfactant Preparation: There are roughly 0.6×10^6 cells covered on the glass slide (1 μL of sample). In a 5 mL solution, there should be roughly 300×106 cells. In this experiment, 1 to 1 dilution was done.

Flow Rate and Droplet Size: Flow rate of oil and aqueous phase is set as 800 μL/h and 60 μL/h, respectively. The droplets were generated during half an hour and the system was stopped for incubation. The monitoring of the responses of the yeast cells is done under inverted fluorescence microscope.

Single Cell Analysis: After all the chambers were filled with only oil phase, yeast solution was sent to the system. Since the solution was dense with cells, initial droplets were generated unstable and large. They coalesced with each other in the first 3 chambers. As the concentration of the yeast cells entered to the system decreased due to the sedimentation of cells in the syringe, droplets generated became more stable and smaller. 30 minutes of droplet generation was enough to fill all the chambers in the chip. Once the system closed, cells were monitored after 1, 2, 3, 6 and 18 hours of incubation. Cells enlarged their areas or they separated from their daughter cells if they had, during the incubation and they were proliferated after 18 hours. Figure 4.31 shows the growth of the cells in the droplets.

Cell Dimensions: It is seen that all the cells grew up as expected. The shrinkage more than 10% means the separation of the daughter and mother cell. 4 cells separated from mother cell after 3 hours incubation. After 18 hours, since they cannot be monitored individually, area of all the cells were monitored. Thus, this explains the great growth of the cells and data loss of some cells (10b, 15b, 21c-2). Table 4.3 and 4.4 shows the area of the cells and the percent change of the areas relative to 1^{st} hour, respectively. Table 4.4 shows the change in area.

For cells 10b and 14b-1 for the first hours, there seems to be shrinkage, however, this is only the Image processing error or the cells changed their positions between these two hours. Figure 4.32 visualize the growth of the cell areas.

Integrated fluorescence density of cells (RPL5 expression): Integrated fluorescence density is the amount of fluorescence that the protein tagged with GFP emits. The integrated fluorescence density of the RPL5 protein decreases for the first 6 hours of incubation. Fluorescence per area decreases as the area of the cells increase, thus,

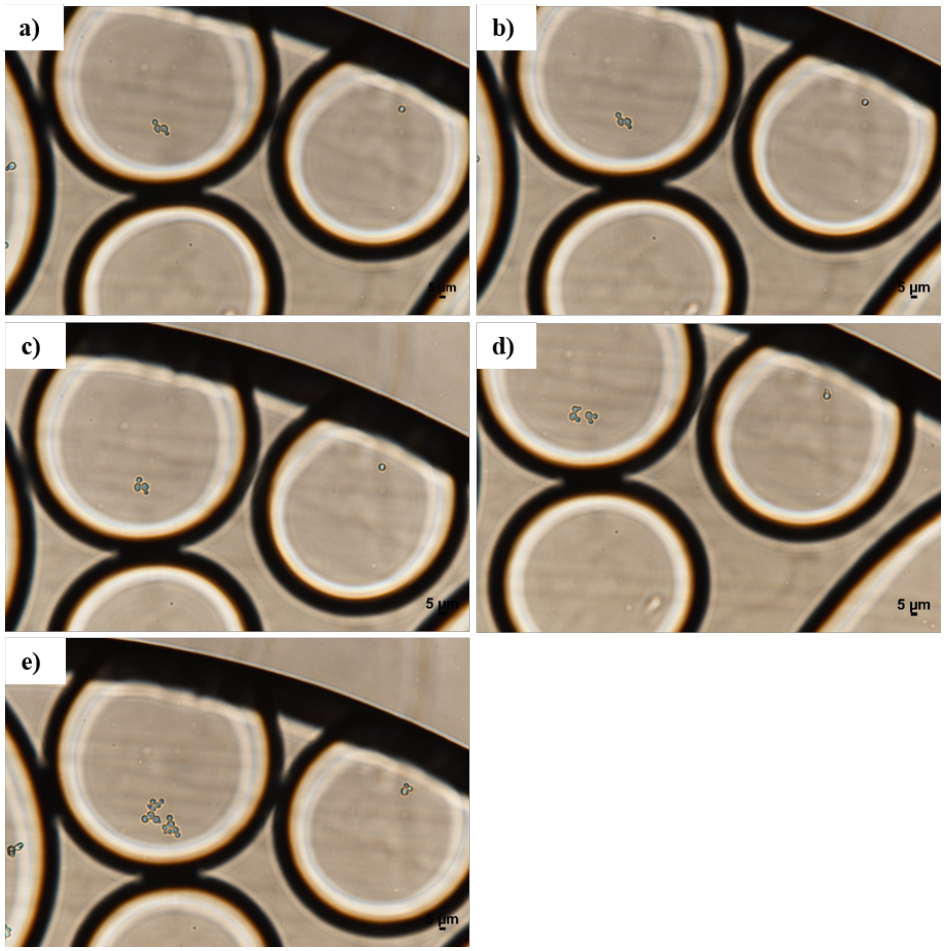

Figure 4.31. a) 1^{st} hour, b) 2^{nd} hour, c) 3^{rd} hour, d) 6^{th} hour, e) 18^{th} hour of incubation for Chamber 15.

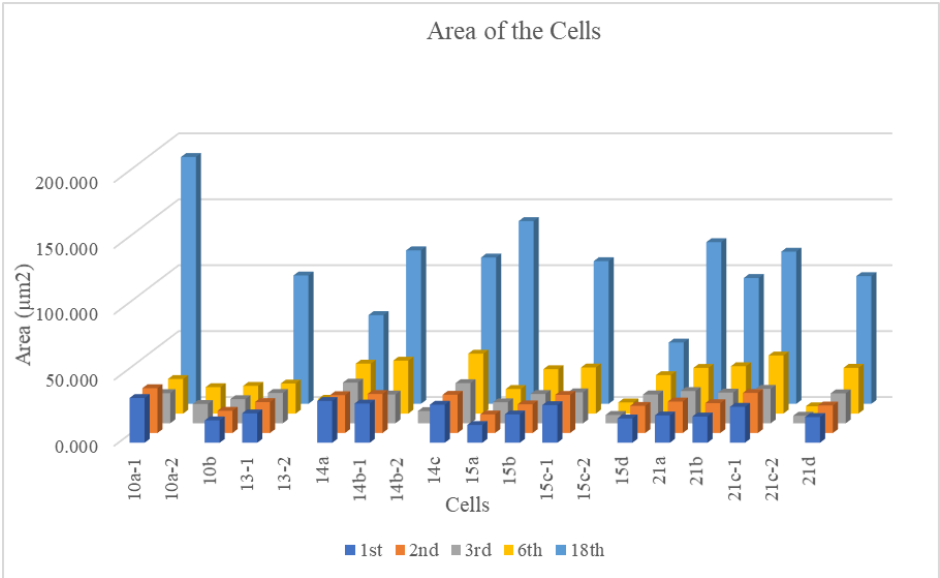

Figure 4.32. Area of the cell vs time.

Table 4.3. Area of the cells for RPL5 tagged strain.

	1st hour (μ**m**^{2})	**2nd hour** (μ**m**^{2})	**3rd hour** (μ**m**^{2})	**6th hour** (μ**m**^{2})	**18th hour** (μ**m**^{2})
10a-1	33.970	34.026	22.883	26.269	187.268
10a-2			14.666	20.070	
10b	16.967	16.895	18.346	21.011	
13-1	22.310	23.496	23.010	22.814	97.412
13-2				11.231	
14a	31.696	28.763	30.890	37.867	67.346
14b-1	29.783	29.655	21.825	40.160	116.468
14b-2			9.271		
14c	28.844	29.052	30.503	45.467	111.029
15a	13.465	14.107	16.008	18.679	138.636
15b	21.516	21.781	22.280	33.648	
15c-1	28.591	28.900	23.486	34.932	108.256
15c-2			6.326	8.487	
15d	18.483	20.595	21.898	29.219	46.491
21a	20.721	23.883	24.520	34.697	122.676
21b	19.891	22.628	F56B00 23.324	35.942	95.486
21c-1	27.256	30.370	26.137	44.125	115.478
21c-2			5.738	5.586	
21d	19.494	20.859	22.746	34.721	96.932

Table 4.4. % change in area relative to 1st hour for RPL5 tagged strain.

	1 to 2	**1 to 3**	**1 to 6**	**1 to 18**
10a-1	0.163379	-32.6378	-22.6705	451.2736
10a-2				
10b	-0.42317	8.125184	23.83568	
13-1	5.314705	3.140324	2.261786	336.6332
13-2				
14a	-9.25296	-2.54355	19.47072	112.4748
14b-1	-0.42878	-26.7201	34.84563	291.0622
14b-2				
14c	0.721816	5.750263	57.6316	284.931
15a	4.766325	18.88558	38.71804	929.5775
15b	1.2312	3.554165	56.39025	
15c-1	1.080752	-17.8569	22.1778	278.6329
15c-2				
15d	11.42389	18.4757	58.08247	151.5322
21a	15.25573	18.32984	67.44477	492.0276
21b	13.76043	17.25847	80.69136	380.0453
21c-1	11.42779	-4.10523	61.8921	323.6881
21c-2				
21d	7.003693	16.68103	78.11327	397.2392

the integrated fluorescence density decreases for the first 6 hours of incubation. After 18 hours, since the cells proliferated and the fluorescence of RPL5 emitted increases, the integrated fluorescence density increases. The fluorescence densities of the cells and the percentage changes are given in Table 4.5 and 4.6 respectively. Figure 4.33 visualizes the change of the fluorescence density for a cell. Table 4.6 shows the change fluorescence density.

Table 4.5. Integrated fluorescence density of cells (raw data) for RPL5 tagged strain.

	1^{st} hour	**2^{nd} hour**	**3^{rd} hour**	**6^{th} hour**	**18^{th} hour**
10a-1	654075	517650	374085	317220	2564535
10a-2			175185	203490	
10b	337365	249390	246585	184875	
13-1	589815	358785	328695	271320	1779135
13-2				133620	
14a	977670	488325	406725	410295	1007250
14b-1	481950	329460	241230	402135	2014245
14b-2			101235		
14c	530145	438090	338130	535500	2014500
15a	362610	177225	234345	244800	1741395
15b	367200	358275	374595	490110	
15c-1	507195	528870	333285	356235	1246695
15c-2			62985	53040	
15d	422280	378165	343740	386835	637755
21a	410805	307275	321300	322320	1302795
21b	436050	341445	278460	334305	1077885
21c-1	745875	411315	341700	401880	1268625
21c-2			97920	83640	
21d	410805	299880	262395	260100	1100835

Table 4.6. Integrated fluorescence density of cells (raw data) for RPL5 tagged strain.

	1 to 2	**1 to 3**	**1 to 6**	**1 to 18**
10a-1	-20.8577	-42.807	-51.501	292.0858
10a-2				
10b	-26.0771	-26.9085	-45.2003	
13-1	-39.1699	-44.2715	-53.9991	201.6429
13-2				
14a	-50.0522	-58.3985	-58.0334	3.025561
14b-1	-31.6402	-49.9471	-16.5608	317.9365
14b-2				
14c	-17.3641	-36.2193	1.010101	279.9904
15a	-51.1252	-35.3727	-32.4895	380.2391
15b	-2.43056	2.013889	33.47222	
15c-1	4.273504	-34.2886	-29.7637	145.8019
15c-2				
15d	-10.4469	-18.599	-8.39372	51.02657
21a	-25.2017	-21.7877	-21.5394	217.1322
21b	-21.6959	-36.1404	-23.3333	147.193
21c-1	-44.8547	-54.188	-46.1197	70.08547
21c-2				
21d	-27.0019	-36.1266	-36.6853	167.9702

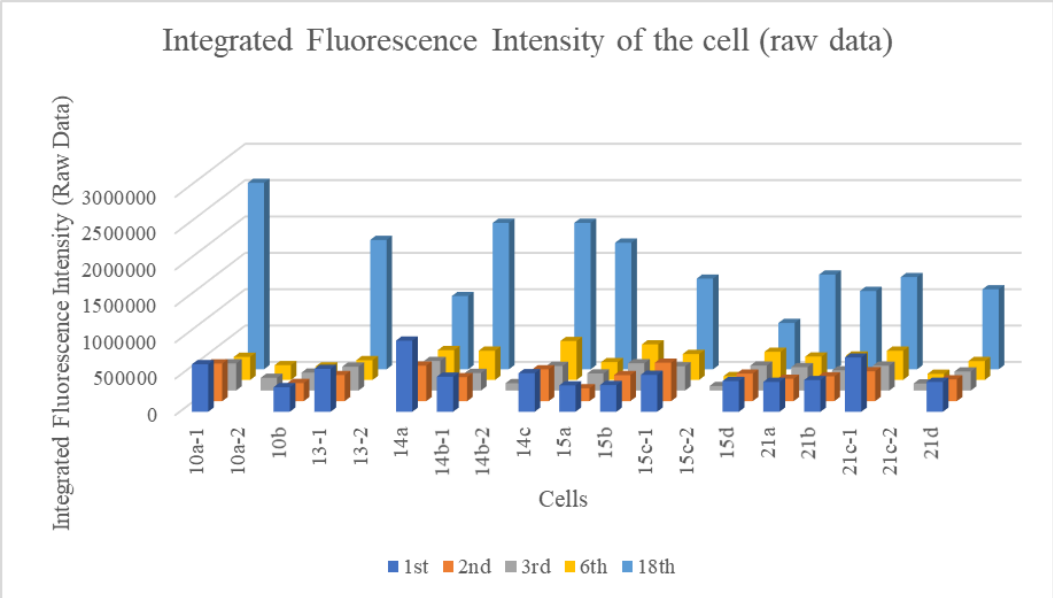

Figure 4.33. The time profile of the integrated fluorescence densities of the cells by using raw data.

4.1.4. Control Experiment with NOP56 Tagged Strain

This experiment is done with RFP tagged NOP56 protein to investigate the growth and proliferation of a yeast cell when there is not ant treatment. The experimental conditions are set as 3% Krytox surfactant in oil phase and 0.075% w/w Jeffamine in aqueous phase.

Yeast Density in Culture: There are roughly 1.99 $\times 10^5$ cells covered on the glass slide (2 μL of sample). In a 5 mL solution, there should be roughly 498×10^6 cells. In this experiment, 1 to 1 dilution was done.

Flow Rate and Droplet Size: Flow rate of oil and aqueous phase is set as 800 μL/h and 60 μL/h, respectively. The droplets were generated during half an hour and the system was stopped for incubation. The monitoring of the responses of the yeast cells is done under inverted fluorescence microscope.

Single Cell Analysis: When the droplets were first generated, the droplets merged in the first 3-4 chambers due to the high concentration of yeast in the syringe. After a while, due to the sedimentation of the cells in the syringe, the concentration of the cell entered to the chip decreased and droplets were generated smaller and more stable. After 30 minutes which means after all the chambers were filled with droplets, of generation, the system was stopped and cells were monitored at their 1^{st}, 2^{nd}, 3^{rd}, 6^{th}, 18^{th} hour of incubation. During 3 hours, cells increased their areas (Figure 4.34a-4.34c) and then they doubled themselves after 6 hours (Figure 4.34d). After 18 hours of incubation, most cells were proliferated, however, since the cells were not on a plane, they cannot be seen individually (Figure 4.34e).

Cell Dimensions: It is seen that cell growth was as expected. First three hours, areas of the cells increased and after 6 hours, some of the cells created bud. After 18 hours, most of the cells were proliferated and the number of cells became countless. Since the boundaries of the cells were not clear, the bulk area was measured for the 18 hour-incubation analysis. Since this is a control experiment, not all the chambers were monitored for cell growth. Table 4.7 and 4.8 shows the area of the cells and the percent change of the areas relative to 1^{st} hour, respectively.

Between the first two hours, it seems decrease of area for several cells (1, 5b, 23a, 23c), however, this shrinkage is smaller than 10%, which means there is a slightly change of areas of these cells. The reason for this shrunk may be the human error when the image is processing. The great downsizing of the cell 5b is stem from separating the daughter cell from the mother cell. The Figure 4.35 visualizes the growth of the cell areas.

Integrated fluorescence density of cells (NOP56 expression): Integrated fluorescence density is the amount of fluorescence that the protein tagged with RFP emits. NOP56 expression seems to decrease in the first 3 hours of incubation, however, since the area of the cell increases, the fluorescence density, which means amount of NOP56 protein per area, decreases and this is the reason why the opposite of the expected results appeared. After 18 hours of incubation, integrated fluorescence density of the

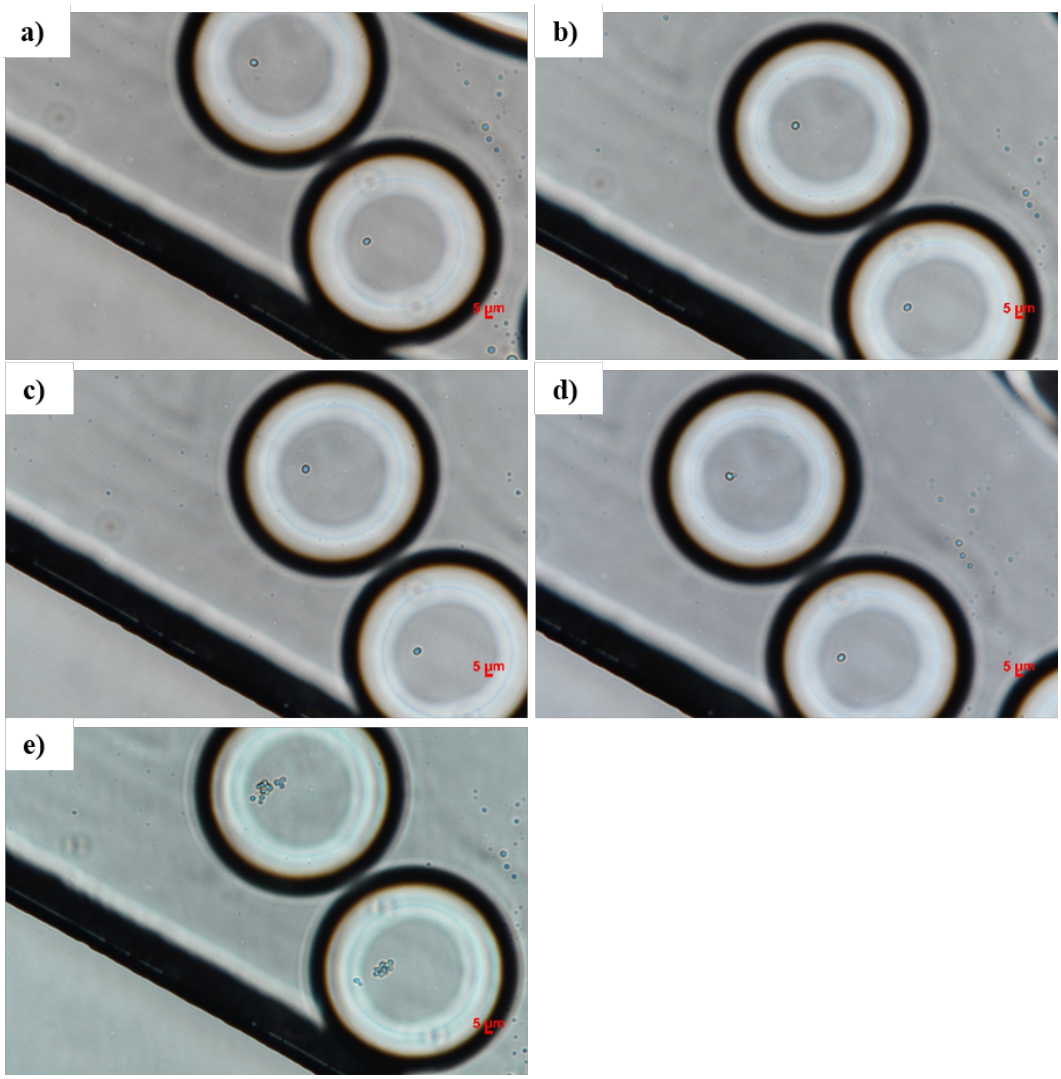

Figure 4.34. a) 1^{st} hour, b) 2^{nd} hour, c) 3^{rd} hour, d) 6^{th} hour, e) 18^{th} hour of incubation for Chamber 3.

Table 4.7. Area of the cells for NOP56 tagged strain.

	1st hour (μ**m**^{2})	**2nd hour** (μ**m**^{2})	**3rd hour** (μ**m**^{2})	**6th hour** (μ**m**^{2})	**18th hour** (μ**m**^{2})
1	15.2684	14.2688	15.7192	19.551	82.3445
3a	22.2852	22.5351	23.912	28.0378	69.6535
					34.8831
					16.2386
					9.7608
3b	18.2427	19.012	20.3595	21.9961	94.6631
					16.4003
5a	16.7776	17.5273	18.6396	19.6294	226.3996
5b	27.9447	25.2056	29.3216	20.0998	
5b-2				8.3692	
11	14.798	14.798	17.0863	15.5281	58.996
23a	16.2876	15.6702	16.7482	18.4387	51.254
23b	10.0646	10.7163	11.6228	11.074	50.8963
23c	22.148	21.8442	22.2705	22.9222	60.3239
23c-2		12.495	12.9409	13.8474	
23d	11.4268	13.6416	12.9752	12.7204	38.5826

Table 4.8. % change in area relative to 1^{st} hour for NOP56 tagged strain.

	1 to 2	**1 to 3**	**1 to 6**	**1 to 18**
1	-6.54685	2.952503	28.04878	439.3132
3a	1.121372	7.299912	25.81354	212.555
	No data for the 1^{st} hour			
3b	4.217029	11.60355	20.57481	418.9095
	No data for the 1^{st} hour			
5a	4.468458	11.09813	16.99766	1249.416
5b	-9.80186	4.927231	-28.0729	
5b-2	No data for the 1^{st} hour			
11	0	15.46358	4.933775	298.6755
23a	-3.79061	2.827918	13.20698	214.6811
23b	6.47517	15.48199	10.02921	405.6962
23c	-1.37168	0.553097	3.495575	172.3673
23c-2	No data for the 1^{st} hour			
23d	19.3825	13.5506	11.32075	237.6501

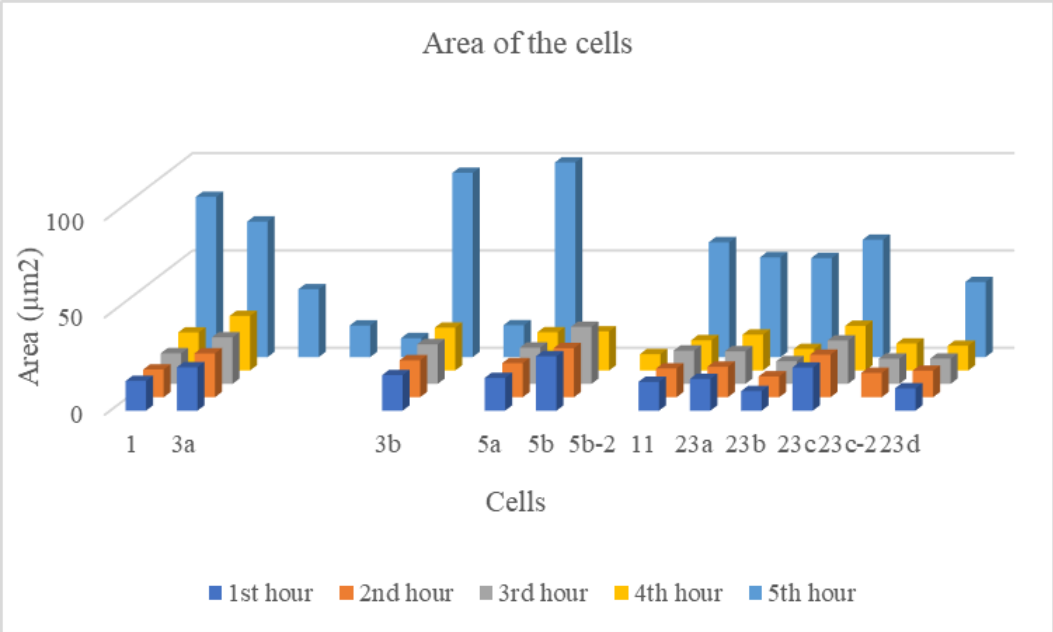

Figure 4.35. Area of the cell vs time.

cells becomes the highest, since it is measured for whole yeast bulk. The fluorescence densities of the cells and the percentage changes are given in Table 4.9 and 4.10 respectively. Figure 4.36 visualizes the change of the fluorescence density for a cell.

4.2. Drug Effect - HU

HU is inhibitor of ribonucleotide reductase (RNR) which synthesize deoxyribonucleotides (dNTP) from ribonucleotides (NTP) [48]. dNTPs are the monomers of DNA and they are used in replication and repair of DNA. RNR regulates the production of dNTPs, and dNTPs are accumulated in pools at G1/S [49]. When a cell faces with HU treatment, RNR cannot produce dNTP, and thus DNA synthesis cannot be completed, and cell cycle is arrested at G1/S phase by Mec1/Rad53 pathway, which regulates late replication origins [37]. So, replication of DNA starts but cannot be completed since the dNTP level is not sufficient for completing all the strand of the DNA.

Table 4.9. Integrated fluorescence density of cells (raw data) for NOP56 tagged strain.

	1st hour	2nd hour	3rd hour	6th hour	18th hour
1	275145	129285	303124	196095	1162800
3a	406215	184110	119340	157590	896070
					323085
					163455
					105825
3b	221850	202215	143565	325890	866745
					91800
5a	214965	109905	214200	118830	
5b	359040	142035	350115	118320	1854360
5b-2				26520	
11	261375	277950	218790	146115	278460
23a	221340	120105	225930	47175	464100
23b	156570	127245	73185	107100	395250
23c	434520	284325	151980	162690	
23c-2		152745	90780	117555	446250
23d	240465	72675	125970	48450	315180

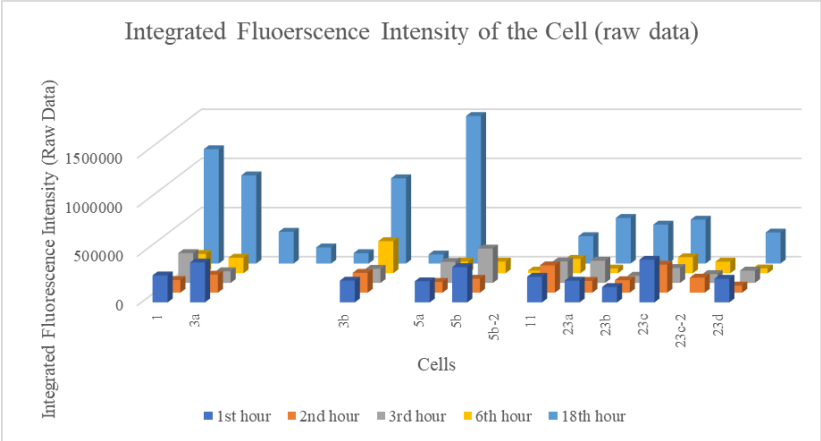

Figure 4.36. The time profile of the integrated fluorescence densities of the cells by using raw data.

Table 4.10. % change in the integrated fluorescence intensity compared to first hour (raw data) for NOP56 tagged strain.

	1 to 2	**1 to 3**	**1 to 6**	**1 to 18**
1	-53.012	10.16882	-28.7303	322.6135
3a	-54.6767	-70.6215	-61.2053	120.5901
	No data for the 1^{st} hour			
3b	-8.85057	-35.2874	46.89655	290.6897
	No data for the 1^{st} hour			
5a	-48.8731	-0.35587	-44.7212	762.6335
5b	-60.4403	-2.4858	-67.0455	
5b-2	No data for the 1^{st} hour			
11	6.341463	-16.2927	-44.0976	6.536585
23a	-45.7373	2.073733	-78.6866	109.6774
23b	-18.7296	-53.2573	-31.5961	152.443
23c	-34.5657	-65.0235	-62.5587	2.699531
23c-2	No data for the 1^{st} hour			
23d	-69.7773	-47.614	-79.8515	31.07105

4.2.1. 200 mM HU (2%Krytox, 1:1 dilution, diploid type, RPL5:GFP)

4.2.1.1. Yeast Density in Culture. For this experiment, the BY4743 diploid yeast strain with RPL5:GFP is used. There are roughly 2.19×10^5 cells covered on the glass slide (2 μL of sample). In a 5 mL solution, there should be roughly 547×10^6 cells.

In this experiment, 1 to 1 dilution was done. Without dilution of the yeast culture in inoculum, aqueous flow became unstable and the droplets tended to coalesce because of the surface tension of the yeast wall. Thus, 1 to 1 dilution is considered to be sufficient to maintain the flow stability.

4.2.1.2. Flow Rate and Droplet Size. Flow rate is set to 800 μL/h for oil phase and 60 μL/h for yeast aqueous phase. With these flow rates, droplet size becomes the smallest size (120 - 200 μm diameter). After about 15 minutes, drug solution is loaded to the chip. Also, HU solution flow rate is set to 60 μL/h, same as the yeast phase. In a short while, to sustain the steady state flow in the chip, both the yeast flow and the drug phase flow rate are increased to 70 μL /h. Drug treatment is applied for almost 20 minutes, because the generated droplets pass all the chambers roughly in 20 minutes. The flow into the microfluidic device is stopped for the incubation of the yeast cells.

As the drug phase entered into the chip, the molarity of the drug solution is halved due to its mixing with the aqueous yeast solution. Thus, the real molarity of the drug that affects the cells become 100 mM.

4.2.1.3. Single Cell Analysis. Roughly, 1 mL of 1 to 1 diluted cell culture was sent to the chip. Since the cells create adhesion to the walls, and that in turn creates deterioration of the steady state, the droplets were generated in different sizes. Only a few droplets were generated in small sizes, otherwise, the droplets coalesced while they were generated. In the first nine chambers, there are several droplets that contain 1 to 10 cells in them; but, after 24 hours of incubation, these droplets were merged together (Figure 4.37), and the response of the cells could not be observed (Figure 4.38).

From Chamber 12 onwards, the coalescence of droplets was less, and several droplets stayed stable (Figure 4.39). As it can be seen in the droplets (Figures 4.40 and 4.41), 100 mM HU treatment did not arrest cell growth and after 24 hours, the number of cells increased while the fluorescence of the cells decreased. On the other hand, in some of the droplets in Chamber 18, growth was slower, which means 100 mM HU treatment affected the cells and decreased the cell growth (Figure 4.42). In the last (24^{th}) chamber, the droplets were large and far away from each other (Figure 4.43). There are two little droplets pinched under the traps. The fluorescence of these droplets decreased after 24 hours of incubation (Figures 4.44 and 4.45), which means HU treatment decreased the RPL5 expression. In brief, some of the cells were affected by HU, some are not affected at all. Fluctuating results in terms of cell growth were observed under HU application. It is decided that this amount of HU is not sufficient and should be increased (by 2-fold) in the next experiment.

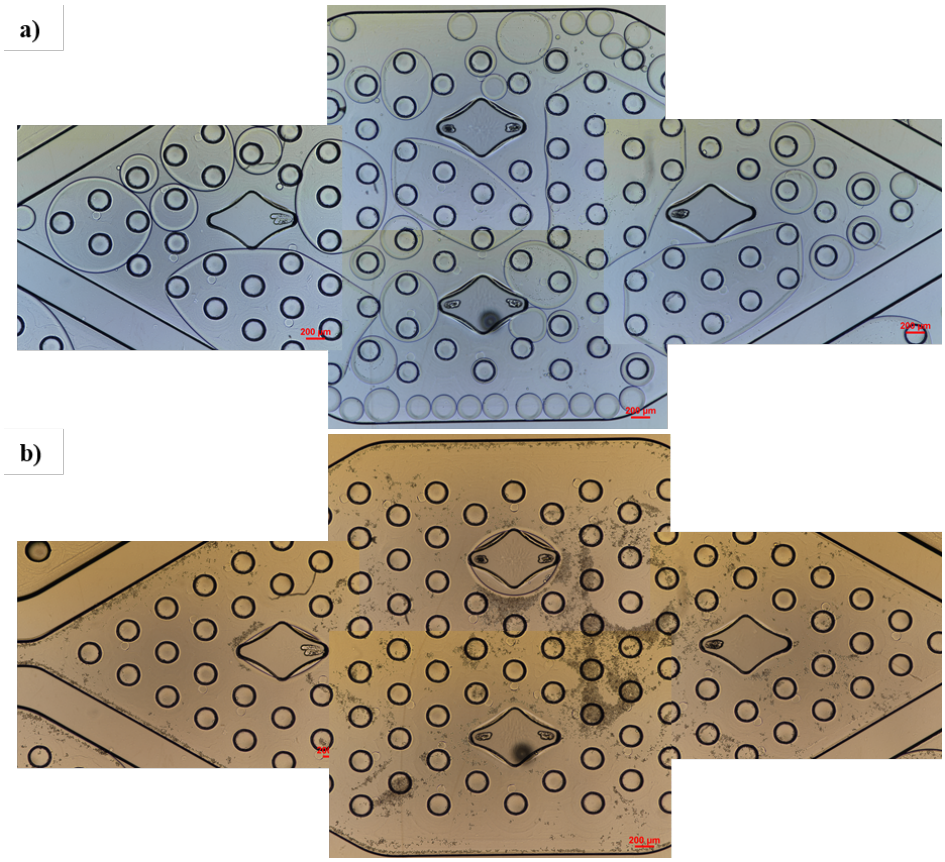

Figure 4.37. Chamber 5 a) After 2 hours, b) After 24 hours.

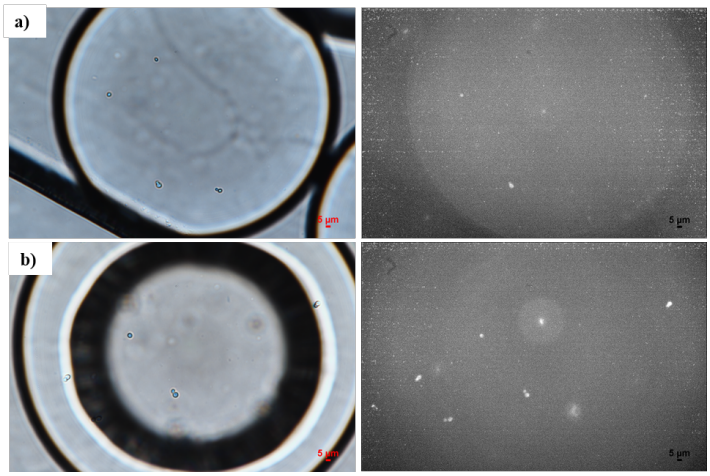

Figure 4.38. a) Cells in a droplet in Chamber 8 (2 hrs.), b) cells in a droplet in Chamber 9 (24 hrs.).

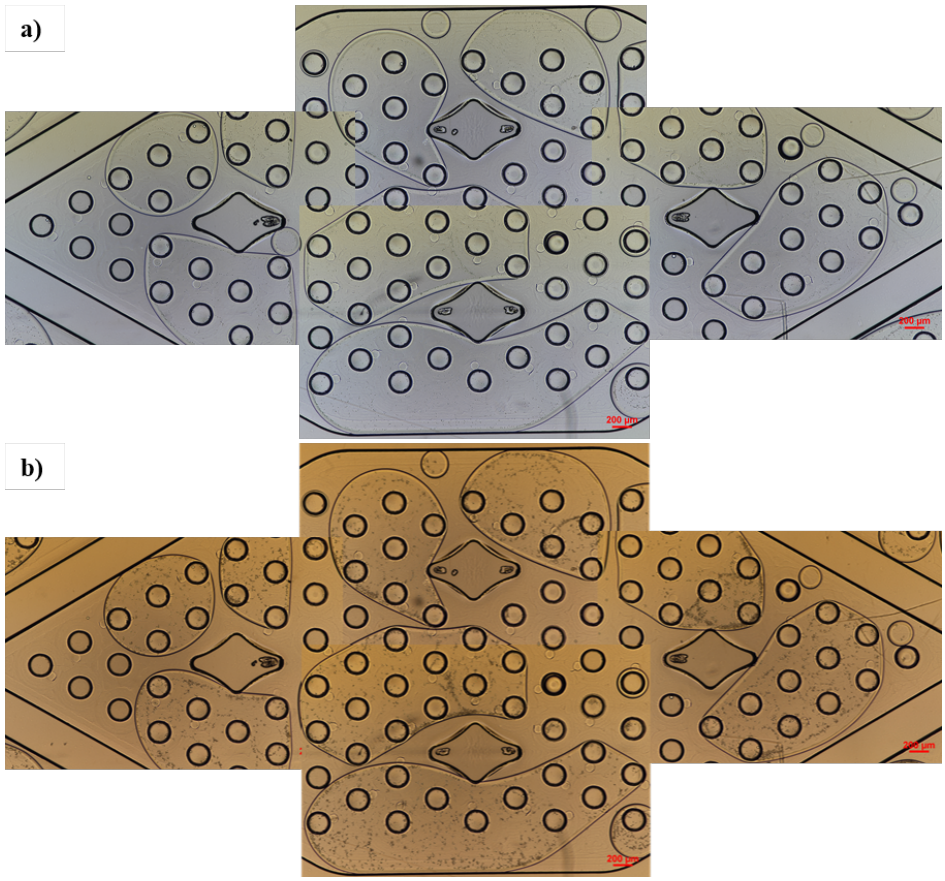

Figure 4.39. Chamber 12 a) After 2 hours, b) After 24 hours.

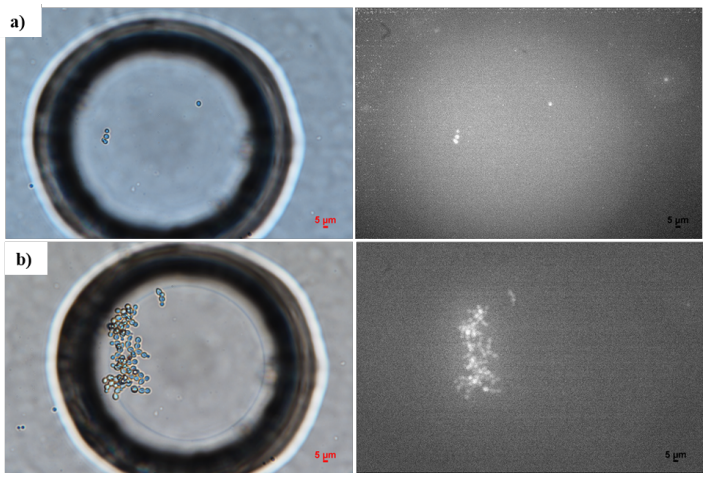

Figure 4.40. a) Cells in a droplet in Chamber 12 (2 hrs.), b) cells in a droplet in Chamber 12 (24 hrs.).

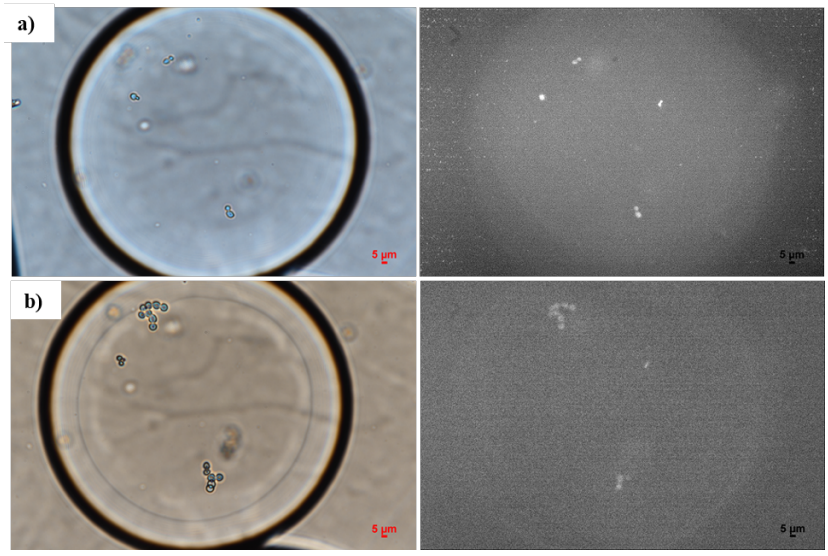

Figure 4.41. a) Cells in a droplet in Chamber 12 (2 hrs.), b) cells in a droplet in Chamber 12 (24 hrs.).

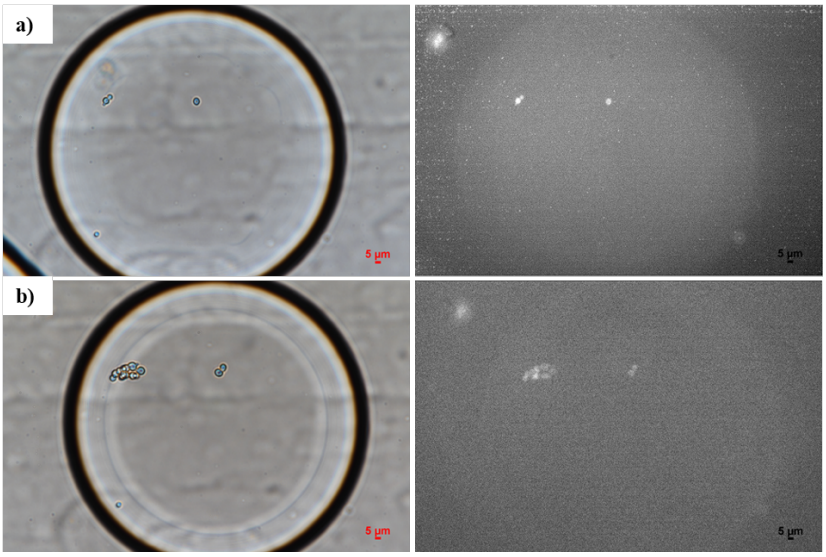

Figure 4.42. a) Cells in a droplet in Chamber 18 (2 hrs.), b) cells in a droplet in Chamber 18 (24 hrs.).

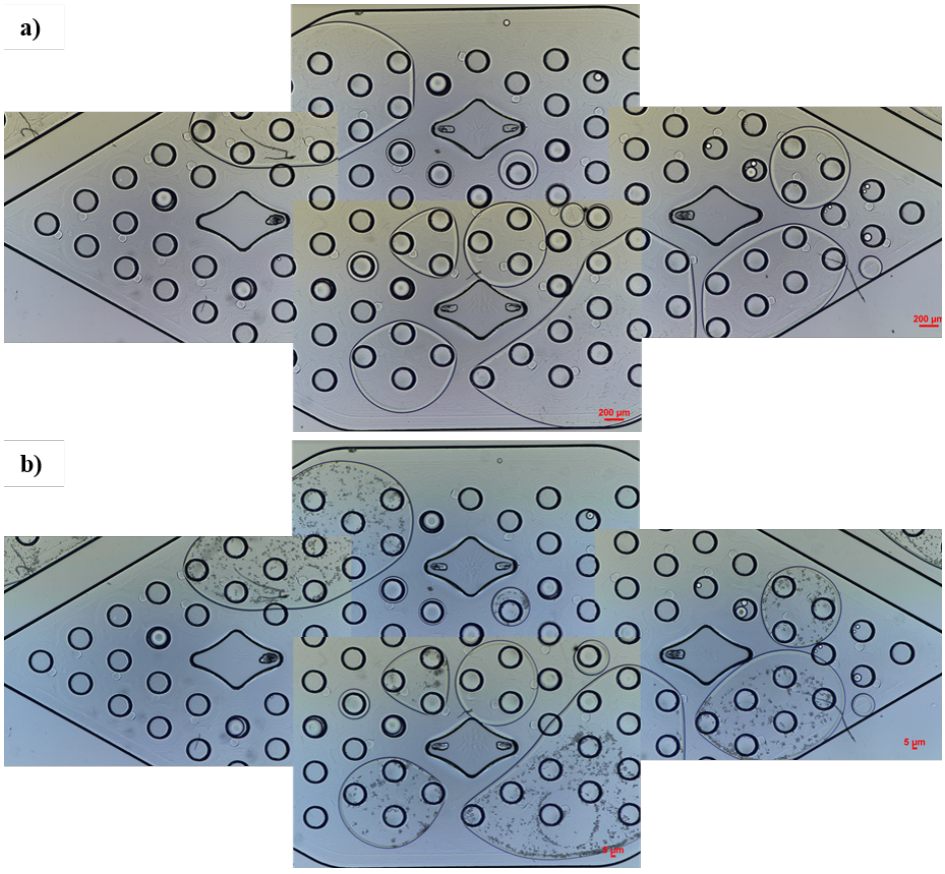

Figure 4.43. Chamber 24 a) After 2 hours, b) After 24 hours.

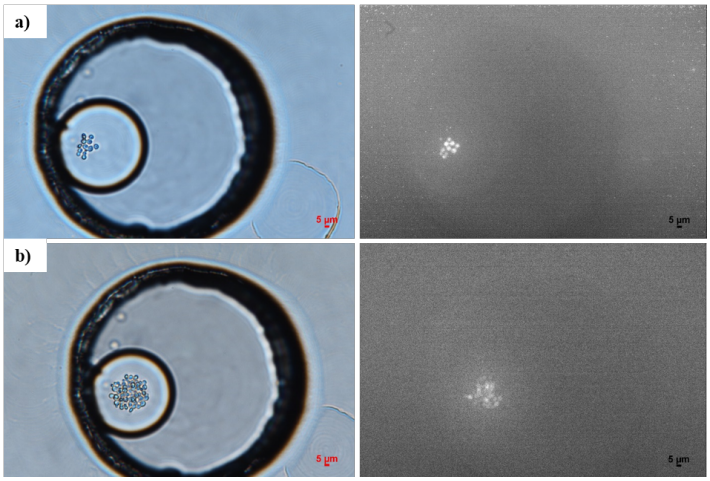

Figure 4.44. a) Cells in a droplet in Chamber 24 (2 hrs.), b) cells in a droplet in Chamber 24 (24 hrs.).

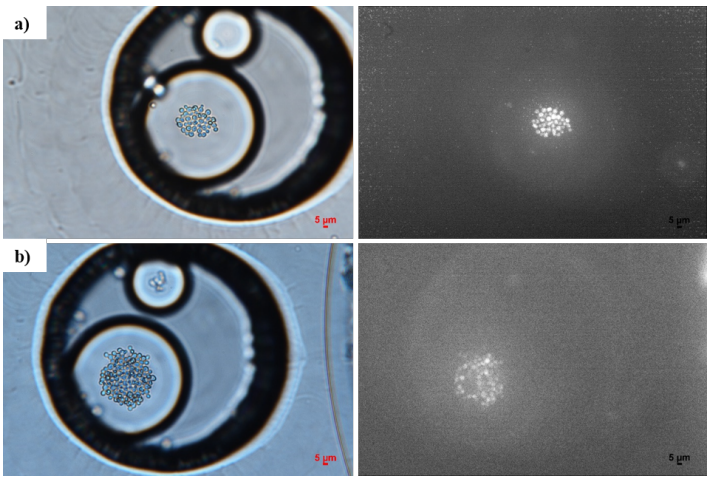

Figure 4.45. a) Cells in a droplet in Chamber 24 (2 hrs.), b) cells in a droplet in Chamber 24 (24 hrs.).

4.2.2. 400 mM HU (3%Krytox, 1:1 dilution, diploid type, RPL5:GFP, Jeffamine)

In this experiment, the drug HU concentration was increased by two-fold in order to enhance its effect on yeast cells and the surfactant concentration was also increased to 3 % to stabilize the droplets and to prevent the coalescence of the formed droplets.

The experiment is done using BY4743 diploid yeast strain with GFP tagged RPL5 protein to investigate the effect of hydroxyurea, by following the fluorescence and hence protein expression in BY4743 yeast strain. The experimental conditions are 3% Krytox surfactant in oil phase and 0.075% w/w Jeffamine in aqueous phase.

4.2.2.1. Yeast Density in Culture. There are roughly 1.12×10^5 cells covered on the glass slide (1 μL of sample). In a 5 mL solution, there should be roughly $562\times^6$ cells. In this experiment, 1 to 1 dilution was done.

4.2.2.2. Flow Rate and Droplet Size. Flow rate is set to 800 μL/h for oil phase and 60 μL/h for yeast aqueous phase at the beginning of the experiment. Droplet diameters vary between 100-200 μm with these flow rates. The flowrate of drug solution (400 mM HU) is set to 100 μL/h. The molarity of the drug is assumed to be halved when it is sent to the chip. 20 minutes of HU treatment is applied to the cells, as the generated droplets pass all of the chambers in roughly 20 minutes. Then the device is stopped for the incubation. The monitoring of the responses of the yeast cells is done under inverted fluorescence microscope.

4.2.2.3. Single Cell Analysis. Some of the droplets merged together while most of them protected their stability and remained as its small size. After 3 and 24 hours of drug treatment, the pictures of 3 cells were taken. It is seen that the proliferation of the cells was slower than expected (Figure 4.46-4.49). The areas of the cells after 3 hours and 24 hours treatment are shown in the Table 4.11. While the cell in the chamber 18 enlarged its area, the cell in the chamber 21 shrunk, although it created

a bud. After 5 hours of incubation, the pictures of two different cells in two separate droplets were taken every 5 minutes for 2.5 hours to monitor the cell cycle of the cells under the drug treatment.

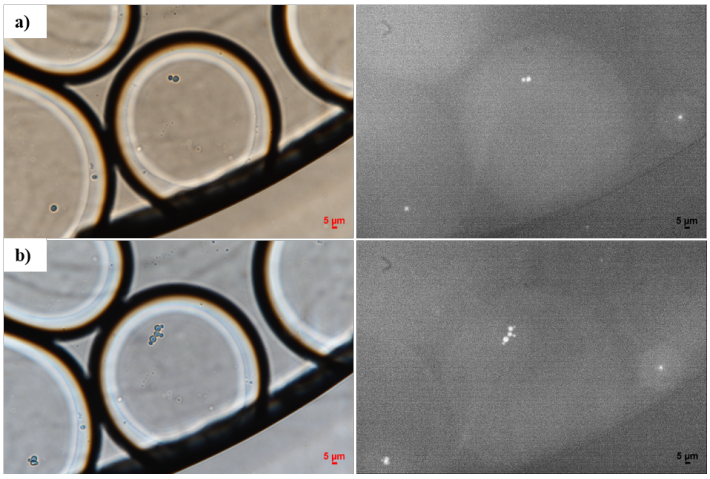

Figure 4.46. a) Cells in a droplet in Chamber 13 (3 hrs), b) cells in a droplet in Chamber 13 (24 hrs.).

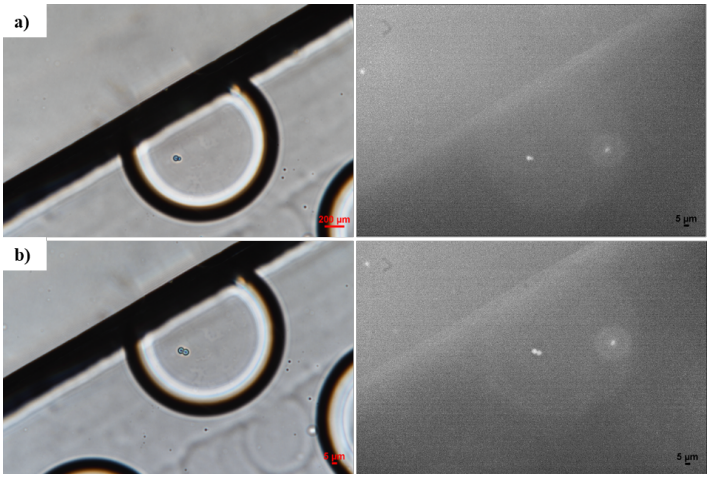

Figure 4.47. a) Cells in a droplet in Chamber 18 (3 hrs), b) cells in a droplet in Chamber 18 (24 hrs.).

The monitoring of cell cycle at every 30 minutes is shown in Figure 4.50. Cells do not proliferate for 2.5 hours however; they are alive as can be seen from the slightly color changes in the nucleus and the slight change in movement. 200 mM HU in a

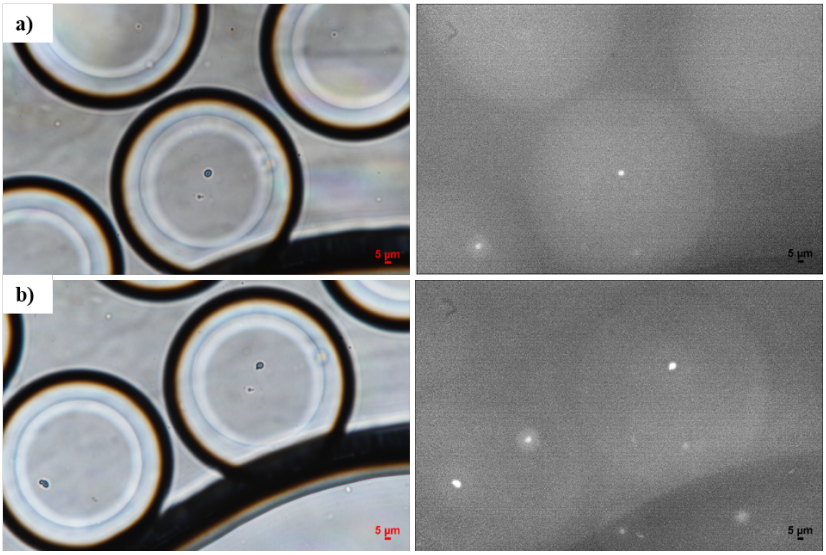

Figure 4.48. a) Cells in a droplet in Chamber 21 (3 hrs), b) cells in a droplet in Chamber 21 (24 hrs.).

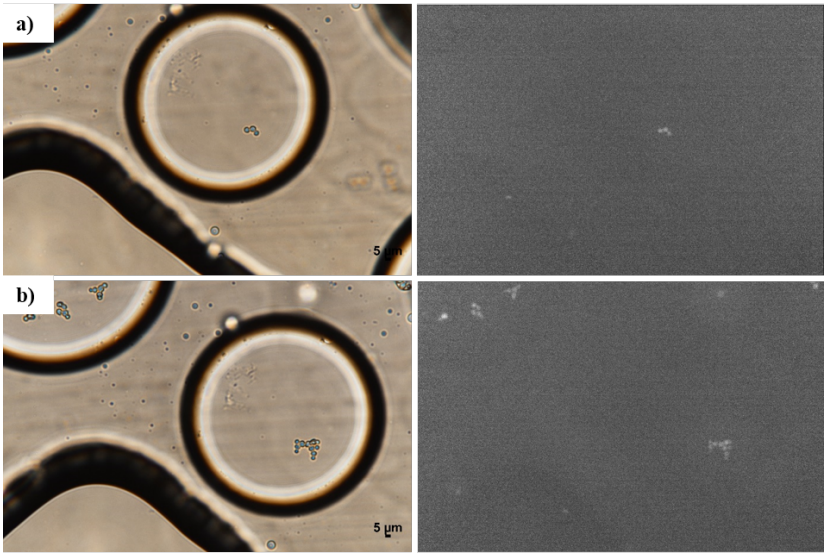

Figure 4.49. a) Non-treated cell at 3rd hour of incubation, b) Non-treated cell at 18th hour of incubation.

droplet is enough to prevent proliferating of the cells. Table 4.12 shows the areas of the cells during the time lapse.

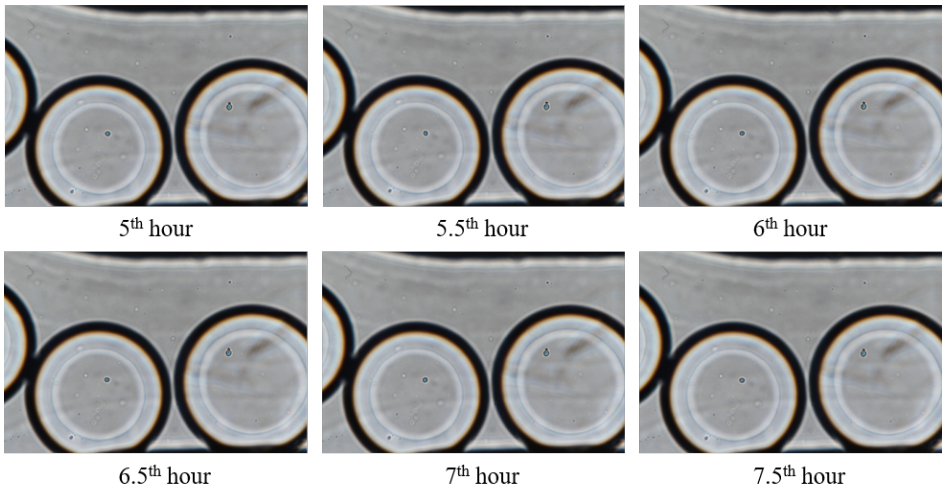

Figure 4.50. Cell cycle for 2.5 hours under HU treatment.

Table 4.11. % change in the integrated fluorescence intensity compared to first hour (raw data) for NOP56 tagged strain.

	Area after 3 h (μm^2)	**Area after 24 h (μm^2)**
Cell in Chamber 18	35.45	65.84
Cell in Chamber 21	33.95	30.73
Cells in Chamber 13	Number of cells are tripled after 24 hours of treatment.	

4.2.3. 400 mM HU (3%Krytox, 1:1 dilution, haploid type, NOP56:RFP, Jeffamine)

In this experiment, the drug HU concentration and the surfactant concentration were kept same as the previous experiment, but the yeast strain was changed from diploid to haploid type. The RFP tagged NOP56 protein was used to follow the fluorescence and hence the protein expression in haploid EY0987 yeast strain.

Table 4.12. Areas of cells during time lapse imaging.

	Cell 1 (μm^2)	**Cell 2 (μm^2)**
5th hour	16.80	28.09
5.5th hour	16.93	27.25
6th hour	16.62	26.63
6.5th hour	18.08	27.34
7th hour	17.59	27.82
7.5th hour	18.78	29.19

4.2.3.1. Yeast Density in Culture. There are roughly 1.4 $\times 10^5$ cells covered on the glass slide (2 μL of sample). In a 5 mL solution, there should be roughly 352$\times^6$ cells.

4.2.3.2. Flow Rate and Droplet Size. Flow rate is set to 800 μL/h for oil phase and 60 μL/h for yeast aqueous phase at the beginning of the experiment. The flowrate of drug solution (400 mM HU) is set to 100 μL/h. When the drug phase is entered into the chip (Figure 4.51), the molarity of the drug is assumed to be halved as the yeast cells are also entering into the system in the aqueous medium. Thus, the real molarity of the drug that affects the cells becomes 200 mM. Droplet diameters vary between 100-200 μm. In the first three chambers, there are coalescence between the droplets due to the instability of the generated droplets caused by a large amount of yeast cells.

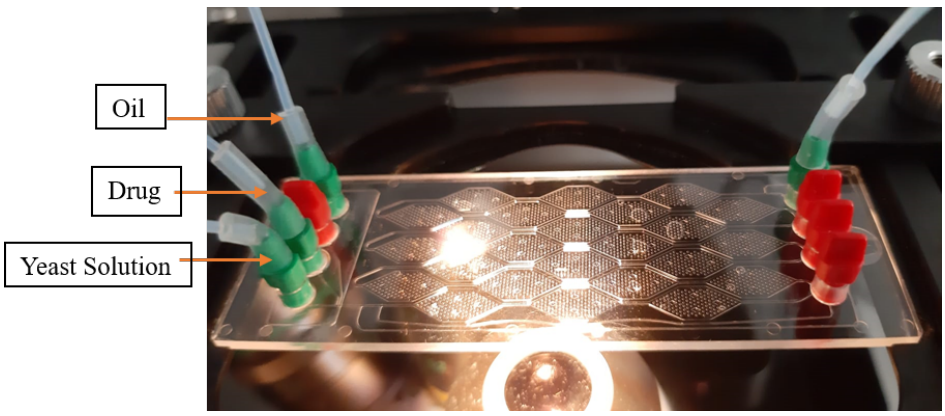

Figure 4.51. System with the drug phase.

4.2.3.3. Single Cell Analysis. Since it was a continuous system and it required time for the culture medium to fill all the chambers, the size of the cells before the HU treatment could not be observed. Thus, when the analysis began, the cells were already facing the HU treatment. Cells were pictured in their 1^{st}, 3^{rd}, 6^{th} and 18^{th} hours of treatment.

32 different cells, some of which were found to be in the same droplet, were examined throughout the experiment. The results are tabulated in Tables B.1-B.7 and Tables 4.13-4.14 and also given in Figures 4.52-4.55.

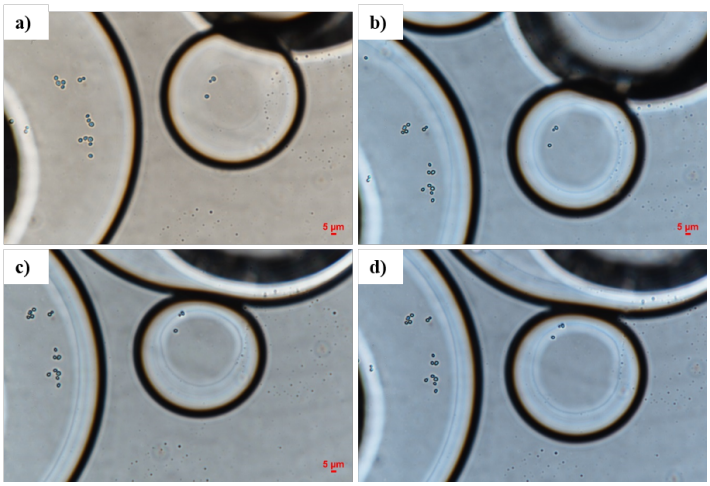

Figure 4.52. Droplets in Chamber 2, a) 1^{st} hour, b)3^{rd} hour c)6^{th} hour , d) 18^{th} hour

In chamber 2, in the small droplet (121 μm diameter) there are only two cells: one with bud and the other without bud, these cells are named as 2a-1 and 2a-2, respectively (Figure 4.52). There is an obvious shrinkage in dimensions of both cells. The bud of the cell did not separate from its mother and there was no growth in any cell including the cells in the larger droplets.

Figure 4.53 shows the change of the morphology of the cells and the growth in chamber 19. In a 130 μm diameter droplet (small one) in chamber 19 (where the cell with a bud is named as 19a), there are only two cells. There are many cells in the larger droplet (160 μm diameter). The cell 19a seems to shrink and there is no bud separation from the mother cell during the 18 hours of HU treatment. On the other hand, the cells in the larger droplet enlarge their areas (so volumes) until the 6th hour

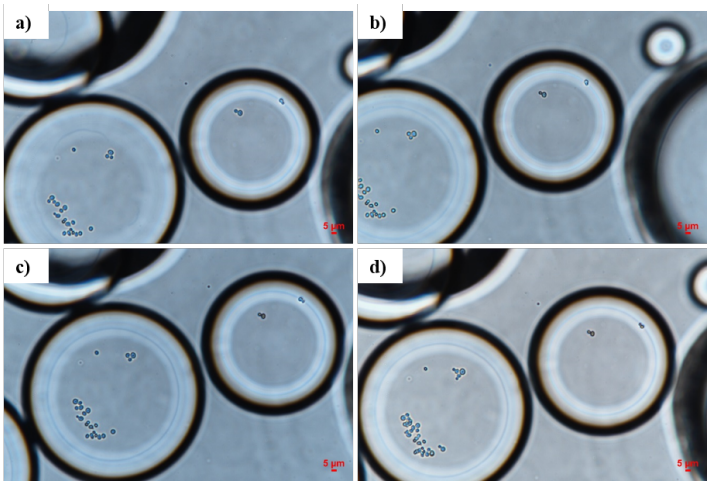

Figure 4.53. Droplets in Chamber 19, a) 1^{st} hour, b)3^{rd} hour c)6^{th} hour , d) 18^{th} hour

of treatment and after that, they grow up (double their number) until the 18th hour of HU treatment. Normally, when there is no drug application on cells, they proliferate at a higher rate than those in the large droplet. Although it cannot be definitely said there is exactly 400mM HU in the large droplet, but there is some drug, and that slows down the growth.

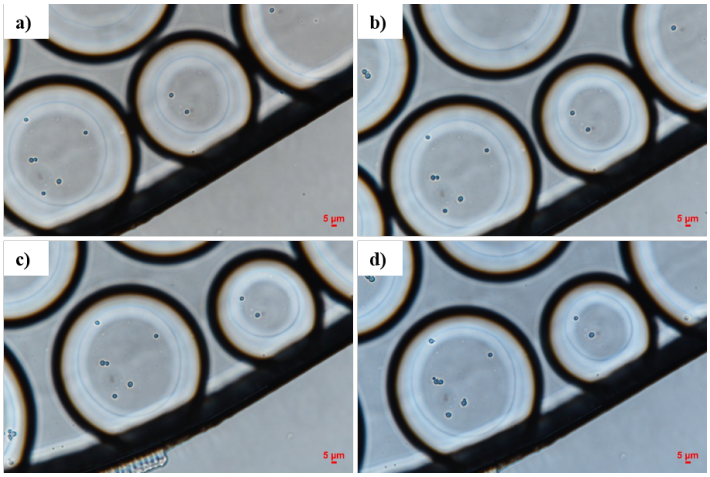

Figure 4.54. Droplets in Chamber 22, a) 1^{st} hour, b)3^{rd} hour c)6^{th} hour , d) 18^{th} hour

In chamber 22, two droplets are monitored, which have diameters 134 μm and 100 μm, and they contain 5 cells and 2 cells, respectively. All cells except one, which is named as 22a-1 in the smaller droplet and shrink, are increased their areas until the 6th hour of the treatment, and after that, they create buds as observed at the 18th

hour of the treatment. Figure 4.54 shows the change of the morphology of the cells and the growth pattern in chamber 22.

4.2.3.4. Cell Dimensions. The results obtained by image processing using ImageJ program shows that, 8 of 32 cells (25%) always shrink compared to first hour of treatment (1a, 2a-1, 2a-2, 9a, 12a-1,12a-2, 19a, 22a-1). Also, 4 of 32 cells (12.5%) always largen their areas (11a, 16a, 21a, 22a-2). 6 of 32 cells (18.75%) enlarge their areas until the 6th hour of treatment (4a-1, 13a, 14a, 15a-1, 15a-3, 17a), and then they shrink at the 18^{th} hour of treatment, compared to first hour of HU treatment. The dimensions of the remaining 14 cells enlarge or shrink at different times of HU treatment (Table 4.13 and B.1-B.2, and Figure 4.55). In fact, the information for some of the cells could not be obtained properly, i.e. these cells either could not be found in the chamber while picturing again, or they change their location in the droplet, so they become invisible due to the depth under microscope.

Since the changes in the areas of the cells can be confusing between the hours, the comparisons with the former measurement are also mentioned below. After two hours of treatment, 5 cells largen their area more than 10% and 2 cells shrink more than 10%. After three hours of treatment (compared to 2^{nd} hour), 12 cells have larger areas (more than 10%) while 3 cells have smaller area (more than 10% of area shrink) and 6 cells have no information since they could not be monitored continuously during the analysis. After 6 hours of treatment (compared to 3^{rd} hour), the area of 4 cells decrease more than 10% and the area of 6 cells increase more than 10%. The change of area of 7 cells could not be observed. When the area of the cells after 18 hours of treatment is compared with the sixth hour of treatment, it is seen that, only 7 of the 32 cells have larger area, and the area of the 18 cells decreased dramatically (Table B.2). 4 of these 18 cells enlarge their areas until 6^{th} hour of treatment. Remaining 14 cells showed different response during the HU treatment.

4.2.3.5. Integrated fluorescence density of cells (NOP56 expression). Integrated fluorescence density is the amount of the fluorescence that the protein tagged with RFP

Table 4.13. % change in the area relative to 1^{st} hour for NOP56 tagged strain.

	1 to 2	**1 to 3**	**1 to 6**	**1 to 18**
1a	-21.31	-13.35	-18.61	-28.41
2a-1		-2.68	-9.08	-18.45
2a-2		-24.35	-4.19	-24.61
3a	-10.22	1.98	-7.72	-13.56
4a-1	0.60	21.28	22.25	-2.66
4a-2	-9.15		15.46	-18.61
4a-3	-5.51		57.48	16.93
5a	0.00	23.81	-13.28	0.00
6a	-5.67		28.36	-4.20
7a	-11.01		19.15	0.56
8a	2.46		37.43	3.01
9a	0.73	-26.55	-13.09	-2.36
10a	-1.69	26.38	15.90	-0.23
11a	-2.79	34.88	25.00	5.12
12a-1	-2.90	-16.75	-17.23	-3.38
12a-2	-12.11	-28.63	-23.79	-8.81
13a	3.46	13.21	18.19	-0.61
14a	5.66	11.89	24.91	0.00
15a-1	-3.11	15.33	16.40	-6.00
15a-2	-4.81			-11.54
15a-3	9.50	9.25	27.50	-4.50
15a-4	-20.00	4.67	-14.67	19.67
16a	19.68	13.89	27.55	5.56
17a	8.41	22.55	19.53	-4.96
18a	-1.53	15.28		-16.38
19a	-5.77	-7.51	-11.75	-2.94
20a	3.87	9.28	3.87	-6.08
21a	15.76	7.07	9.93	3.53
22a-1	2.27	-0.91	-23.81	-7.94
22a-2	5.11	7.80	27.69	47.85
23a	-7.12	7.69	2.64	-17.34
24a	-0.62	17.72	-4.31	-2.77

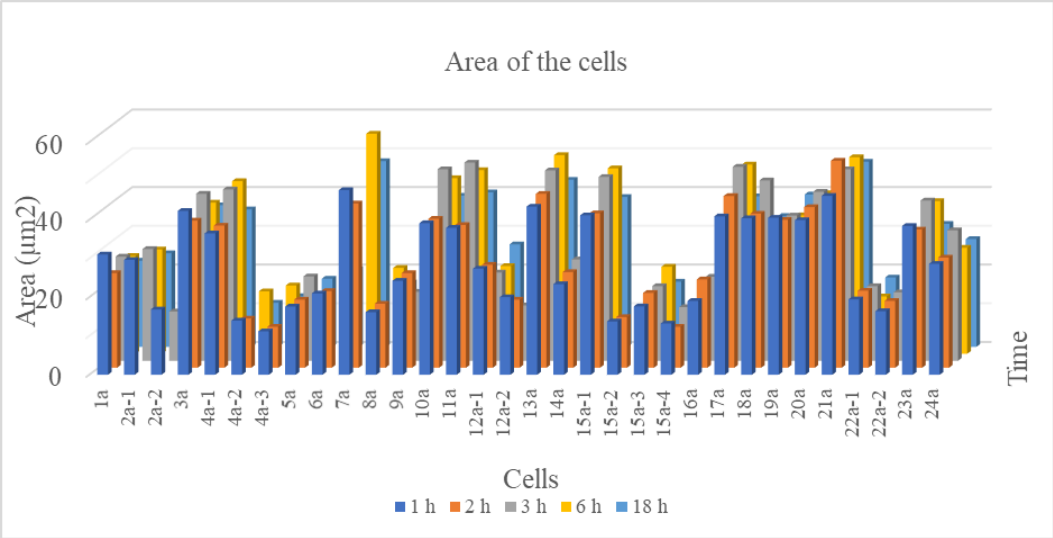

Figure 4.55. Area of the cell (Nop56:RFP) vs time.

emits. Compared to the integrated fluorescence density of the first hour raw data, the fluorescence of the cells usually changes (Figure 4.56). 7 of the 32 cells have slightly lower density after 2 hours of treatment compared to first hour of HU treatment while 5 of them have slightly higher fluorescence density. That can be considered as no change in fluorescence density in two hours of treatment. On the other hand, 13 cells have much lower integrated density and 6 cells have much more density compared to first hour of treatment. At the 6^{th} hour of the treatment, 14 cells have higher density value and 7 cells have lower density value compared to first hour treatment. 7 of 32 cells have much lower fluorescence density after 18 hours compared to 1 hour, while 9 of them have much higher fluorescence density. The changes in percentages (Table 4.14) are too high to give any efficient information.

None of the cells tends to continuously increase or decrease fluorescence density. However, 13 cells have a great decrease in fluorescence density after 18 hours of treatment compared to 6^{th} hour of treatment. This particular result is in agreement with the change (increase) in the area after 6 hours of treatment (Table B.3-B.4).

Integrated fluorescence density results are also investigated on log2 base to get rid of noises, i.e. small changes of fluorescence density. According to these results, the

Table 4.14. % change in the integrated fluorescence intensity compared to first hour (raw data) (Nop56:RFP).

	1 to 2	**1 to 3**	**1 to 6**	**1 to 18**
1a	621.4286	671.4286	567.8571	542.8571
2a-1	-100	-66.7797	5.762712	-45.7627
2a-2	-100	-83.5821	8.955224	-44.0299
3a	-74.8837	-84.6512	20.46512	-15.814
4a-1	-39.3162	-29.4872	-2.13675	-1.7094
4a-2	-81.0976		-6.09756	-17.0732
4a-3	25.97403		-98.7013	1.298701
5a	-65.1852	-68.8889	-51.8519	8.148148
6a	-6.03015		2.512563	-4.0201
7a	-72.3032		27.69679	-53.0612
8a	-5.40541		94.59459	83.78378
9a	1.930502	-71.0425	-38.2239	0.3861
10a	-21.2121	8.080808	88.88889	57.57576
11a	-44.5283	-8.30189	34.33962	6.792453
12a-1	0	257.5758	518.1818	203.0303
12a-2	-3.0303	10.60606	65.15152	-6.06061
13a	1.363636	21.81818	37.72727	-0.90909
14a	4.504505	-86.036	-47.7477	6.756757
15a-1	-1.97183	-64.7887	-18.8732	-3.38028
15a-2	77.27273			19.69697
15a-3	181.1321	-81.1321	175.4717	52.83019
15a-4	265.2174	195.6522	104.3478	182.6087
16a	32.53012	125.3012	1.204819	15.66265
17a	-11.6618	-2.62391	-4.37318	-4.66472
18a	-79.9517	-94.686		-16.4251
19a	-48	-16.3077	-8	-1.53846
20a	-3.69004	73.43173	-44.6494	-4.05904
21a	-81.8182	-3.55731	18.97233	12.64822
22a-1	-0.9009	-39.6396	51.35135	-7.20721
22a-2	8.080808	-32.3232	154.5455	-2.0202
23a	-9.13349	-73.0679	-79.8595	-68.8525
24a	4.471545	-19.5122	7.317073	4.065041

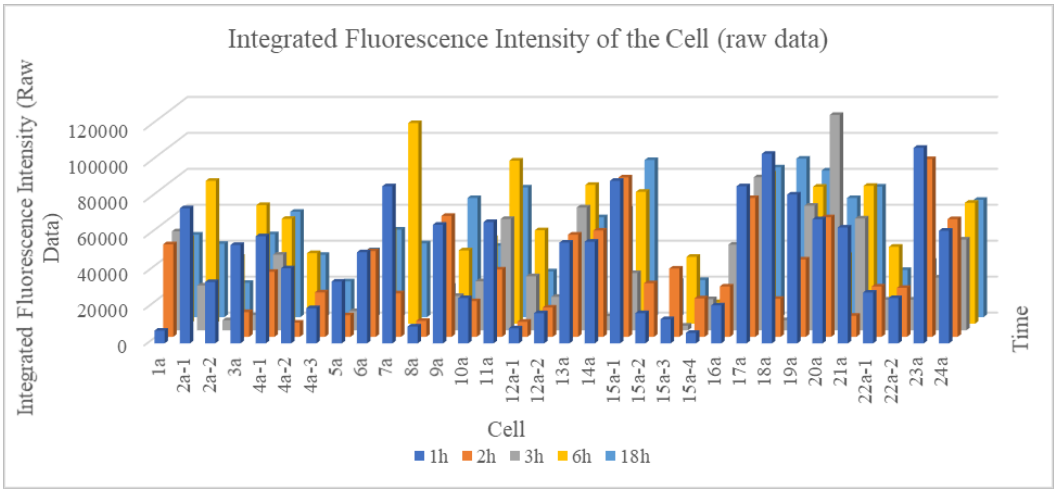

Figure 4.56. The time profile of the integrated fluorescence densities of the cells by using raw data (Nop56:RFP).

changes of fluorescence density of the cells are not as dramatic as the raw data results (Appendix Table B.5-B.6, Figure B.1). After 2 hours of treatment (compared to first hour), fluorescence density of 3 cells increase while the fluorescence density of 6 cells decreases. After 6 hours of treatment, 3 cells increase the fluorescence intensity while 2 cells decrease compared to the first hour of treatment. After 18 hours of HU treatment, fluorescence density of 3 cells increased while only that of 1 cell decreased compared to first hour treatment. According to the log2 base data (Table B.7), integrated density of the 19 cells decreases after 6 hours of treatment until 18^{th} hour.

In Table 4.15, the number of the cells is given according to the change in cell dimension and fluorescence intensity during the HU treatment. The changes in the number of the cells are compared with the measurement of previous time, rather than comparing with the first hour of the HU treatment to indicate the change between the time intervals, especially the great changes between the 3^{rd} to 6^{th} hour and 6^{th} to 18^{th} hour of the treatment. The number of cells increasing in area and fluorescence are in agreement. Nevertheless, there are some fluctuations in data.

The reason of the inconsistency between the changes of the cells may be the unequal amount of drug entered into the droplets. The cells can fight with the low

Table 4.15. Number of cells changing between the time intervals during HU treatment (log2 base).

Time passed after HU treatment (hr)	**1 to 2**	**2 to 3**	**3 to 6**	**6 to 18**
Number of cells enlarged (10%)	2	12	6	7
Number of cells shrunken (10%)	5	3	4	18
Number of cells with no proper (continuously) information	2	8	7	2
Number of cells with Fluoresence density increased (raw data, 10%)	6	11	18	9
Number of cells with Fluoresence density decreased (raw data 10%)	13	13	6	13
Number of cells with Fluoresence density increased (log2 base, 10%)	3	2	6	1
Number of cells with Fluoresence density decreased (log2 base, 10%)	6	5	0	0

amount of drug (less than 200mM of HU) during the 6 hour and then, they may grow up again. When lots of drug (more than 200 mM of HU) enter into the droplet, the cell cannot fight, and shrink in size. This may also explain the similar behavior of the cells which are in the same droplet.

4.2.3.6. The relationship between the fluorescence density and the cell area. Figure 4.57 shows the relation between the fluorescence density and the areas of the different cells at the same time points. For 1^{st}, 6^{th} and 18^{th} hours, the data show a reasonable agreement between the fluorescence density and the cell area (R^2=0.5161, R^2=0.4883, R^2=0.5023). However, at the 2^{nd} and 3^{rd} hours of HU treatment, the fluorescence density is not linearly dependent on area (R^2=0.0286, R^2=0.2916).

Figure 4.58 shows the relation between the fluorescence density and the area of each cell with respect to time. 19 cells are investigated, only few have acceptable R^2 values (R^2,1a= 0.5916; R^2,2a-2= 0.8094; R^2,4a-3=0.936; R^2,6a=0.7202; R^2,7a=0.7553; R^2,13a=0.9667; R^2,15a-1=0.5716), and unfortunately most R^2 values are not acceptable for linear regression.

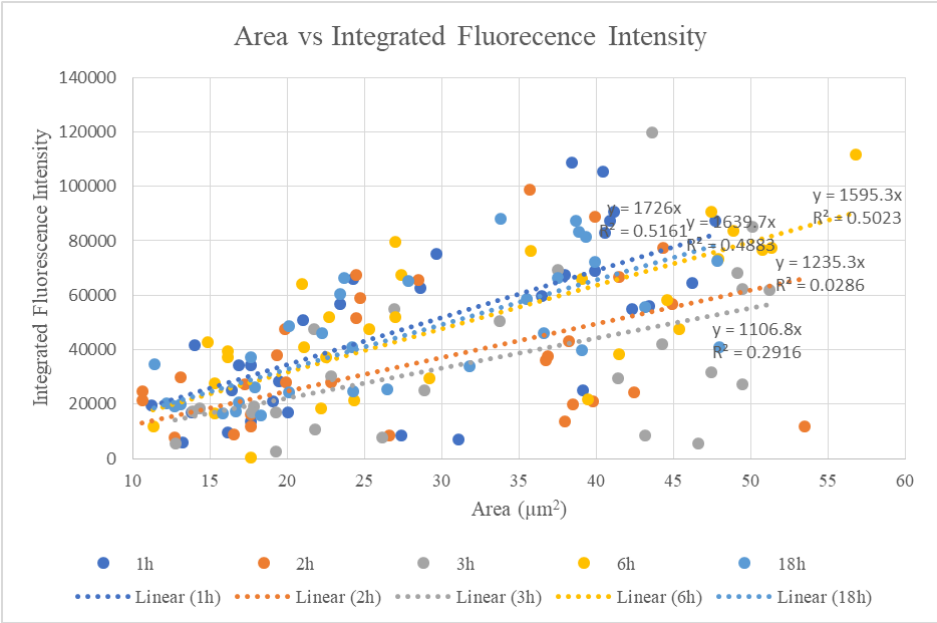

Figure 4.57. The change of fluorescence density by the cell area at the same time point.

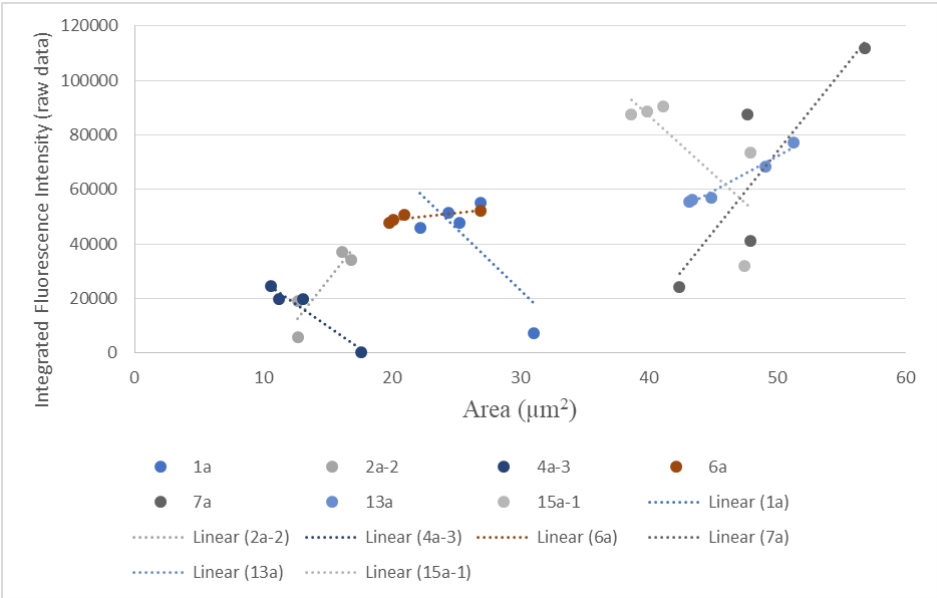

Figure 4.58. The change of fluorescence density by the cell area for each cell.

4.2.3.7. Discussion. HU is known as an inhibitor enzyme of ribonucleotide reductase, which is a catalytic enzyme that converts ribonucleotides to deoxyribonucleotides. This means, when the ribonucleotide reductase enzyme is inhibited, there is not sufficient amount of deoxyribonucleotides for the synthesis of DNA [50]. Thus, HU treatment slows the growing of the cells as also can be observed from the droplet based microfluidic experiments. When the cell growth slows down, the need for ribosome biogenesis decreases leading to reduction of NOP56 synthesis. However, after 18 hours of HU treatment, the DNA content is doubled in the cell and the cell is separated from mother cell. This result is also supported by the study of Alvino *et al.* [37].

Similarly, RPL5 amount decreases under HU treatment. Since HU treatment also inhibits rRNA synthesis, the need for ribosomal proteins to produce ribosome decreases. Under HU treatment, rather than producing ribosomes, ribosomal proteins like RPL5 hinder the activity of MDM2, which controls p53 levels, and subsequent increase in p53 level causes cell cycle arrest [31]. Consequently, this experiment also supports this study through decreasing the integrate fluorescence density of the RPL5.

As the experimental results show some fluctuations and inconsistency, we further investigated the effect of HU application on yeast cells by computational means, i.e. by integrating the gene expression data reported in literature. A co-expression network was constructed and analyzed by self-organizing map method, i.e. cluster of genes, which show similar features, were identified employing the microarray data produced by Krippleber *et al.* [45] for HU treatment of BY4741 wild type yeast strain.

4.3. Coexpression Analysis for HU Treatment

4.3.1. SOM Analysis

Self-organized maps are a machine learning system, which is generated by Kohonen in 1980s. Later, SOM was modified for use in gene expression investigation. SOM combines sampled and gene- centered data and allows to visualize the groups in the form of mosaics. These mosaics are like a prototype of mini clusters (metagenes) of

resembled genes in terms of expression profiles and they are determined by the algorithm according to the similarity in the behavior of the genes. The arrangement of the genes is adjusted during the process of the self-organizing algorithm, i.e. they are arranged as decreasing the distance in the map as the degree of similarity between metagenes increases [51]. The benefit of the SOM is to reduce the data dimension and make the interpretation of the data easier. Further gene enrichment analysis provides a complementary information on the samples and the gene clusters [52].

In this present study, the data of Krippleber *et al.* for hydroxyurea treatment on S. cerevisiae wild type strain BY4741 is used for SOM analysis. During 4 hours of treatment, Krippleber *et al.* obtained expression data at 0^{th}, 1^{st}, 2^{nd} and 4^{th} hours. Using these data, self-organizing maps are created by oposSOM package in Rstudio program. SOM mosaic is created as 30x30 array, thus, there are 900 metagenes that represent the clusters of genes, which show similar features. The population map is given in Figure 4.59 and it shows the number of the genes in the metagenes.

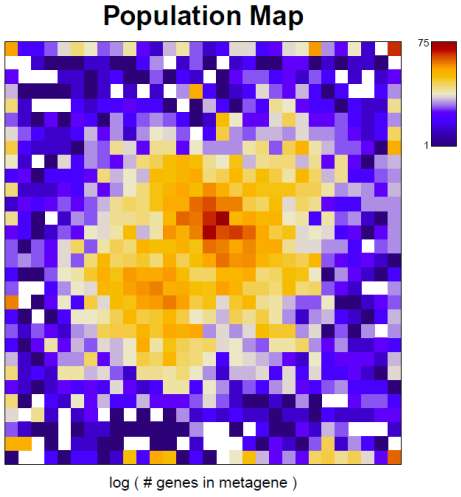

Figure 4.59. Population map.

4.3.1.1. Expression Portraits. Expression portraits show the expression of the metagenes according to the time at which the samples are taken. As can be seen in the expression portraits (Figure 4.60), the expression of the genes placed on the left top

of the map was low before the HU treatment. After an hour of the treatment, these genes are overexpressed. Similarly, the genes placed on the right bottom of the map are highly expressed before HU treatment while they are underexpressed after HU treatment.

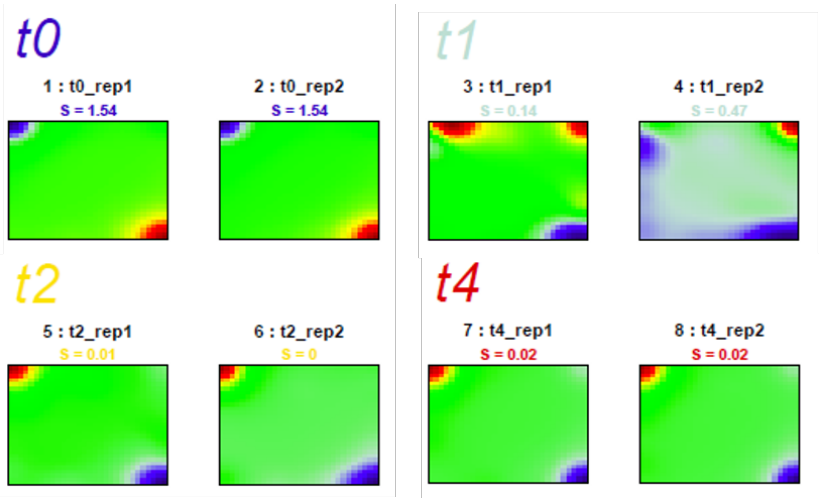

Figure 4.60. Expression Portraits.

4.3.1.2. Data Distribution. Data distribution shows the distribution of the expression levels of the genes. Many genes are expressed at 0-15 levels (Figure B.2). Since there are a few genes expressed at high levels, log2 expressions are also high and they extend the data distribution map.

4.3.1.3. Overexpression Spots. Overexpression spots show the strongly expressed metagenes at any time during the HU treatment. In Figure 4.61, the legend also shows the gene enrichment of the spots, which may give idea about the biological context of the genes in the spots. In this study, there are three spots overexpressed.

In spot A, the right bottom corner of the map, there are three metagenes and 40 genes, and these genes are especially overexpressed before the treatment (Figure 4.61). Top ten overexpressed genes in spot A are tabulated according to their maximum expression level (Table B.8). GO enrichment analysis of the genes in spot A indicates

that these genes are related to cytoplasmic translation as biological process, ribosome as cellular component and structural constituent of ribosome as molecular function (Table B.9). In spot A, genes have high p-value, which means they are not significant for this cluster. YKL156C has the lowest p-value, and the gene product is putative uncharacterized protein, but it has overlapping data with the verified gene RPS27A.

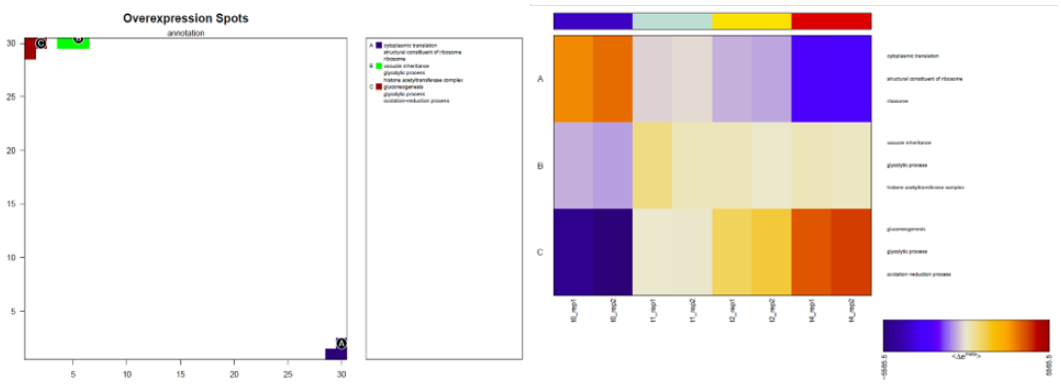

Figure 4.61. Overexpression Spots.

Spot B and spot C are placed in the left top of the map. In overexpression spot B, there are 3 metagenes and 25 genes. This spot is placed in the left top of the map and it is overexpressed mainly in the first hour of the HU treatment. The genes in this spot B are related to vacuole inheritance, glycolytic process as BP, histone acetyltransferase complex as CC and peptidyl-prolyl cis-trans isomerase activity as MF. Top ten overexpressed genes and GO enrichments results of the genes are tabulated (Table B.10 and B11). Similar to overexpression spot A, the genes in this spot have high p-values and YGR209C (TRX2), which transcripts a cytoplasmic thioredoxin isoenzyme, has the lowest.

Overexpression spot C is placed in the left top corner of the map. In this spot, there are 3 metagenes and 29 genes. These genes are overexpressed mainly after 2 hours of HU treatment. The result of the GO enrichment analysis shows that these genes are related to gluconeogenesis, glycolytic process and oxidation-reduction process (BP), cytosol (CC) and oxidoreductase activity, acting on the aldehyde or oxo group of donors (MF). Top ten overexpressed genes and GO enrichments analysis results of the genes are tabulated (Table B.12 and B13). The lowest p-value (with known function) belongs

to YGR180C (RNR4) which is the ribonucleotide-diphosphate reductase (RNR) small subunit and it catalyzes the rate-limiting step in dNTP synthesis.

The significant genes and their related functions, biological processes and cellular components in the cell in response to drug application are given in Tables B.8-B.13 in Appendix B. The genes of our interest, RPL5, NOP56 and NOP58 genes, are not placed in any overexpression spot.

4.3.1.4. Underexpression Spots. Underexpression spots show the strongly underexpressed metagenes during the HU treatment. For the HU treatment, there are two underexpressed spots (Figure 4.62). Spot a is placed at the left top corner of the map. This spot is underexpressed before the treatment. There are 3 metagenes and 29 genes in spot a and these genes are related to gluconeogenesis, glycolytic process and oxidation-reduction process. Underexpression spot b is placed at the right bottom corner of the map and there are 9 metagenes and 83 genes. These genes are underexpressed after 1-hour HU treatment and they are related to cytoplasmic translation, structural constituent of ribosome and ribosome. Neither NOP56 nor NOP58 is involved in underexpression spots. RPL5 is also not placed in any underexpression spot.

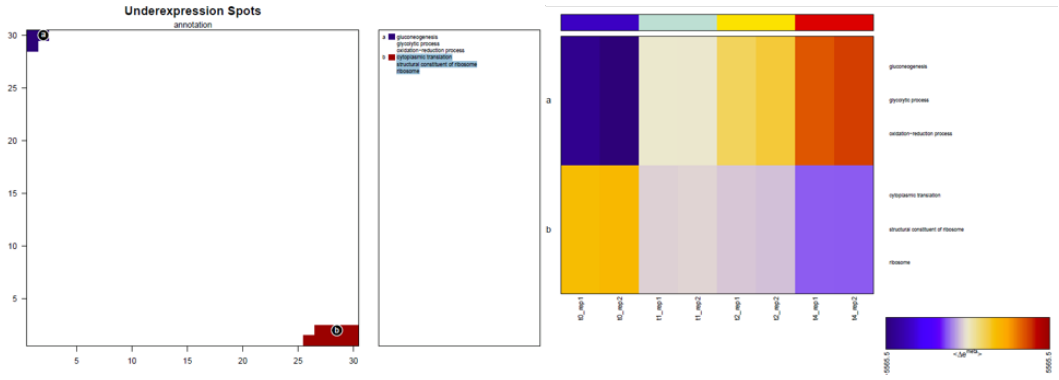

Figure 4.62. Underexpression Spots.

4.3.2. Geneset Z-score (GSZ score)

Overrepresented gene sets are identified for each sample set (i.e. samples that replicated). Overrepresentation of a gene set in a sample is calculated by using Z-score statistics. Hypergeometric enrichment score, which is weighted with the differentially expressed test scores, is used to find the GSZ. Basically, the z-score gives the number of standard-deviations, that a value is away from the mean of all the values in the same group (same gene). For example, a z-score of -3 for the gene X in sample A means that this value is 3 standard-deviations lower than the mean of the values for gene X in all the samples (A, B, C...). When a gene is differentially expressed in two groups (like treated and control or diseased and healthy), then the z-scores of samples will be (mostly) positive in one group and (mostly) negative in the other group. The heatmaps are created according to GO terms, i.e. biological process, molecular function and cell component. For the replicated samples, the geneset rankings are close to each other for each replicate of the sample.

The following graph (Figure 4.63) shows the GSZ-score heatmap of the biological process of all samples. In terms of biological process, GSZ score is low for glycolytic process and gluconeogenesis before the treatment (Table B.14), while the scores of these processes increases at the 4^{th} hour of the treatment (Table B.17). Also, GSZ scores of cell redox homeostasis and DNA damage check point are also low before the treatment. GSZ score of translation and cytoplasmic translation is very high before the treatment however, right after the treatment begins, GSZ scores of these processes decrease and become the lowest scores (Figure 4.63). Figure 4.64 shows the heatmap of the GSZ-scores of the cellular components. For cellular component, intracellular, cytosolic large and small ribosomal subunits and ribosome have the highest GSZ-score before the treatment. 1 hour after the treatment the GSZ-scores of these components decrease. Figure 4.65 shows the heatmap of the GSZ-score of the molecular function. For the molecular function, there is not any strong high value of GSZ-score; however, structural constituent of ribosome is relatively high before the treatment and it has the lowest value after the HU treatment.

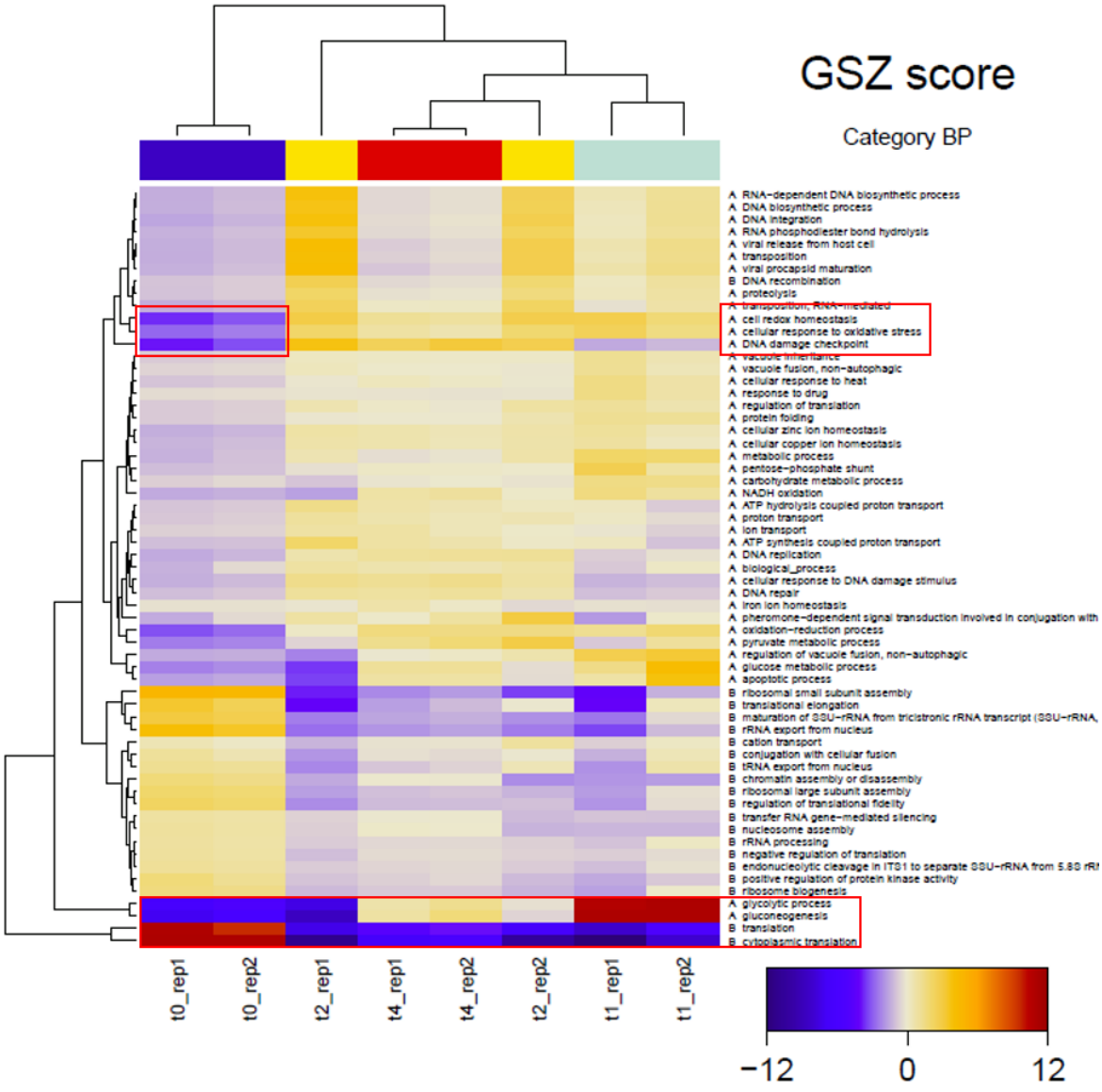

Figure 4.63. GSZ-score for Biological Process.

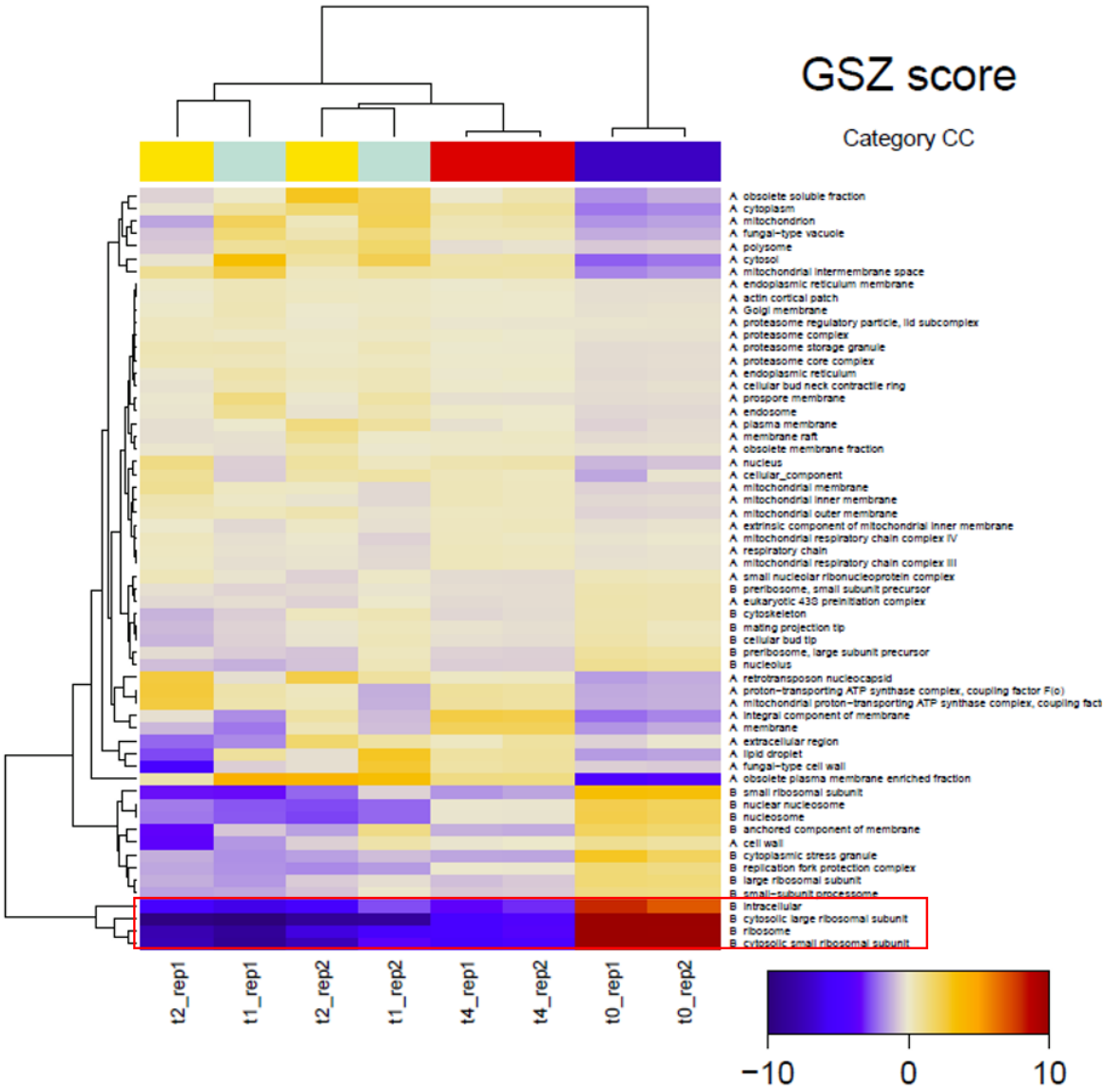

Figure 4.64. GSZ-score for Cellular Component.

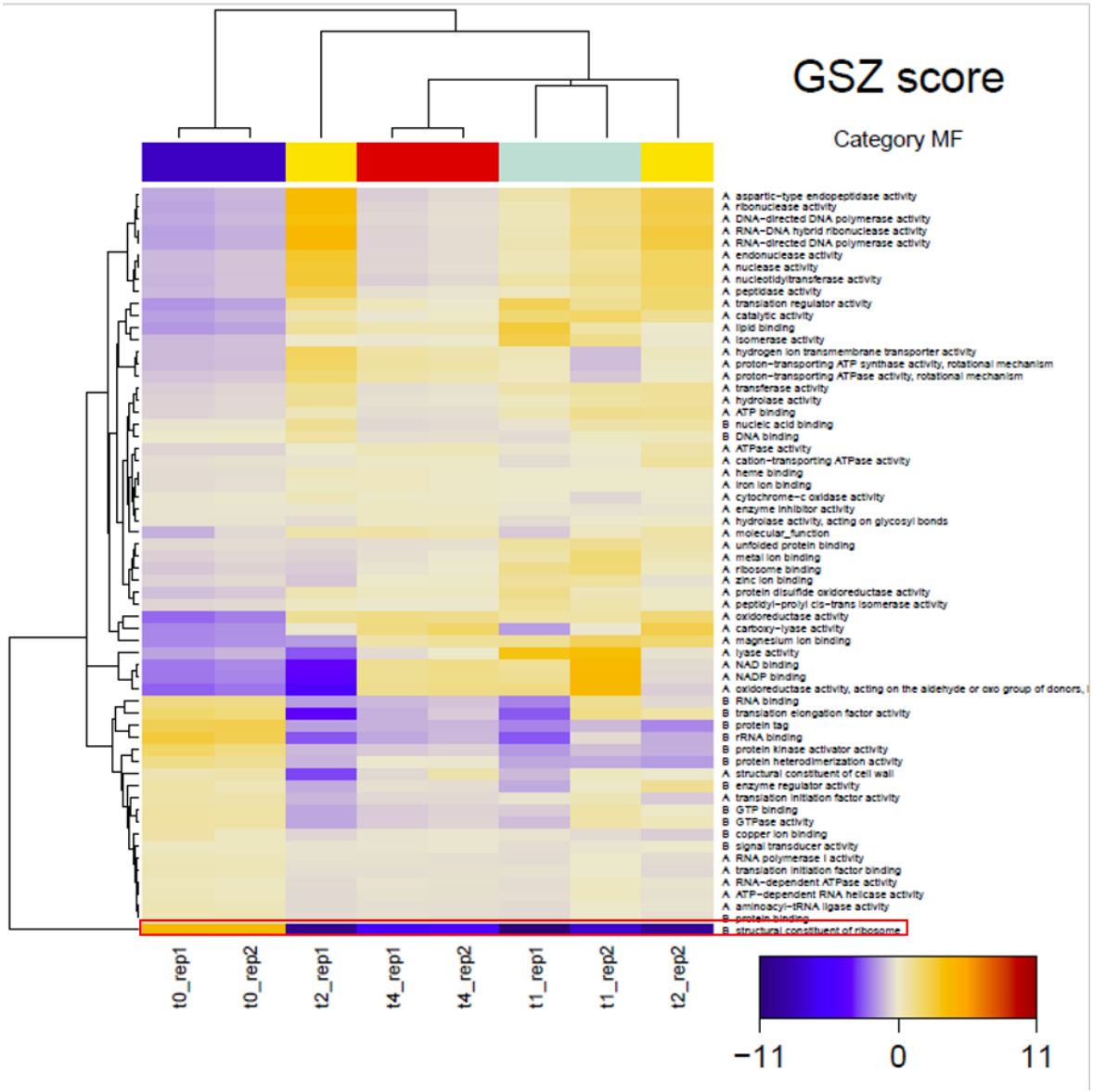

Figure 4.65. GSZ-score for Molecular Function.

Tables B.14-B.17 in Appendix B show the upregulated and downregulated gene sets by time during treatment. According to the Table B.14, when there is not any treatment, cytoplasmic translation has the highest Z-score where the gluconeogenesis has the lowest Z-score. Table B.15 shows the changes after 1 h of treatment, and the upregulated geneset is involved in gluconeogenesis and glycolytic process, while the downregulated geneset is involved in cytoplasmic translation. After 2 hours and 4 hours treatments, downregulated genesets are similar which are cytoplasmic translation and structural constituent of ribosome (Table B.16-B.17). Table B.16 shows that the upregulated genesets are involved in viral procapsid maturation and viral release from host cell after 2 hours treatment. After 4 hours treatment, upregulated genesets are involved in processes related to DNA damage checkpoint and integral component of membrane (Table B.17).

4.3.3. Clustering Approaches

Different clustering approaches such as D-clustering, K-clustering, Pearson clustering are used to group the gene expression data and estimate the relationship among the genes of interest and related pathways and finally the crosstalk among these pathways. Clustering methods and the related GO Terms for NOP56 and NOP58 containing clusters are summarized in Table 4.17 at the end of the part 4.3.

4.3.3.1. D-Cluster. D-clustering is a clustering approach based on similarities between the metagenes and calculated based on the distances between each pair of the gene. For this clustering, oposSOM uses Euclidian distance as distance statistics. This statistic measures the similarity between gene expression and the dominant eigenvector expression. Higher value indicates the higher similarity between the metagenes [53].

In this analysis, there are two clusters. Cluster A is placed in the top left corner of the map and cluster B is placed in the right bottom corner of the map (Figure 4.66). Neither NOP56 nor NOP58 genes are placed in D-clusters.

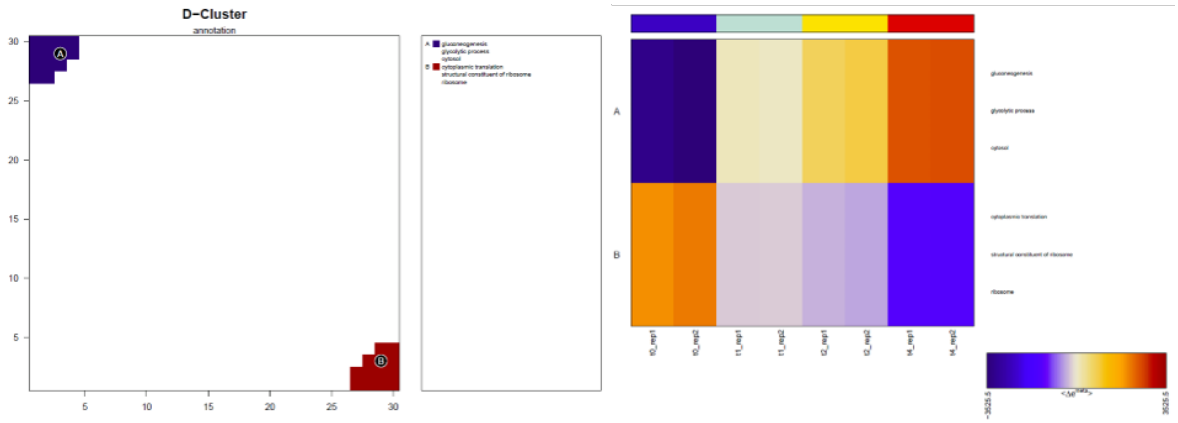

Figure 4.66. D-cluster Spots and Heatmap.

In cluster A, there are 13 metagenes and 52 genes. Table B.18 in Appendix B shows the top 10 genes of this cluster according to their maximum expression level and Table B.19 in Appendix B shows the results of GO enrichment analysis. According to the GO enrichment analysis of this cluster, the genes in this cluster are mainly related to gluconeogenesis, glycolytic process and cytosol. According to the Table B.18, YMR046W-A, which is unlikely to encode a functional protein, and YGR180C (RNR4), which is ribonucleotide-diphosphate reductase (RNR) small subunit, have the lowest p-values.

In cluster B, there are 13 metagenes and 82 genes. Table B.20 in Appendix B shows the top 10 genes of this cluster according to their maximum expression levels and Table B.21 shows the GO enrichment results. YOR182C (RPS30A) is the most meaningful gene, which transcripts 40 S ribosomal subunit and has one of the lowest p-value in this spot. GO enrichment analysis is done to these genes and the results show that this cluster is related to cytoplasmic translation, ribosome and structural constituent of ribosome (Table B.21). Although many ribosomal protein (RP) related genes are placed in D-cluster B, RPL5 is not involved in this cluster, however, it is placed close to this cluster (28x4 metagene).

4.3.3.2. K-means Cluster. In this method, the number of clusters is set to 15, arbitrarily, to make the numbers of the metagenes in a spot close to each other. 15 random examples are initial centroids and these centroids create clusters by assigning each

metagene to closest centroid. Then, these 15 centroids are moved by averaging the metagenes in each cluster. Clusters are partly arranged based on the over- or under-expressions of metagenes. This is a coarser fragmentation of the map and it enables the gapless sorting of genes. Also, the gene enrichment analysis is applied to the clusters. NOP56 gene is in Spot A and NOP58 is in Spot C (Figure 4.67). RPL5 gene is in Spot E. Top three GO enrichment analysis results of the spots are given in the Table B.22 in Appendix B according to their p-values.

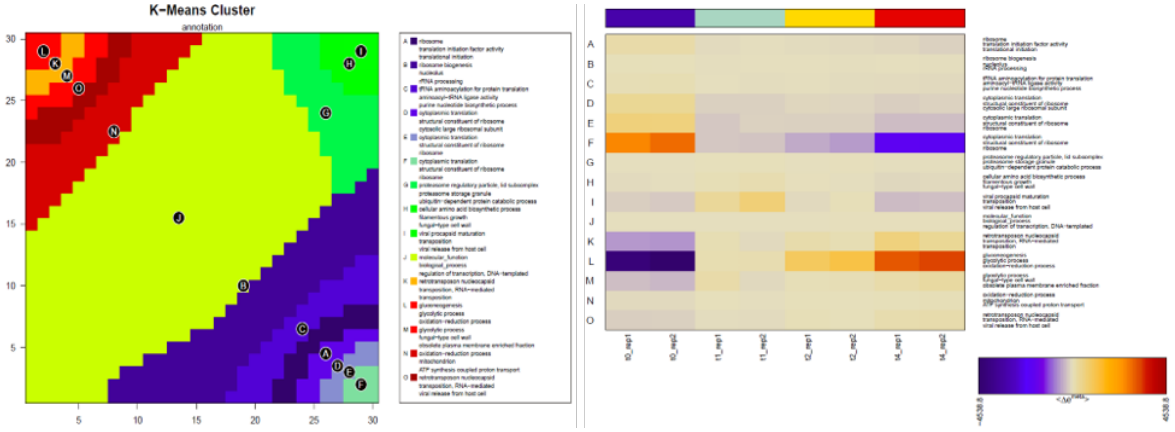

Figure 4.67. K-means Clusters and Heatmap.

4.3.3.3. Correlation Cluster-PCC. Another spotting alternative is the Pearson correlation clustering. In this method, spots are selected from highly correlated metagenes. The correlation spots tend to fragment the regions along the border of the map, which refer to the metagenes of strongest variability of their expression profiles [54]. Each colored area represents a group of metagenes, which strongly correlate each one with another with a correlation coefficient of $r > r_{threshold} = 0.9$. The equation of r is given below. When X and Y are assumed as expression levels of genes, r gives the correlation between the genes X and Y.

$$r = \frac{\sum XY - \frac{(\sum X)(\sum Y)}{n}}{\sqrt{(\sum X^2 - \frac{(\sum X)^2}{n})(\sum Y^2 - \frac{(\sum Y)^2}{n})}} \tag{4.1}$$

The following figure (Figure 4.68) may help to understand what the correlation means.

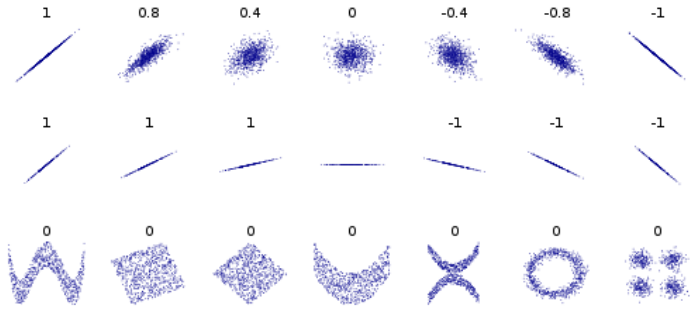

Figure 4.68. Correlation Coefficient of Data Distribution [55].

Here, the metagenes are clustered by their Pearson correlations. Each cluster represents the metagenes that are strongly correlated with each other (Figure 4.69). The correlation threshold is taken as 0.9. NOP56, NOP58 and RPL5 are in Cluster B (Figure 4.69). The genes in the cluster B are highly expressed before the treatment while they are downregulated after the treatment. Genes in the cluster B are related with cytoplasmic translation, structural constituent of ribosome and translation. On the contrary, cluster K, which is related with oxidation-reduction process, membrane and oxidoreductase activity, is lowly expressed before treatment while it is highly expressed at 4th hour of the HU treatment. Expression levels of the other clusters do not change too much as the treatment is applied.

In general, the metagenes in the clusters are highly correlated with each other; however, the genes in the clusters, individually, are not correlated with each other that strongly. In general, the correlations between the metagenes are higher than 0.9 while the correlation between the genes in the clusters are low. Genes are placed in metagenes according to their expression profiles. It means that the genes that are in different metagenes show different expression profiles. Thus, the reason of having low correlation coefficient between genes in a cluster may be the different expression profiles of each gene in the metagenes. On the other hand, mean expression level of the metagenes may be close to each other; thus, their correlation coefficient is high. In general, Pearson correlation coefficient of the metagenes in a cluster is higher than 0.9 while it is around 0.5 and 0.6 for individual genes (Figure 4.69).

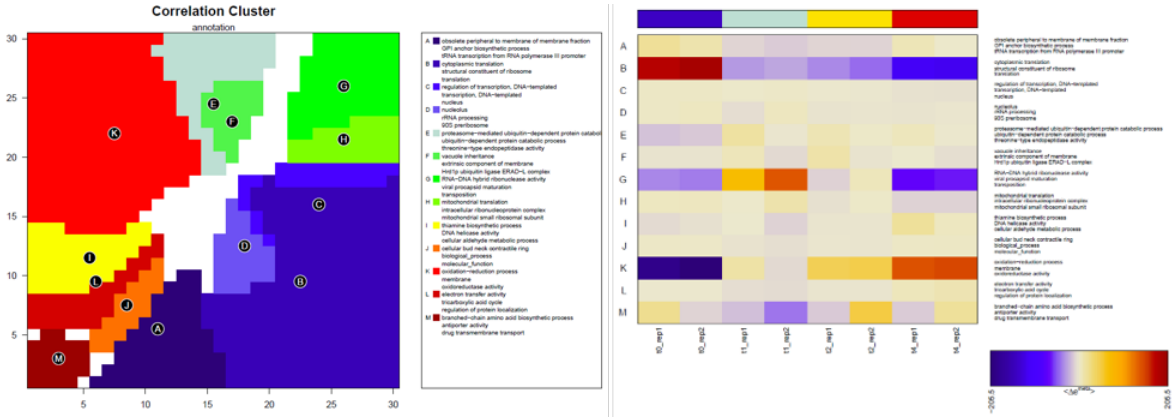

Figure 4.69. Correlation Cluster.

4.3.3.4. Correlated Genes with NOP56. There are 193 proportionally correlated genes with NOP56 which have Pearson correlation coefficient higher than 0.95 (Table B.23). According to the GO enrichment analysis, the genes proportionally related with NOP56 protein under HU treatment are generally related to ribosome biogenesis and biosynthetic process as the biological process terms. As the molecular function term, these genes are related to structural constituent of ribosome and RNA binding. As a cellular component, these genes are related to ribonucleoprotein complex (Table B.25).

Also, there are 163 inversely correlated genes with NOP56, which have Pearson correlation coefficient less than -0.95 (Table B.24). According to the GO enrichment analysis, the genes inversely correlated with NOP56 are related to biological process of telomere maintenance while they are related to helicase activity as a molecular function. However, there is not any cellular component that these genes are related with (Table B.26).

Two different heatmaps are created for the highly correlated genes according to PCC. First one (Figure 4.70) displays the expression levels of highly correlated genes. In this heatmap, the samples are hierarchically clustered. Two-way clustering, which makes combined sample clustering with gene clustering, identifies the genes, that are the most important for sample clustering. According to the hierarchical clustering, the data before the HU treatment create one major cluster and the data after 4 hours treatment are separated from 1 and 2 hours treatment. It can be said that, the cells

responded to the treatment immediately, and after 4 hours, the response is the strongest (Figure 4.70).

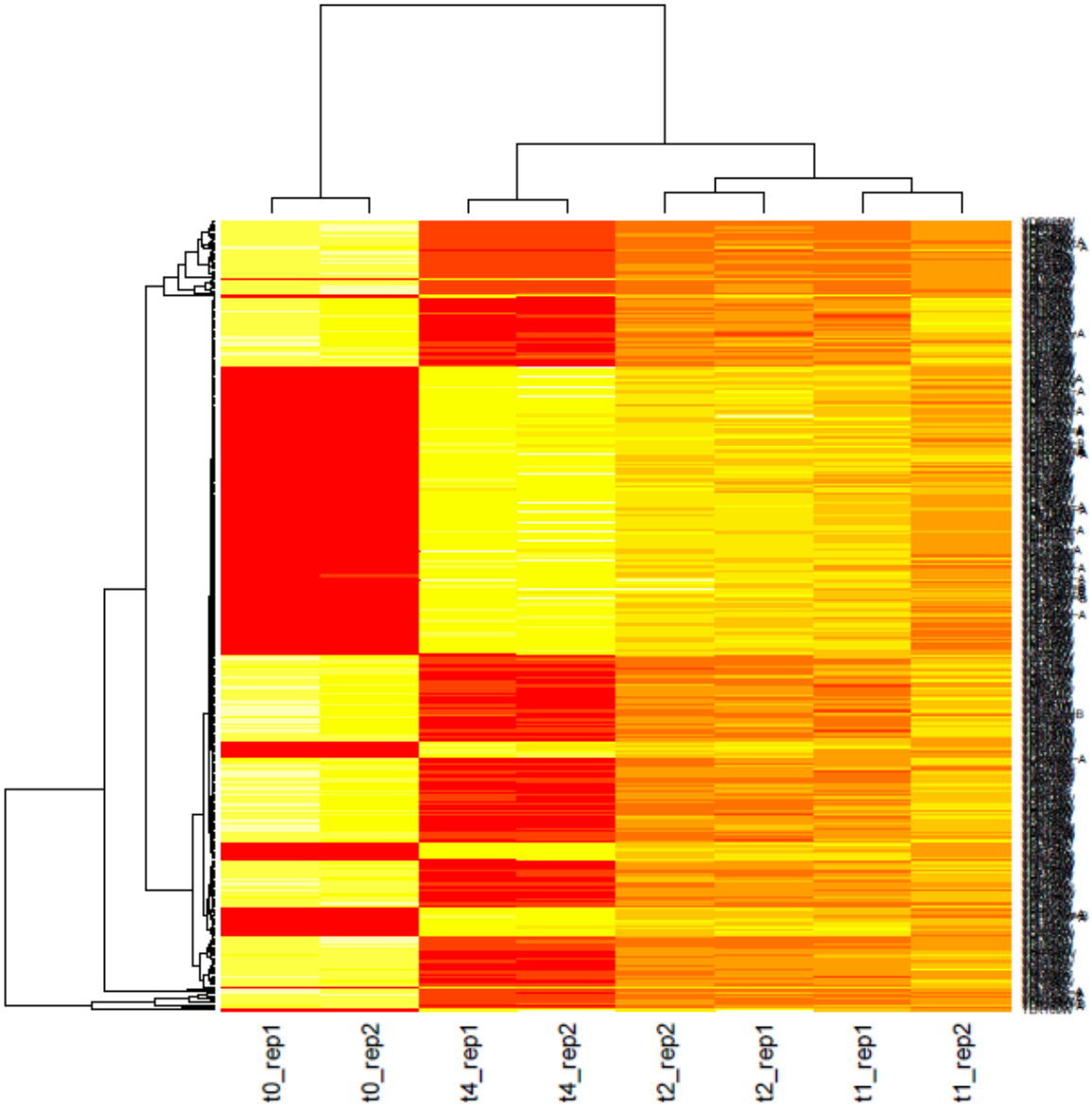

Figure 4.70. Heatmap of highly correlated genes.

The genes are also clustered to discover the co-regulated and functionally related genes. Second heatmap (Figure B.3) is created according to the Pearson correlation coefficients of the genes. This heatmap (Figure B.3) shows the pairwise correlation of highly correlated genes. Since these genes are highly correlated with a correlation coefficient value higher than 0.95 or lower than -0.95, there seems to be only two colors,

which are red and blue, however, the colors slightly change. The diagonal has always the value of 1.

4.3.4. Response of Yeast Cells to HU Application

Using the data of Krippleber *et al.* for hydroxyurea treatment on S. cerevisiae wild type strain BY4741 (expression data obtained at 0^{th}, 1^{st}, 2^{nd} and 4^{th} hours), self-organizing maps are created by oposSOM package in Rstudio program. In this section, several analyses are done on these maps focusing on RPL5 NOP56 and NOP58 genes. RPL5 is in the 28x4, NOP56 is in the 26x7 metagene and NOP58 is in the 24x7 metagene. The other co-expressed genes in these metagenes (28x4, 26x7 and 24x7) are listed in Table 4.16.

Table 4.16. Metagenes that contain RPL5, NOP56 and NOP58.

26x7	**24x7**	**28x4**
SES1	SUP45	RPL16A
NOP56	NPL3	**RPL5**
SUN4	GUS1	
	NOP7	
	NSR1	
	MES1	
	LIA1	
	NOP58	

The GO enrichment analysis cannot be done to the metagenes containing NOP56 and RPL5 genes, because there are insufficient number of genes in each metagene. For Nop58 containing metagene 24x7, the genes in the metagene are related to RNA metabolic process as biological process, mRNA binding as molecular function and ribonucleoprotein complex as cellular component. Clustering methods and the related GO Terms for NOP56 and NOP58 containing clusters are summarized in Table 4.17.

Table 4.17. Clustering methods and the related GO Terms.

Method	**GO process**	**GO component**	**GO function**	**NOP56/ NOP58/ RPL5**
Overexpressed, A	Cytoplasmic translation	Ribosome	Structural constituent of ribosome	-
Overexpressed, B	Vacuole inheritance	Histone actyltransferase complex	Peptidyl−prolyl cis−trans isomerase activity	-
Overexpressed, C	Gluconeogenesis	Cytosol	Oxidoreductase activity	-
Underexpressed, A	Gluconeogenesis	Cytosol	Oxidoreductase activity	-
Underexpressed, B	Cytoplasmic translation	Ribosome		-
D-cluster A	Gluconeogenesis	Cytosol	Oxidoreductase activity	-
D-cluster B	Cytoplasmic translation	Ribosome	Structural constituent of ribosome	-
K-means cluster, A	Translation initiation	Ribosome	Translational initiation factor activity	NOP56
K-means cluster, C	tRNA aminoacylation for protein translation	Nucleolus	Aminoacyl-tRNA ligase activity	NOP58
K-means cluster, E	Cytoplasmic translation	Ribosome	Structural constituent of ribosome	RPL5
Pearson Correlation Clustering, B	Cytoplasmic translation	Cytosolic large ribosomal subunit	Structural constituent of ribosome	NOP56, NOP58, RPL5

4.4. Transcription Factor Analysis for HU Treatment

4.4.1. Transcription Factor Activity for the Genes in D- Clustering Under HU Application

In order to get an insight on the regulation of ribosome biogenesis related processes under HU treatment, the transcription factors of the genes in D-cluster B, which are related to ribosome biogenesis, are found and used in the SOM analysis. D-cluster is selected for this analysis since D-clustering is the most analytic and efficient clustering of all the clustering methods in the SOM analysis.

The transcription factors of 75 genes out of 82 genes in Cluster B are identified by using Yeastract website. 82 genes are indicated in Sheet1 of the supplementary excel file. Sheet 2 in the supplementary excel file shows the transcription factors of each gene in the cluster. Then, a table is prepared for the transcription factors and the genes, where the first row with the numbers shows the number of transcription factors of the gene and first column with the numbers shows the number of genes that TF targets. Number "1" indicates that the TF targets the gene in the column while "0" indicates that TF does not target the gene in that column. According to the table, 158 different transcription factors are found. Of these, Rap1p, Yap1p, Sfp1p, Gcr1p, Cst6p, Ace2p and Swi5p are the most common transcription factors for the genes in the cluster B. In the Sheet 4, the descriptions of the common transcription factors are given.

The color code for the fold changes of the genes under HU treatment with respect to those without HU treatment are given in Figure 4.71.

Rap1 (repressor activator protein), which is the transcription factor of 67 out of 75 genes in the cluster B, is an essential DNA-binding transcription regulator that binds many loci; involved in transcription activation, repression, chromatin silencing, and telomere length maintenance. The proteins interacting with this TF are identified [56] and given in Figure 4.72. This protein is related to Spt15p, which is TATA-binding protein (TBP), that in turn is essential for viability [57]. Underexpression of this

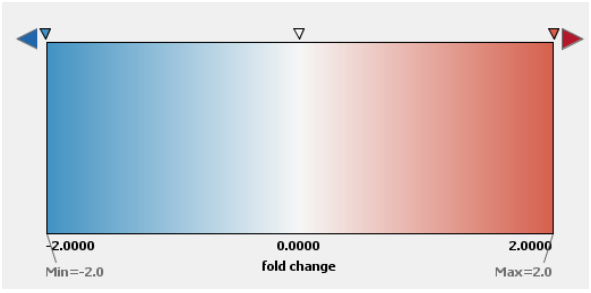

Figure 4.71. Fold change distribution of the genes in cluster B.

protein means the viability of the cell is decreased. Also, Rap1 is generally interacting with the TAF proteins, which are TBP-associated factor. TAF proteins are mainly involved in RNA polymerase II transcription initiation and in chromatin [58]. There are many subunits of TAF protein related to Rap1 and they are also underexpressed under HU treatment. When the polymerase II transcription initiation is decreased, cell proliferation is also decreased. Contrary to TAF proteins, Rif proteins which bind to Rap1p and control telomere length by establishing telomeric silencing, are slightly overexpressed, which is also meaningful in terms of preventing the DNA replication [59]. Rap1 gene product interacts with Gcr1p, which is also one of the most common transcription factors of the D-cluster B.

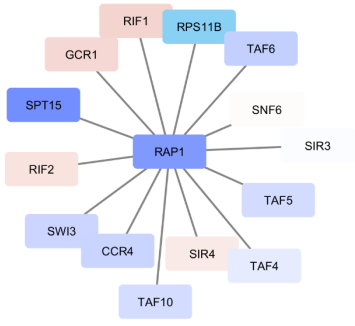

Figure 4.72. Interactions of RAP1.

Gcr1 is a transcriptional activator of genes involved in glycolysis (GlyColysis Regulation), which also interacts with transcriptional activator Gcr2p [60]. Literature survey shows that Gcr1, Gcr2 and Rap1 gene products work together [61]. Moreover, as shown in Figure 4.73, Gcr1 interacts with Pom gene products (Pore Membrane), which are subunits of the transmembrane ring of the nuclear pore complex (NPC)

and contribute to nucleocytoplasmic transport, NPC biogenesis and spindle pole body duplication [62, 63]. According to Wozniak *et al.*, overexpression of Pom152 inhibits cell growth, however, under HU treatment, Pom152 is underexpressed. This means, HU treatment does not affect Pom152 in a way that prevents the cell growth [64].

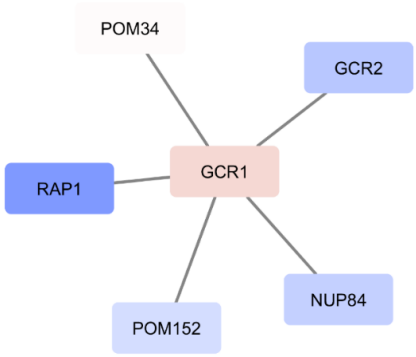

Figure 4.73. Interactions of GCR1.

Yap1 is one of the most common TFs in the D-cluster, and it is basic leucine zipper transcription factor, which is basically required for oxidative stress tolerance [65]. Under HU treatment, overexpression of Yap1 gene shows abnormality of the cell cycle progression and increase in the resistance to chemicals. Kap (karyopherin) genes, which are interacting with Yap1 (Figure 4.74), are underexpressed under HU treatment. Kap genes provide the transport of the molecules from cytoplasm to nucleus or vice versa. When these genes are underexpressed, the amount of protein imported to the nucleus decreases and it may cause abnormalities in microtubule stability [66]. Yap1 also interacts with Crm1 (major karyopherin), which exports proteins, RNAs and ribosomal subunits from nucleus. Crm1 gene is slightly overexpressed under HU treatment, which means decrease in growth and increase in chromosome loss [67].

As shown in Figure 4.75, Crm1 also interacts with Ace2, which is an activator protein of Cup1, provides resistance to high concentrations of copper and cadmium. It is involved in negative regulation of transcription by RNA polymerase II process, i.e., overexpression of this gene leads to decrease in transcription by RNA polymerase II. Ace2 is the paralog gene of Swi5 gene and both of them are interacting with Cdc28. Clb2 and Clb3, which are also interacting with Crm1, activates Cdc28 to promote the G2 to M phase transition and it may have a role on DNA replication. Overexpression

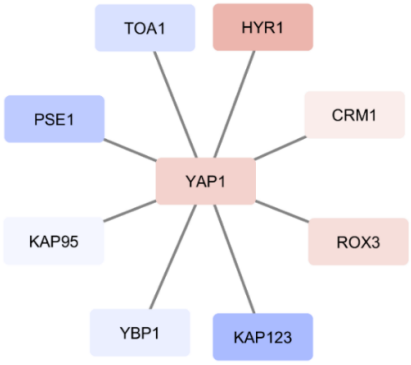

Figure 4.74. Interactions of YAP1.

of Clb2 and underexpression of Clb3 lead to the abnormal activities of cell cycle progression [68]. Cdc28 (Cell Division Cycle) is the major regulator of the mitotic cell cycle and it is involved in all phases of the transitions. Overexpression of Cdc28 leads complication in protein distribution during the cell cycle.

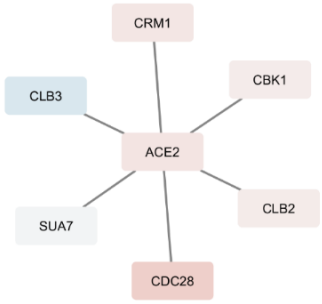

Figure 4.75. Interactions of ACE2.

Similar to Ace2, Swi5 is not affected from HU treatment too much. Swi5 interacts with both Cdc28 and Cdc14 (Figure 4.76). Cdc28 activates transcription of genes expressed at the M/G1 phase boundary and in G1 phase. On the contrary to Cdc28, Cdc14 is slightly underexpressed under HU treatment. Cdc14 has a role on terminating the cell cycle. Cdc14 stays inactive during the cycle, and at the end of the cycle it is released from the nucleolus to terminate the cell cycle. Underexpression of Cdc14 may mean that cell cycle exit cannot occur.

Finally, Sfp1 (Figure 4.77) is also a common transcription factor in D-cluster B in SOM analysis. It has a role on G2/M transition phase during cell cycle. It is slightly underexpressed under HU treatment together with CKA genes. Cka1 and Cka2 genes

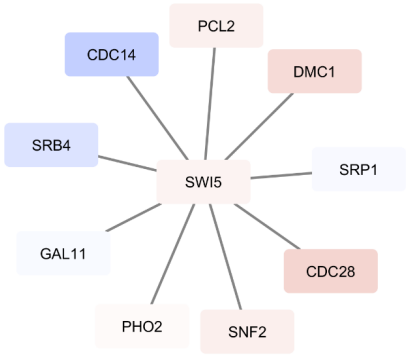

Figure 4.76. Interactions of SWI5.

are catalytic subunits of casein kinase 2, which has a role in proliferation and cell growth [69]. Underexpression of these genes may also lead to a decrease in cell growth.

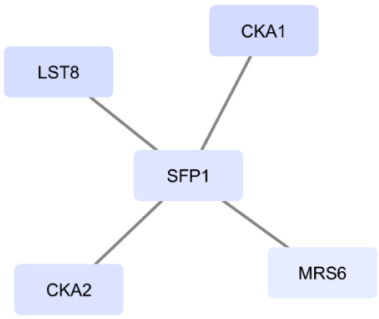

Figure 4.77. Interactions of SFP1.

The general interaction between the most common transcription factors is shown in the following figure (Figure 4.78). Because most of the TFs are in similar biological process (cell cycle), they are related to each other.

Nop56 is connected with these proteins indirectly. The interactions between the Nop56 protein and the proteins interacting with TFs are shown in the Figure 4.79. Nop1 is interacting with Yap1 through the interaction of the Pse1 protein. Also, Nop58 is interacting with Utp8, which is interacting with Pom152. Since Pom152 is interacting with Gcr1, and thus with Rap1, it can be said that, NOP56 is associated with these transcription factors.

Nop58 produces mature rRNA and synthesis of 18S rRNA. Nop58 is highly homologous with Nop56, and they both are in the nucleolus of the cell and vital for the

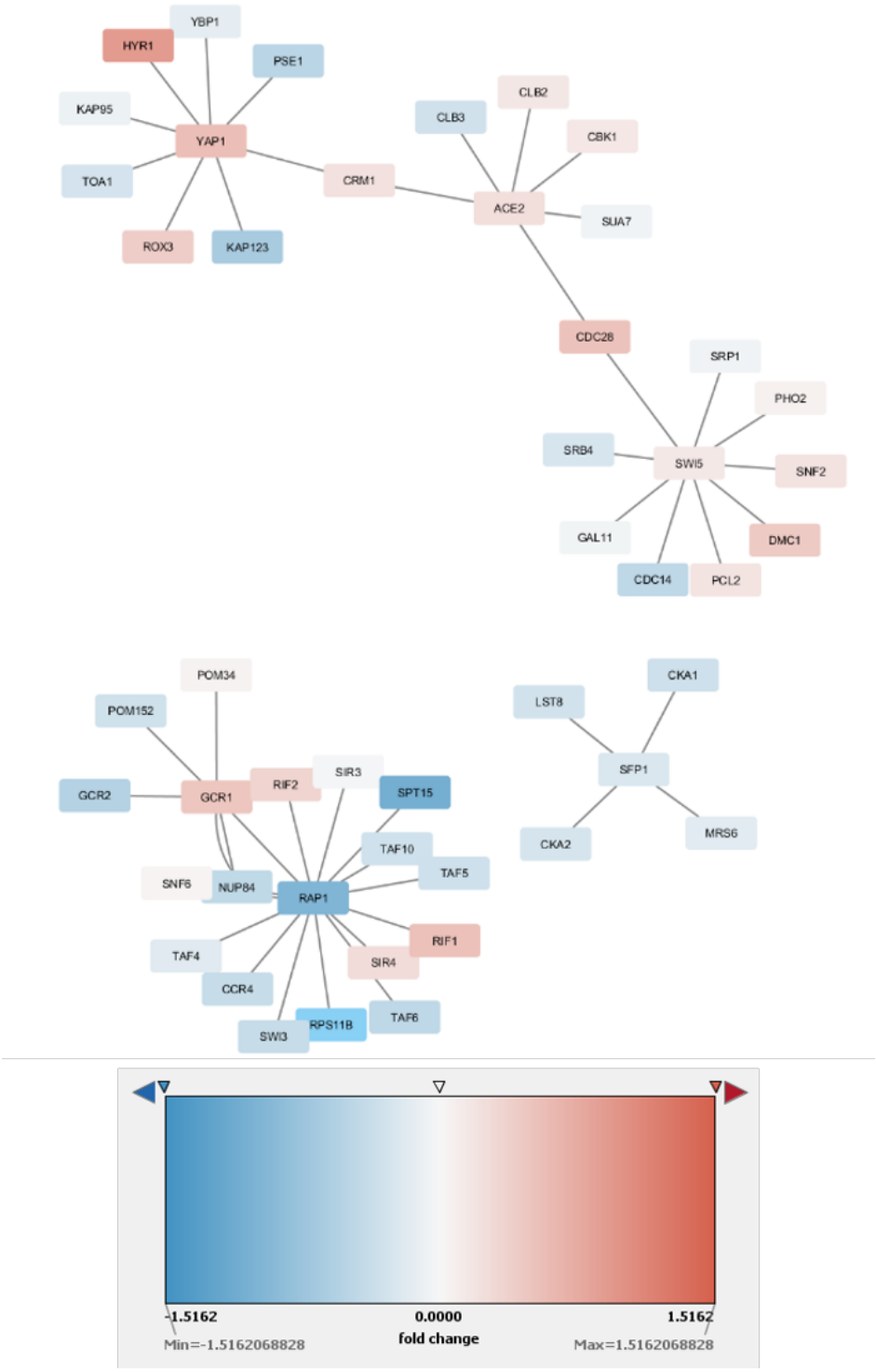

Figure 4.78. Interactions of all TFs.

cell [70]. Underexpression of this protein under HU treatment may impede the ribosome biogenesis. Utp8 (U Three Protein, U3) protein functions in rRNA processing and assembly of small ribosomal subunit. Underexpression of this protein indicates a decrease in 18S rRNA production [71]. As mentioned above, Pom152, which is responsible for inhibiting the cell growth, is interacting with Utp8 and connects the Nop56 protein with the transcription factors of Rap1p, Yap1p, Sfp1p, Gcr1p, Cst6p, Ace2p and Swi5p through Nop58.

4.4.2. Transcription Factors of the Genes Correlated with NOP56

In addition to the TFs of genes in D-cluster B in SOM analysis, the transcription factors of the genes correlated with NOP56 are also found, i.e. the Pearson Correlation Coefficients (PCCs) are calculated between NOP56 gene and all the other genes. There are 22 genes proportionally correlated with NOP56, i.e. having a PCC value higher than 0.99. Yeastract database is used to find the transcription factors of these genes. Figure 4.80 shows a sample of transcription factors of each gene (a total of 22 genes). Figure 4.81 shows the sample of transcriptions factors versus the correlated genes. First row with the numbers shows the number of transcription factor of the gene and first column with the numbers shows the number of genes that the TF targets. Number "1" indicates that the TF targets the gene in the column while "0" indicates that TF does not target the gene in that column. Whole tables are given in the Supplementary file 2.

4.5. Drug Effect: Rapamycin derivatives against TOR

Temsirolimus (Toricel), a gift of Pfizer, is a drug for targeted therapy of cancer and it is designed to inhibit the mTOR pathway and it is a derivative of rapamycin (Sirolimus). It interferes with the proliferation, growth and survival of tumor cells. In the present section, the results of the experiments performed with temsirolimus will be explained and its effect on yeast cells will be discussed.

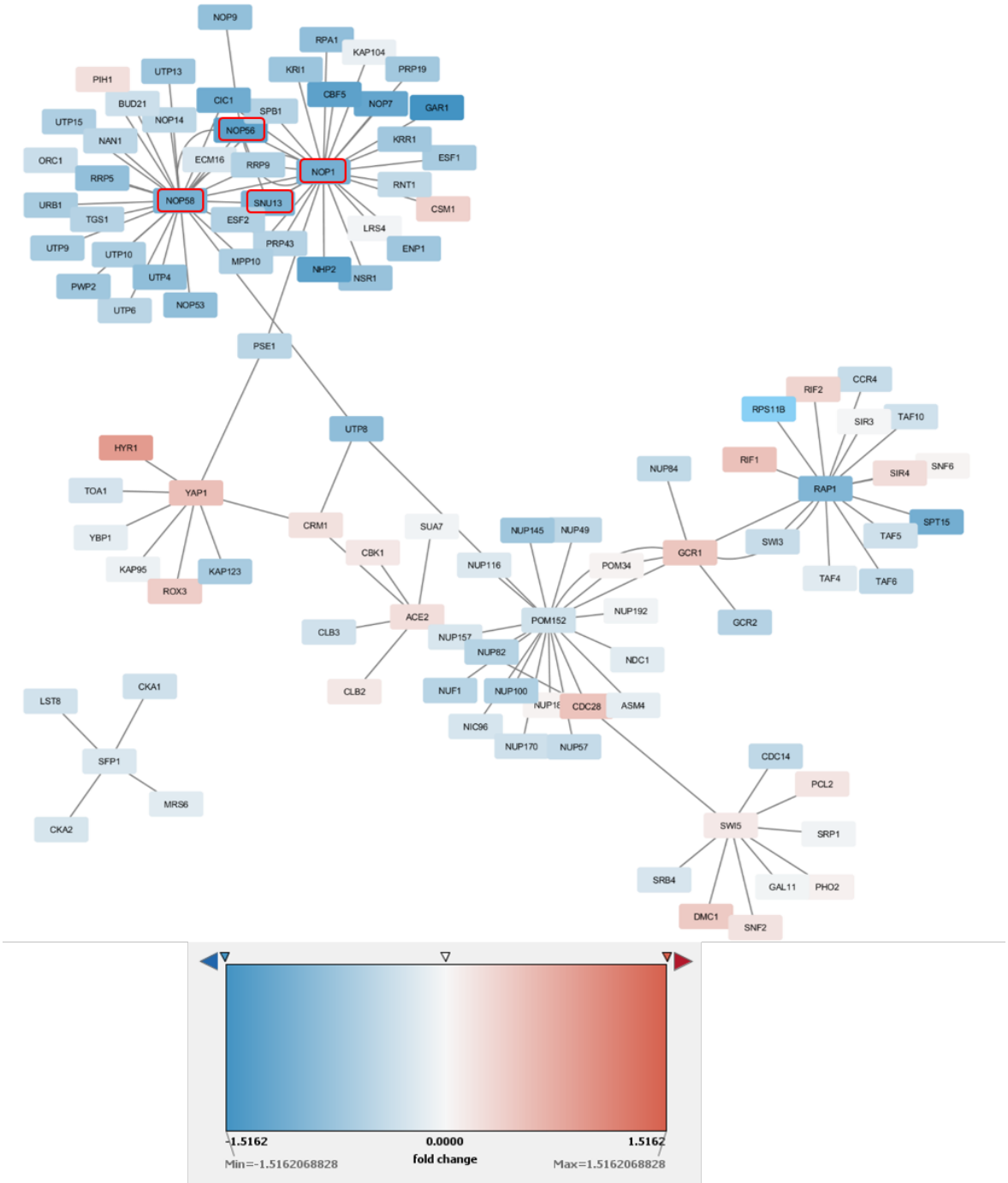

Figure 4.79. Interaction of all TFs and NOP56 and the expression fold changes.

YLR197W/ NOP56	YGR264C/ MES1	YJR070C/ LIA1	YOR335C/ ALA1	YGR265W	YDL208W/ NHP2	YBR121C/ GRS1	YDL051W/ LHP1	YIL078W/ THS1	YPR069C/ SPE3	YJR063W/ RPA12	YOL097C/ WRS1
Sfp1p	Sfp1p	Yap5p	Reb1p	Rox1p	Yox1p	Abf1p	Cbf1p	Rpn4p	Gcn4p	Sfp1p	Sfp1p
Rpn4p	Hap1p	Yap1p	Yox1p	Rpn4p	Sfp1p	Mig1p	Tye7p	Arr1p	Sfp1p	Abf1p	Ndt80p
Arr1p	Ume6p	Sfp1p	Aft1p	Arr1p	Abf1p	Sfp1p	Met4p	Sfp1p	Ste12p	Gcn4p	Arr1p
Yap1p	Yap1p	Msn2p	Ndt80p	Ste12p	Aft1p	Rap1p	Sfp1p	Ste12p	Yap1p	Gln3p	Bas1p
Met4p	Hap2p	Met4p	Hap2p	Sfp1p	Msn2p	Yap1p	Gln3p	Ndt80p	Ndt80p	Cad1p	Cbf1p
Oaf1p	Cst6p	Ndt80p	Mal33p	Cst6p	Gcn4p	Ndt80p	Gcn4p	Ume6p	Opi1p	Dal82p	Ecm22p
Pdr3p	Tup1p	Rox1p	Cst6p	Tup1p	Gln3p	Arr1p	Rdr1p	Hap2p	Arr1p	Haa1p	Fkh2p
Gcn4p	Gcr1p	Bas1p	Tup1p	Hsf1p	Cin5p	Bas1p	Rtg3p	Cst6p	Cbf1p	Hap2p	Gcr2p
Gln3p	Hsf1p	Fkh2p	Cup9p	Met31p	Reb1p	Ecm22p	Urc2p	Tup1p	Gcr2p	Yap5p	Haa1p
Arg80p	Sok2p	Gcr2p	Gcr1p	Yox1p	Cup9p	Fkh2p	Cst6p	Gcr1p	Ixr1p	Ace2p	Mga2p
Bas1p	Mig3p	Cst6p	Hsf1p	Yhp1p	Gal4p	Haa1p	Tup1p	Hsf1p	Mga2p	Aro80p	Mss11p

Figure 4.80. TF of the Genes.

	Genes	YLR197W /NOP56	YGR264C /MES1	YJR070C/ LIA1	YOR335C /ALA1	YGR265 W	YDL208W /NHP2	YBR121C /GRS1	YDL051W /LHP1	YIL078W/ THS1	YPR069C/ SPE3	YJR063W /RPA12	YOL097C/ WRS1	YER165W /PAB1	YBR143C /SUP45	YJR071W
TF	573	42	19	36	20	16	26	30	17	20	29	29	31	17	18	18
Sfp1p	22	1	1	1	1	1	1	1	1	1	1	1	1	1	1	1
Cst6p	21	1	1	1	1	1	0	1	1	1	1	1	1	1	1	1
Tup1p	19	1	1	1	1	1	0	1	1	1	1	0	1	1	1	1
Yap1p	18	1	1	1	0	0	1	1	1	1	1	1	0	1	1	1
Gcr1p	18	1	1	1	1	0	0	1	0	1	1	1	1	1	1	1
Ace2p	16	1	1	1	1	0	1	1	1	1	1	1	1	1	0	0
Swi5p	15	1	1	1	0	0	1	1	1	1	1	1	1	1	0	0
Hsf1p	14	1	1	1	1	1	0	0	0	1	1	0	0	1	1	0
Rap1p	13	1	0	1	1	0	0	1	0	1	1	0	0	1	0	0
Abf1p	13	1	1	1	0	0	1	1	1	0	0	1	0	1	1	0
Hap2p	12	1	1	0	1	0	0	1	0	1	0	1	0	1	1	0
Ash1p	12	1	1	1	0	0	1	1	0	0	1	0	0	1	0	0
Sok2p	11	1	1	1	1	0	1	1	0	1	1	0	1	0	0	0
Gln3p	10	1	0	0	0	0	1	1	1	0	1	1	1	0	0	0
Ndt80p	10	0	0	1	1	0	0	1	0	1	1	0	1	0	1	0
Arr1p	9	1	0	1	0	1	0	1	0	1	1	0	1	0	0	0
Gcn4p	9	1	0	0	0	0	1	0	1	0	1	1	0	0	0	0
Fkh2p	9	1	0	1	0	0	0	1	0	0	0	0	1	0	0	0
Aft1p	9	1	0	0	1	0	1	0	1	0	1	0	0	0	0	0
Bas1p	8	1	0	1	0	0	0	1	0	0	0	0	1	0	1	1
Msn2p	8	1	0	1	1	0	1	0	0	0	0	0	0	0	0	1
Fkh1p	8	1	0	0	0	0	1	1	1	0	0	0	0	0	0	0
Spt23p	8	1	1	1	0	0	0	0	0	0	0	1	0	1	0	0
Rim101p	8	1	1	0	0	0	1	0	0	0	0	0	1	0	0	0
Reb1p	8	0	0	1	1	0	1	0	0	0	0	0	0	0	1	0
Skn7p	8	0	0	0	1	0	0	1	0	1	1	0	1	1	0	0
Met4p	7	1	0	1	0	0	0	0	1	0	0	0	0	1	0	0
Gcr2p	7	1	0	1	0	0	0	0	0	0	1	0	1	1	1	0
Mga2p	7	1	0	0	0	0	0	0	0	0	1	0	1	0	0	0
Yox1p	7	1	0	1	1	1	1	0	0	0	0	1	0	0	0	0
Ste12p	7	1	1	0	0	1	0	0	0	1	1	0	0	0	0	0
Mcm1p	7	0	0	1	1	0	0	1	0	1	0	0	0	0	0	0
Rpn4p	6	1	0	1	0	1	0	1	0	1	0	0	1	0	0	0
Msn4p	6	1	0	1	1	0	1	1	0	0	0	0	0	0	0	1
Zap1p	6	0	0	1	0	1	1	0	0	0	1	0	0	0	0	1
Yrm1p	6	0	0	0	0	1	0	0	0	0	0	1	0	1	1	0
Pip2p	6	0	0	0	0	0	1	0	0	0	0	1	0	0	0	1
Ume6p	5	1	1	0	0	0	0	0	0	1	0	0	1	0	0	1
Swi4p	5	1	0	1	0	0	0	0	0	0	1	0	1	0	0	1
Ixr1p	5	0	1	1	0	0	0	0	0	0	1	0	0	0	0	0
Cin5p	5	0	0	1	0	0	1	0	0	0	1	1	0	0	0	0
Gal4p	5	0	0	0	0	0	1	0	0	0	0	1	1	0	0	0
Haa1p	5	0	0	0	0	0	0	1	0	0	0	1	1	0	0	0
Oaf1p	4	1	0	0	0	0	0	0	0	0	0	0	1	0	0	1
Rtg3p	4	1	0	0	0	0	0	0	1	0	0	0	0	0	0	0
Stb5p	4	1	0	1	0	0	0	0	0	0	0	0	0	0	0	0
Yhp1p	4	1	0	1	0	1	0	0	0	0	0	1	0	0	0	0
Yap5p	4	0	0	1	0	0	0	0	0	0	0	1	0	0	0	1
Rox1p	4	0	0	1	0	1	0	0	0	0	0	0	0	0	0	1

Figure 4.81. TFs vs the Correlated Genes.

4.5.1. 400 μM Temsirolimus (3% Krytox, 1:1 dilution, RPL5:GFP, Jeffamine)

This experiment is done with GFP tagged RPL5 protein to investigate the effect of temsirolimus, by following the fluorescence and hence protein expression in EY0987 yeast strain. Surfactant concentration in oil phase is used as 3% and Jeffamine concentration is used 0.075% w/w in aqueous phase for two experiments. In both experiments, the results are contrary to expectations. The expectations were to stop growth and proliferation of the cells under temsirolimus treatment. However, when the cells were treated with temsirolimus, they proliferated much more than they were not under any treatment.

4.5.1.1. Yeast Density in Culture. For the first experiment, there are roughly 1.49×10^5 cells covered on the glass slide (2 μL of sample). In a 5 mL nutrient solution, there should be roughly 374×10^6 cells. For the second experiment, there are roughly 1.44×10^5 cells covered on the glass slide (2 μL of sample). In a 5 mL nutrient solution, there should be roughly 360×10^6 cells. Therefore, both cultures were diluted with the YNB medium at a ratio of 1:1.

4.5.1.2. Flow Rate and Droplet Size. For both experiments, first, the chip is filled with only oil and the air was taken out. Then, drug phase with a concentration of 0.4 μg/mL temsirolimus, was sent to the microfluidic system at 80 μL/h. After the system becomes stable, yeast solution was sent to the chip at 60 μL/h. It was assumed that the concentration of the drug phase is halved due to the mixing of the yeast phase. Time to time, yeast phase repressed the drug phase, so, most of the droplets were generated drug free. Also, after the droplets were generated and they moved to chambers, they coalesced with each other. The non-coalesced droplets were impossible to detect whether they were drug free or not. The diameter of the droplets which remained non-coalesced vary between 100 to 250 μm. Especially in the second experiment, there was discontinuous flow regime where the yeast phase and the drug

phase were meeting. So, the number of cells in the droplets in the second experiment was generally more than 1.

4.5.1.3. Single Cell Analysis. Most of the droplets merged with each other, nevertheless there were several droplets remained stable in both experiments. The pictures of the cells were taken after the 1^{st}, 2^{nd}, 3^{rd}, 6^{th} and 18^{th} hour of the treatment. The area of the cells and the integrated fluorescence density were obtained by using ImageJ program. A few cells for each experiment was processed for this study, however, more cells can be observed which are proliferated under temsirolimus treatment. Figure 4.82 and Figure 4.83 show the growth of the cells under temsirolimus treatment for the first and second experiments, respectively. In the first experiment (Figure 4.82), two cells

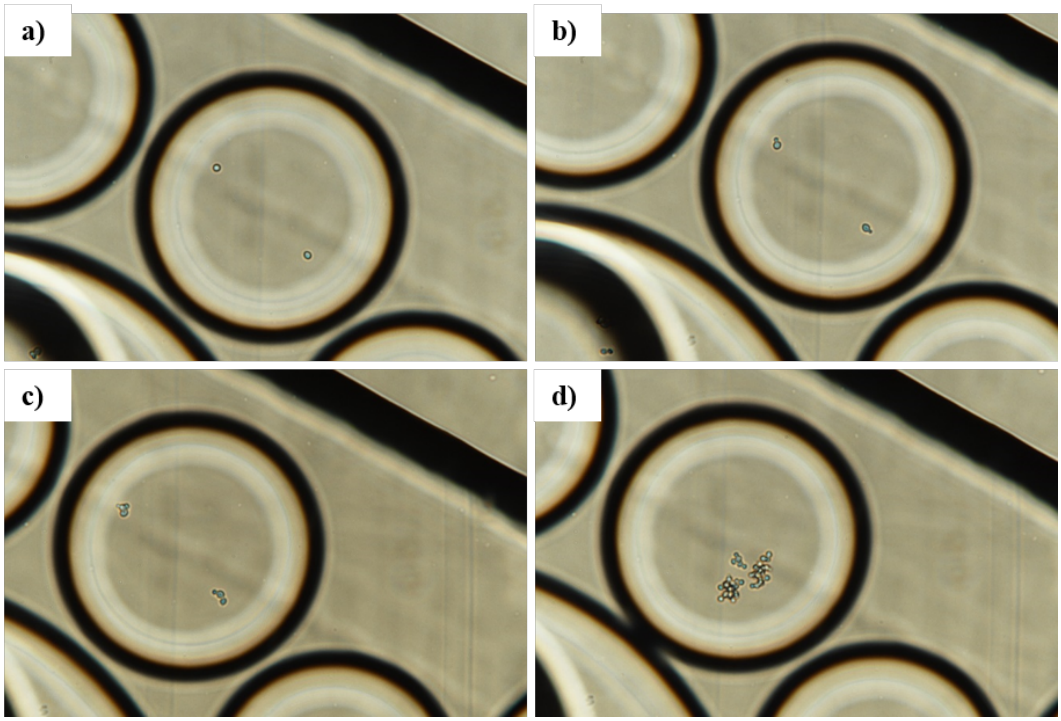

Figure 4.82. Cells in first experiment a) 1^{st} hour, b) 3^{rd} hour, c)6^{th} hour, d)18^{th} hour.

monitored in a droplet are given as a representative example of the whole chip. This droplet has 187.5 μm diameter. At the beginning of the treatment, there are two single cells, but after 3 hours of treatment, these single cells create bud. After 6 hours, the buds (daughter cells) separate from the mother cells and then, the mother cells create

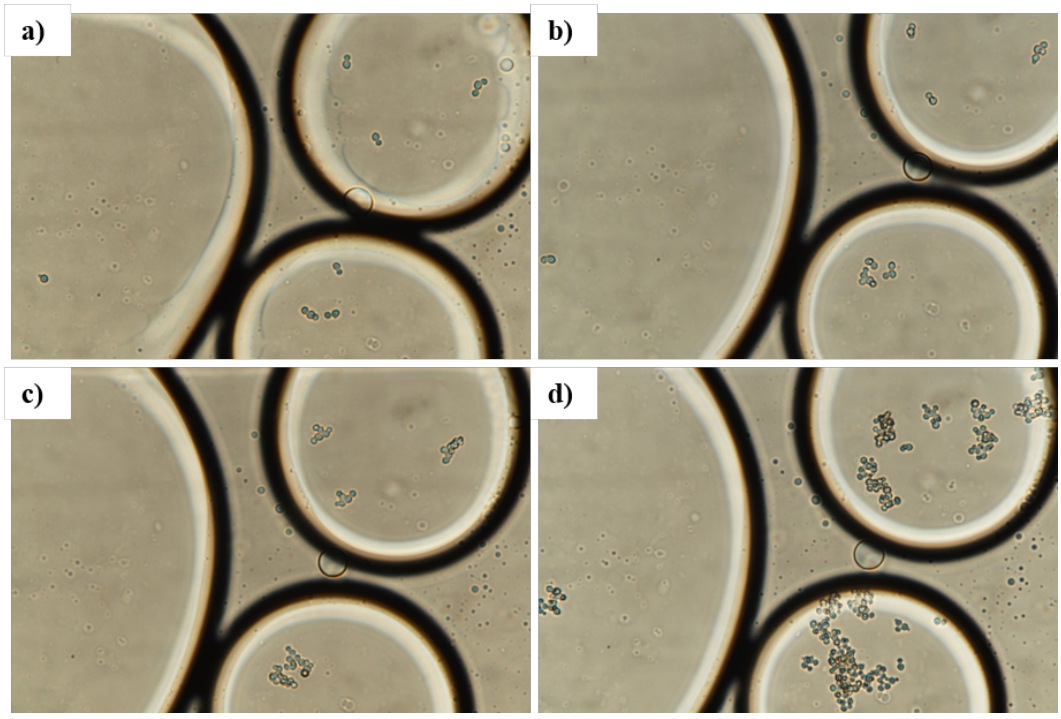

Figure 4.83. Cells in second experiment a) 1^{st} hour, b) 3^{rd} hour, c)6^{th} hour, d)18^{th} hour.

one more bud. Finally, after 18 of hours treatment, cells proliferate as if there is no treatment in the droplet. The proliferation can be explained by absence of drugs in the droplets. Similarly, in the second experiment (Figure 4.83), there are lots of cells in two different droplets. The upper droplet has 181.5 μm diameter and the lower droplet has 200 μm diameter. Cells in these droplets already have buds and, after three hours they proliferated more. Table 4.18 and Table 4.19 gives the area and the change of the area of the cells, respectively.

Table 4.18. Areas of the cells under temsirolimus treatment.

	1^{st} Experiment				
	1^{st} h (μm^2)	**2^{nd} h (μm^2)**	**3^{rd} h (μm^2**	**6^{th} h (μm^2)**	**18^{th} h (μm^2)**
11a	22.883	23.128	28.2142	49.4165	179.9525
11b-1	22.4077	23.0153	25.1076	28.6748	200.5962
11b-2				14.2786	
18a	26.4306	27.4449	32.2616	41.5569	110.7841
18b	14.6265	17.346	19.3893	28.7042	110.2598
18c	10.6575	14.5628	16.562	27.2342	57.1585
20a	31.409	33.614	35.8974	66.6057	250.684
	2^{nd} Experiment				
5a	34.5058	36.3776	45.8199	58.8294	282.8133
11a	32.2126	33.6042	47.8485	77.8365	932.0535
11b	39.8958	40.5279	67.8699	113.6898	

4.5.1.4. Integrated Fluorescence density of Cells (RPL5 Expression). Integrated fluorescence density for all measurements is obtained by using ImageJ program. These results are interpreted according to the raw data (Table 4.20 and 4.21). The results in the first experiment show that the fluorescence density of the RPL5:GFP increases during the treatment. On the other hand, the results in the second experiment show that the fluorescence density of the RPL5 decreases until the 18^{th} hour of treatment. There is an inconsistency between the two experiments.

Table 4.19. % changes in area relative to 1^{st} hour.

	1^{st} Experiment			
	1 to 2	**1 to 3**	**1 to 6**	**1 to 18**
11a	1.070664	23.29764	115.9529	686.4026
11b-1	2.711568	12.04898	27.96851	795.211
11b-2				
18a	3.837597	22.06155	57.23026	319.1509
18b	18.59296	32.56281	96.24791	653.8358
18c	36.64368	55.4023	155.5402	436.3218
20a	7.020281	14.29017	112.0593	698.1279
	2^{nd} Experiment			
5a	5.424595	32.78898	70.49134	719.6109
11a	4.320049	48.5397	141.6337	2793.444
11b	1.584377	70.11791	184.9668	

In the first experiment, the increase of the fluorescence density can be explained by great proliferation of the cells when it is assumed there is no drug entered to the droplets. This argument conflicts with the control experiments. In the control experiments (mentioned in part 4.1.3) the fluorescence density decreases until the 18^{th} hour. However, in this experiment, the proliferation of the cells is greater than the proliferation of the control experiment. Thus, this conflict may be ignored.

On the other hand, the result of the second experiment is similar to the control experiment. Thus, it can be said that the monitored droplets in the second experiment have no or trace amount of drug in it. Also, these results are consistent with those of the NOP56 protein.

4.5.2. 400 μM Temsirolimus (3% Krytox, 1:1 dilution, NOP56, Jeffamine)

This experiment is done with RFP tagged NOP56 protein to investigate the effect of temsirolimus, which is a rapamycin derivative, by following the fluorescence and hence protein expression in EY0987 yeast strain. The experimental conditions

Table 4.20. Integrated fluorescence density of cells (raw data).

	1^{st} Experiment				
	1^{st} h (μm^2)	**2^{nd} h (μm^2**	**3^{rd} h (μm^2**	**6^{th} h (μm^2)**	**18^{th} h (μm^2**
11a	379695	386070	367200	347820	2342175
11b-1	334560	276675	383775	549015	3520785
11b-2				258060	
18a	419220	304725	442935	693345	1667955
18b	196605	236130	271320	442425	983280
18c	153510	164475	182325	461295	494700
20a	405195	488835	506175	766785	3657465
	2^{nd} Experiment				
5a	482970	147900	101475	64260	6611895
11a	444720	343230	199665	146880	10111770
11b	578850	482460	385560	158355	

Table 4.21. % change in the fluorescence density compared to 1st hour (raw data).

	1^{st} Experiment			
	1 to 2	**1 to 3**	**1 to 6**	**1 to 18**
11a	1.678979	-3.2908	-8.3949	516.857
11b-1	-17.3018	14.71037	64.10061	952.3628
11b-2				
18a	-27.3114	5.656934	65.38929	297.871
18b	20.10376	38.00259	125.0324	400.1297
18c	7.142857	18.77076	200.4983	222.2591
20a	20.64191	24.92133	89.23851	802.6432
	2^{nd} Experiment			
5a	-69.377	-78.9894	-86.6948	1269.007
11a	-22.8211	-55.1032	-66.9725	2173.739
11b	-16.652	-33.3921	-72.6432	

are kept same as the other drug (HU) application experiments. Thus, 3% Krytox surfactant used in oil phase and 0.075% w/w Jeffamine is used in aqueous phase.

4.5.2.1. Yeast Density in Culture. There are roughly 2.16×10^5 cells covered on the glass slide (2 μL of sample). In a 5 mL nutrient solution, there should be roughly 541×10^6 cells.

4.5.2.2. Flow Rate and Droplet Size. First, the chip is filled with only oil to exit the air from chambers. Then, the aqueous phase which is yeast solution is sent to the chip at 60 μL/h flow rate while oil phase is sent at 800 μL/h flow rate. After the system becomes stable, drug phase is sent to the chip at 100 μL/h. Drug solution has to be sent to the chip at a higher flowrate than the aqueous phase to keep the system continuous and stable. When it is sent to system at 60 μL/h, continuity of the flow is broken and most of the droplets are generated drug free. The concentration of the temsirolumus is prepared as 0.4 μg/mL. It is assumed that the concentration of the drug is halved when the flow of the drug solution is mixed with the flow of aqueous phase so drug treatment (0.2 μg/mL) is applied to the cells. When all the phases are sent to chip, the droplet diameters vary between 100-200 μm.

4.5.2.3. Single Cell Analysis. Yeast cells were loaded to the microfluidic chip continuously by mixing them with the drug phase. Since loading of all the chambers takes time, the analysis started after 1^{st} hour of treatment. Then, the area and the integrated fluorescence density of the cells were obtained by image processing for the 2^{nd}, 3^{rd} and 6^{th} hour of treatment. 60 different cells had been identified in the droplets and they were examined throughout the experiment. Examples of the pictures of the cells are given in the Figures 4.84 - 4.86.

In chamber 6, 6 cells were investigated in two different droplets that have 153.57 μm and 175 μm diameter. 2 of them (red circles in the second droplet, called 6b-2 and 6b-3 from left to right) have already bud and these buds separated from the mother cell after 6 hours completely and they are called 6b-2-2 and 6b-3-2. Also, the dimension

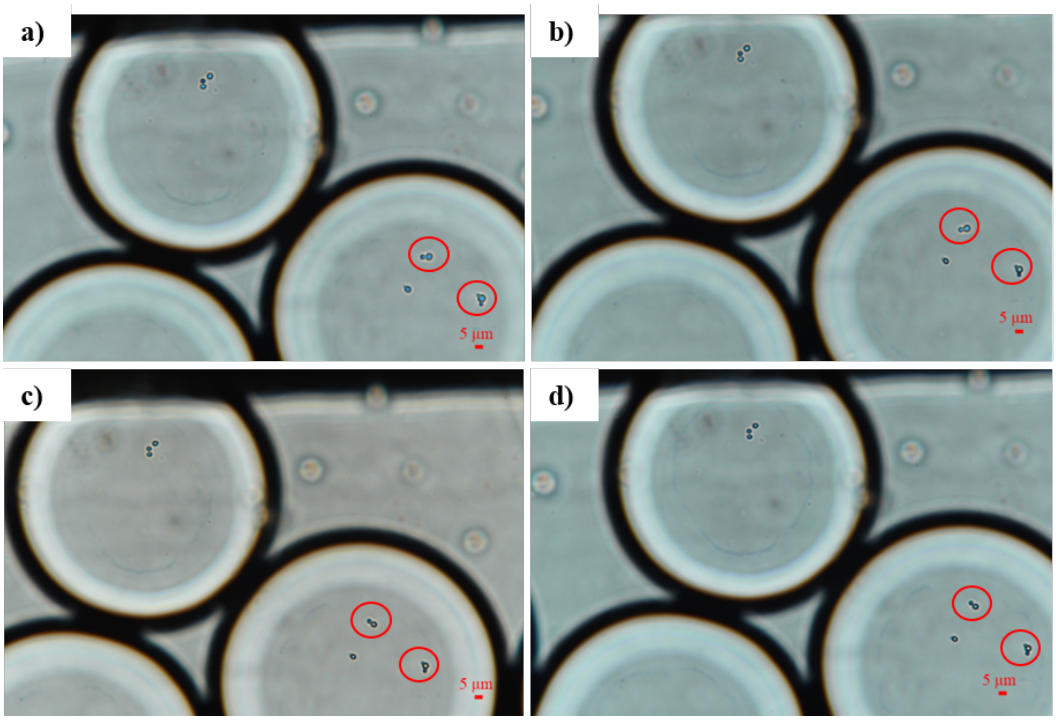

Figure 4.84. Droplets in Chamber 6 (a) 1^{st} hour, b) 3^{rd} hour, c)6^{th} hour, d)18^{th} hour).

of the cells was getting smaller by the time and they didn't create any further bud (Figure 4.84). This means, temsirolumus blocks the growth and proliferation of the cells.

In chamber 12 (Figure 4.85), four cells were investigated in two different droplets, which have 132 μm and 139 μm diameter, and one of them has bud which separated from mother cell at 3^{rd} hour of the treatment. It is seen that, all the cells shrunk by time under the temsirolumus treatment. Also, there were not any proliferation of the cells.

In chamber 19, 4 cells are investigated in two droplets that have 150 μm and 167 μm diameter, from left to right in the Figure 4.86. The morphology of these cells seem to change by time. They were affected by temsirolumus and they shrunk. The area and the integrated fluorescence density of all the 64 cells were analyzed by using ImageJ and the results are given as Tables 4.22 and 4.23, Tables C.1 to C.7 and Figure C.1 in Appendix C.

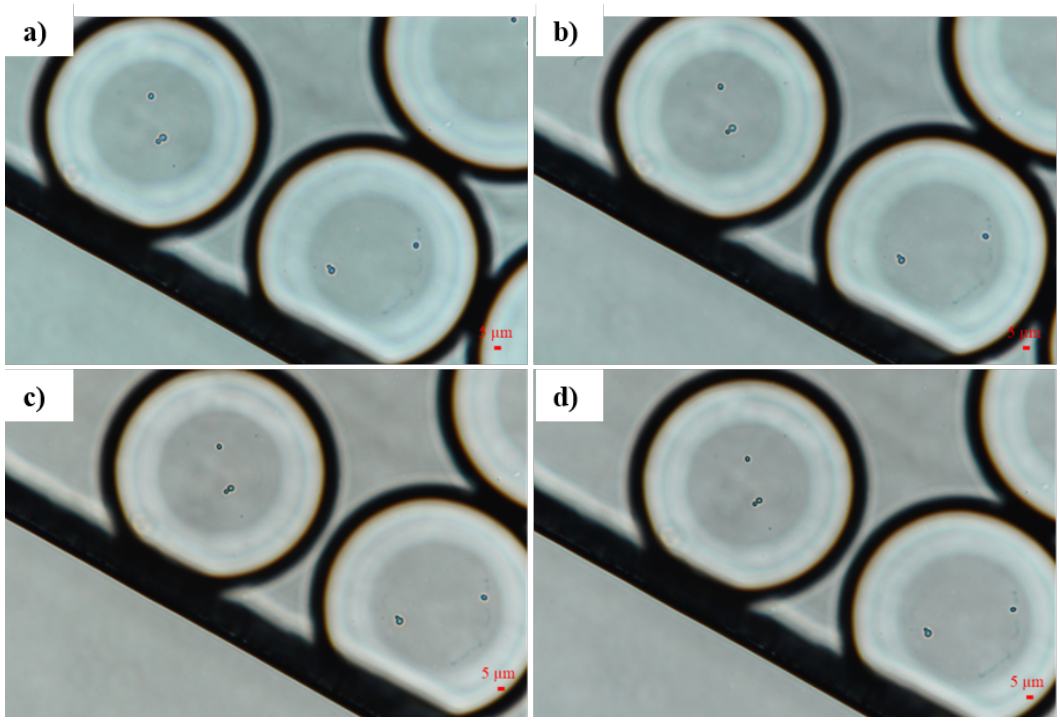

Figure 4.85. Droplets in Chamber 12 (a) 1^{st} hour, b) 3^{rd} hour, c)6^{th} hour, d)18^{th} hour).

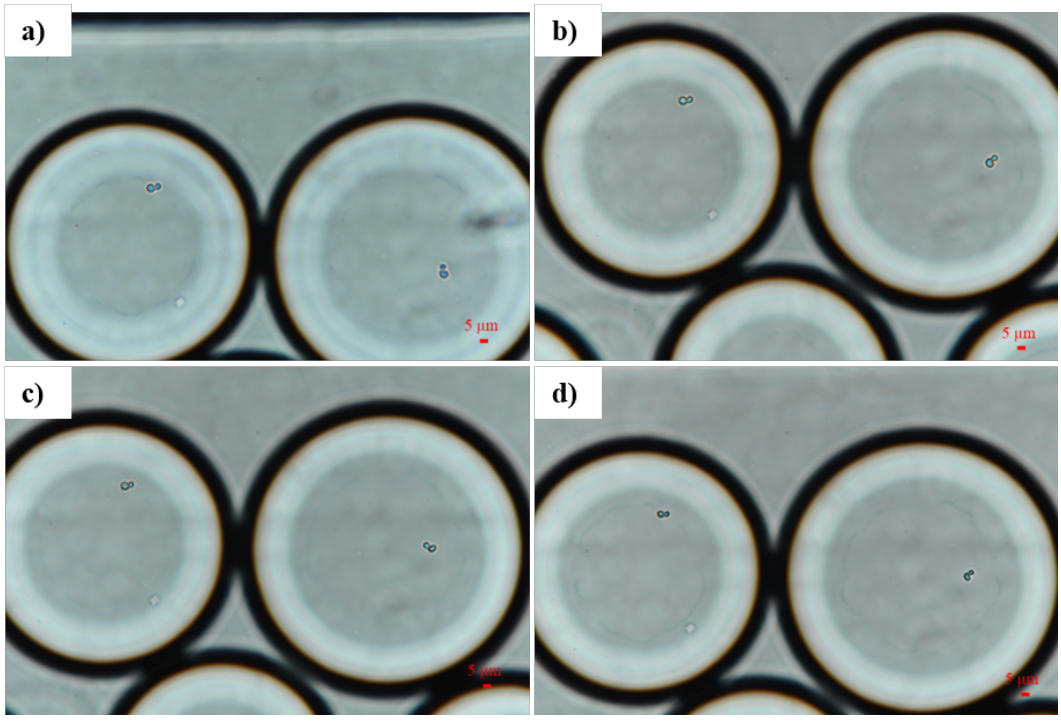

Figure 4.86. Droplets in Chamber 19 (a) 1^{st} hour, b) 3^{rd} hour, c)6^{th} hour, d)18^{th} hour).

4.5.2.4. Cell Dimension. After the image processing is done for all the cells, the area and the fluorescence density of the cells are compared with each other. The result of a measurement is compared with the result of the former measurement. It is seen that 12 out of 60 cells (20%) shrunk consistently. Only one cell slightly increases its area after 2 hours. This cell then shrunk after 3 and 6 hour of treatment. Area of 10 cells (16%) decrease after 2 hours of treatment, but slightly increase after 3 and 6 hours of treatment. Table C.1 shows the areas of the cells throughout the treatment while Table C.2 shows the comparison between the successive measurements, and Figure

Also, comparisons of the measurements according to the 1st hour of treatment are done. It is seen that 59 out of 60 cells (98%) shrunk after 2 hours of treatment compared to the first hour treatment. After 3 hours treatment, 56 cells (93%) have smaller area compared to first hour of treatment. Similarly, after 6 hours of treatment, 56 cells (93%) have smaller area compared to the first hour of treatment. Table 4.22 shows the comparisons of the measurements according to the first hour of treatment.

4.5.2.5. Integrated fluorescence density of cells (NOP56 expression). Integrated fluorescence density for all measurements is obtained by using ImageJ program. These results are interpreted according to the raw data and log2 base data. Fluorescence of 12 out of 60 cells decreased constantly durithe drug treatment. None of the cells emitted consistently increasing fluorescence. This result shows that treatment of temsirolimus has a negative effect on NOP56 expression at any time during treatment. 7 cells have smaller fluorescence after 2 hours treatment but then, their fluorescence increases until the end of the treatment. It can be said that, these cells are affected from temsirolimus only for 2 hours. The reason may be the lower molarity of the drug entered to the droplet when they are generated. Table C.3 shows the raw data of the integrated fluorescence density of the cells, Table C.4 shows the comparison between the adjacent measurements, and Figure 4.88 illustrates the change of the areas visually.

Also, comparisons of the measurements according to the 1st hour of treatment are done for the raw data of integrated fluorescence density data. 42 out of 60 cells

Table 4.22. % change in the area relative to 1^{st} hour of the temsirolumus treatment.

	1 to 2	**1 to 3**	**1 to 6**		**1 to 2**	**1 to 3**	**1 to 6**
1a-1	-15.5056	-4.33507	-6.42112	**12b-2**	-29.8774	-22.9264	-46.0485
1a-2	-12.4462	-38.9579	-34.2305	**13a-1**	-56.3528	-100	-55.6552
2a-1	-5.20679	-1.10682	3.449163	**13a-2**	-51.5853	-47.1294	-51.3282
2a-2	-2.2892	13.26633	-17.1357	**14a-1**	-18.4555	-12.3909	-11.1257
3a-1	-1.07724	8.287293	4.41989	**15a-1**	-22.5865	-15.2095	-13.9041
3a-2	-10.3594	193.3877	11.1413	**15a-2**	-16.3876	-73.7905	-74.6146
3b-1	-3.32223	4.013267	3.117745	**15a-2-2**			
3b-2	-19.576	-17.4253	-16.4868	**16a-1**	-15.7895	-16.5887	-13.0994
4a-1	-15.228	-33.8046	-31.3303	**16b-1**	-18.4317	-17.2471	-17.9815
4a-2	3.459249	-13.3419	-16.5429	**17a-1**	-24.2925	-18.5797	-20.7285
5a	-18.5046	-30.4641	-33.2485	**17a-2**	-27.5246	-23.7414	-37.8016
6a-1	-2.33406	-37.2863	-37.9411	**17a-3**	-18.3213	-17.9331	-22.7953
6a-2	-10.7304	-9.74212	-9.88539	**17a-4**	-24.2963	-22.7778	-18.1481
6a-3	-20.8455	-42.7152	-43.8328	**17b-1**	-29.2181	-29.2181	-20.3143
6b-1	-48.7315	-49.154	-45.215	**17b-2**	-44.8889	-41.9517	-40.7536
6b-2	-12.4855	-78.3429	-78.3984	**18a-1**	-13.9996	-9.74389	-7.79896
6b-2-2				**18b-1**	-14.2088	-16.9024	-15.4209
6b-3	-25.9419	-56.2019	-53.5136	**19a-1**	-15.5453	-21.5888	-47.6973
6b-3-2				**19a-2**	-24.4811	-42.3687	-49.6032
7a-1	-19.9593	-5.12188	-12.8973	**19b-1**	-11.2674	-40.2951	-47.1354
7b-1	-29.8843	-15.83	-38.2996	**19b-2**	-16.6667	-10.5413	-48.0769
7b-2	-11.6587	-41.3793	-43.4986	**21a-1**	-13.0692	-19.2696	-12.6962
8a	-21.1176	-38.1815	-44.9321	**21b-1**	-15.7525	-10.4079	-11.2799
9a-1	-49.0341	-22.7039	-30.5395	**21b-2**	-7.56303	-8.4267	-3.47806
9a-2	-38.6743	-54.7552	-54.5198	**21b-3**	-9.74659	-26.0234	-27.8265
10a-1	-47.6165	-34.139	-39.4092	**22a-1**	-20.8931	-18.4831	-33.2979
10a-2	-39.4705	-25.1852	-26.0784	**22a-2**	-46.7172	-47.2643	-40.0673
11a-1	-26.8485	-28.045	-13.474	**23a-1**	-21.531	-20.7707	-13.3402
12a-1	-29.4154	-43.0912	-52.9202	**23a-2**	-44.819	-39.2426	-33.9992
12a-2	-38.3526	-83.1954	-81.6558	**23b-1**	-11.2951	-13.9637	1.771337
12a-2-2				**24a-1**	-21.7789	-24.0629	-21.1877
12b-1	-32.5889	-20.5615	-22.8351	**24b-1**	-11.1336	-4.53009	-4.32725

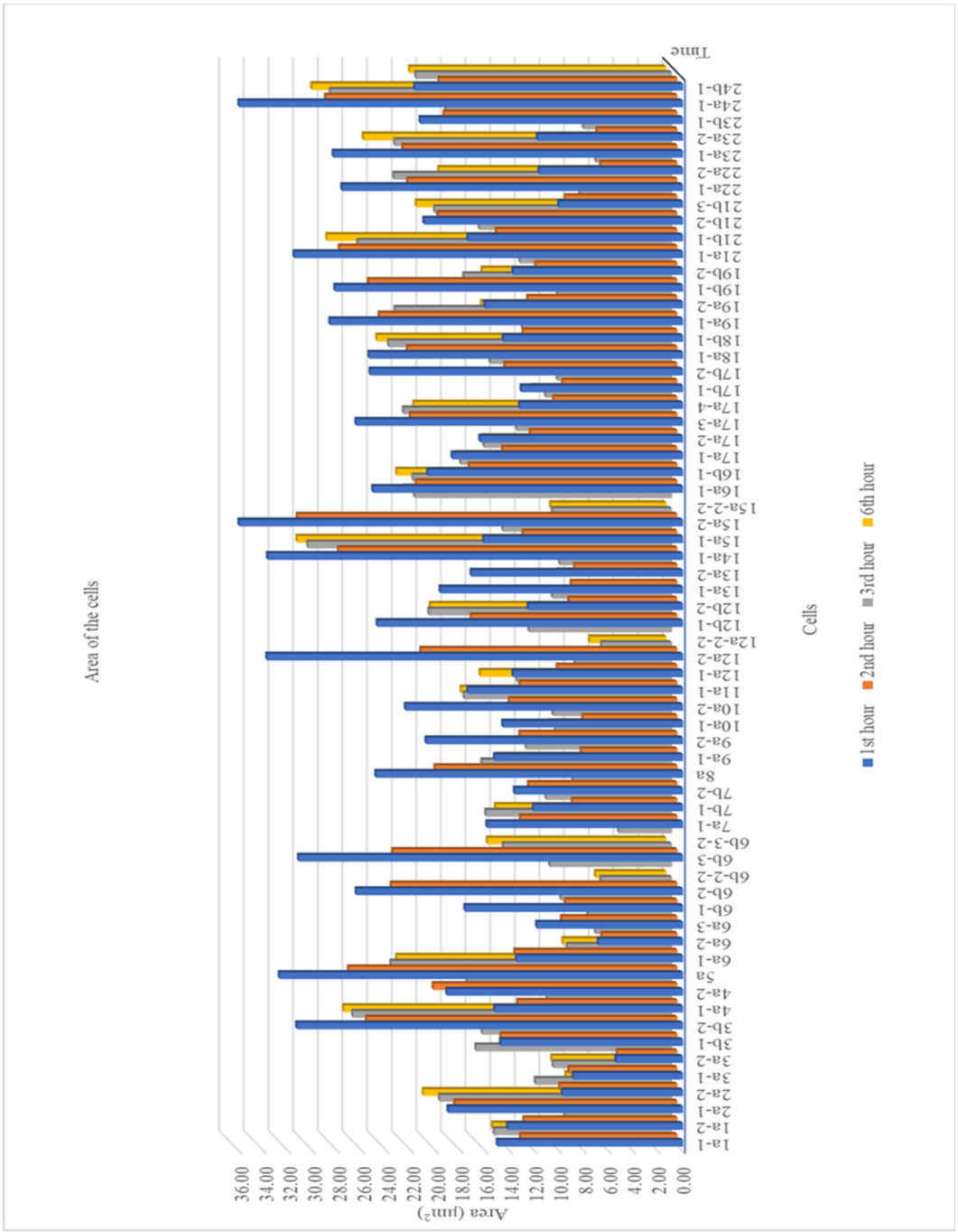

Figure 4.87. Time profile of the cell area during the temsirolumus treatment.

(70%) have lower fluorescence after 2 hours of treatment. After 3 hours of treatment, 52 of all cells (86%) have lower fluorescence density according to the first hour of treatment. Finally, 49 cells (81%) have lower fluorescence density after 6 hours of treatment. These results show that, all the cells are affected by temsirolimus for at least one hour treatment and the expression of NOP56 decreases. Table 4.23 shows the comparisons of the measurements according to the first hour of treatment.

Integrated fluorescence density is also investigated on log2 base. According to the results, change of fluorescence is not as dramatic as raw data. Fluorescence of 12 of 60 cells (20%) always decrease during the treatment. 6 cells (10%) have smaller fluorescence after 2 hours treatment but then, their fluorescence increases until the end of the treatment. This may be interpreted as these cells are affected from temsirolimus only for only 2 hours of treatment. Table C.5 shows the log2 base data of fluorescence density while Table C.6 shows the the comparison between the adjacent measurements, and Figure C.1 illustrates the change of the areas visually.

Also, comparisons of the measurements according to the 1st hour of treatment are done for the log2 base of integrated fluorescence density data. Fluorescence of 43 cells (71%) decrease after 2 hours of tretament. After 3 hours, 52 cells (86%) have less fluorescence density according to the first hour of trteatment. 49 cells (81%) have less fluorescence density according to the first hour of treatment at the end of the treatment. It can be concluded that from these results, temsirolimus treatment decreases the expression of NOP56 at some point of treatment. Table C.7 shows the comparisons of the measurements according to the first hour of treatment.

In Table 4.24, the number of the cells is given according to the change in cell dimension and fluorescence intensity during the temsirolimus treatment. The changes in the number of the cells are compared with the measurement of previous time, rather than comparing with the first hour of the temsirolimus treatment to indicate the change between the time intervals. The number of cells increasing in area and fluorescence are in agreement. Nevertheless, there are some fluctuations in data.

Table 4.23. % change in the integrated fluorescence intensity compared to 1^{st} hour of the measurement (raw data).

	1 to 2	**1 to 3**	**1 to 6**		**1 to 2**	**1 to 3**	**1 to 6**
1a-1	24.26667	-34.8	-10.9333	**12b-2**	-53.5211	-82.6291	-86.5415
1a-2	-29.8348	-37.1234	-31.2925	**13a-1**	27.60943	-100	16.16162
2a-1	0.113379	-27.2109	31.51927	**13a-2**	-3.92157	-4.05229	-16.4706
2a-2	24.67532	-24.531	-12.6984	**14a-1**	-52.856	-39.3584	-38.1455
3a-1	-7.61015	-9.74633	-3.20427	**15a-1**	27.68362	75.14124	-52.5424
3a-2	0	175.8542	-13.8952	**15a-2**	-4.32099	-64.3519	-81.1728
3b-1	44.42308	6.730769	110.3846	**15a-2-2**			
3b-2	-15.9398	-22.8571	-23.8346	**16a-1**	-16.5185	-13.037	-25.1852
4a-1	43.27869	17.54098	19.83607	**16b-1**	-28.3333	-22.6852	-64.1667
4a-2	-7.48201	-37.482	-30.7194	**17a-1**	-50.8621	-82.3755	-53.2567
5a	-24.7752	-18.0755	-23.1565	**17a-2**	-63.3181	-28.9193	-5.17504
6a-1	32.5779	-23.9377	-23.0878	**17a-3**	-55.0617	-37.9012	-7.90123
6a-2	-17.6101	-23.2704	-31.2369	**17a-4**	-90.6695	-80.057	-69.5157
6a-3	21.70543	-67.0543	-30.2326	**17b-1**	-58.7156	-58.002	-64.6279
6b-1	3.303685	-7.36976	5.082592	**17b-2**	-48.0494	-43.0123	-48
6b-2	-45.4373	-71.3561	-70.2788	**18a-1**	21.56309	-7.43879	-49.8117
6b-2-2				**18b-1**	-3.87016	-32.2097	-49.9376
6b-3	-25.7447	-40.7447	-31.0106	**19a-1**	-45.9495	-30.5888	-40.5489
6b-3-2				**19a-2**	6.242197	-14.1074	-28.7141
7a-1	-17.2043	-13.9785	-65.457	**19b-1**	60.30466	-10.9319	1.344086
7b-1	-15.1603	-32.5073	-17.7843	**19b-2**	-56.6971	-68.1887	-56.5449
7b-2	-2.45023	-3.52221	-10.4135	**21a-1**	-51.1001	-55.8856	-52.1452
8a	5.769231	-4.65976	3.994083	**21b-1**	-8.72274	-14.7456	-14.0187
9a-1	-17.9293	35.10101	51.51515	**21b-2**	19.89418	26.87831	-41.164
9a-2	-30.4714	-6.39731	2.020202	**21b-3**	-23.6559	-21.5054	2.329749
10a-1	-72.0564	-91.2106	-92.9519	**22a-1**	-25.3133	-71.345	-79.5322
10a-2	-69.8708	-82.9974	-88.6305	**22a-2**	-59.9696	-38.3562	-45.9665
11a-1	-36.9408	-43.7229	-13.4199	**23a-1**	-5.7971	-11.9807	-70.8213
12a-1	-59.7953	-73.538	-87.4269	**23a-2**	-56.6066	-44.5946	-50.9009
12a-2	8.256173	-79.321	-79.2438	**23b-1**	26.30385	10.77098	13.71882
12a-2-2				**24a-1**	-70.7736	-72.1745	-70.2642
12b-1	-75.1992	-88.6076	-88.2325	**24b-1**	-8.26211	29.91453	-5.27066

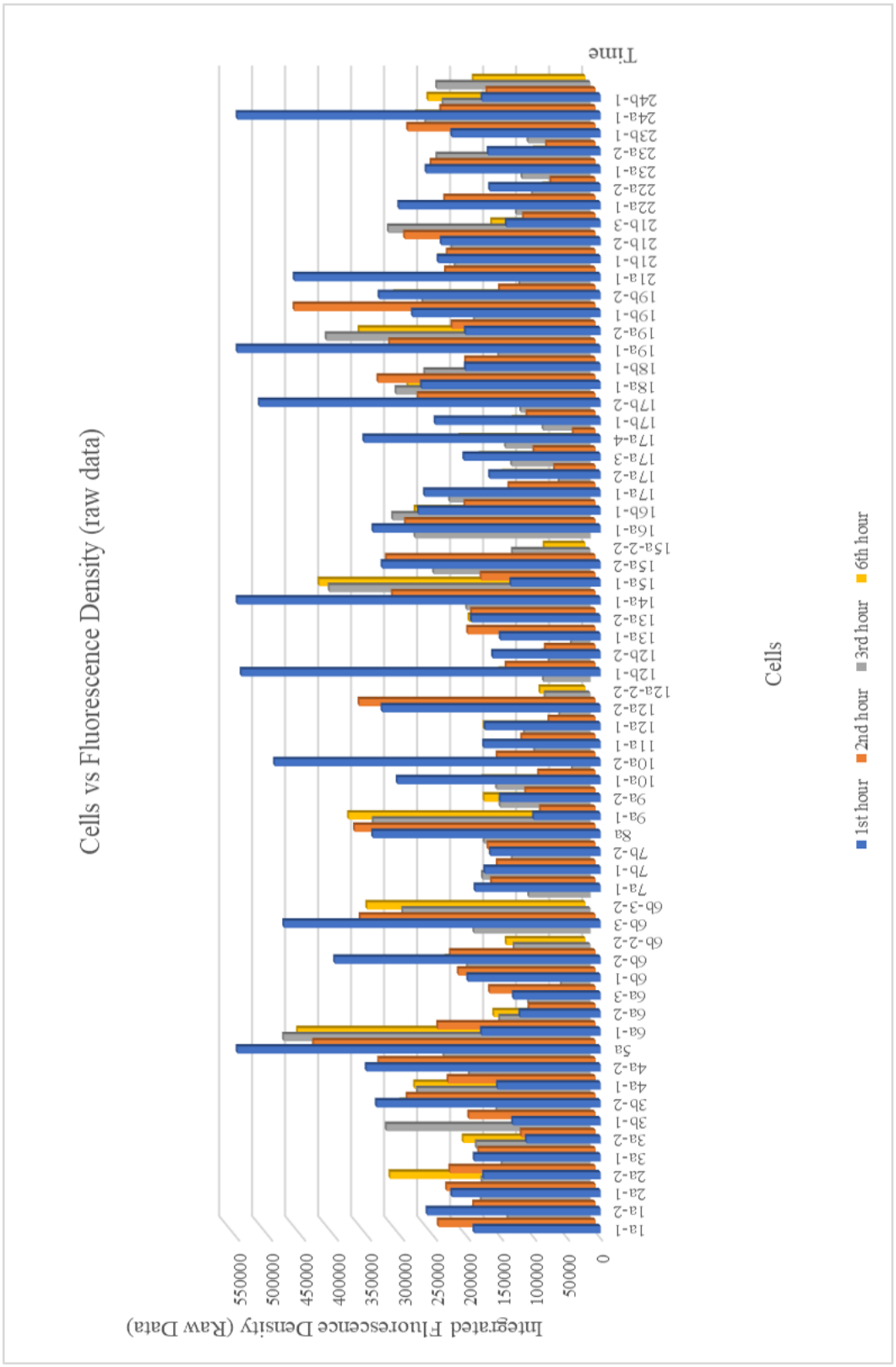

Figure 4.88. Fluorescence density of the cell vs time (raw data).

Table 4.24. Number of cells changing between the time intervals during temsirolimus treatment.

Time passed after HU treatment (hr)	**1 to 2**	**2 to 3**	**3 to 6**
Number of cells enlarged (10%)	0	10	4
Number of cells shrunken (10%)	52	18	13
Number of cells with no proper (continuously) information			1
Number of cells with Fluoresence density increased (raw data, 10%)	11	12	19
Number of cells with Fluoresence density decreased (raw data 10%)	33	29	24
Number of cells with Fluoresence density increased (log2 base, 10%)	0	0	0
Number of cells with Fluoresence density decreased (log2 base, 10%)	3	3	1

As the time goes, the effect of the temsirolimus decreases. This information is supported by both the decrease in the number of shrunken cells and by the increase in the number of cells with increasing fluorescence density (Table 4.24, line 2 and 4). The reason of the inconsistency between the changes of the cells may be the unequal amount of drug entered into the droplets. The cells can fight with the low amount of drug (less than 200nM of temsirolimus) for 3 hours and then, they may grow up again. When lots of drug (more than 200 nM of temsirolimus) enter into the droplet, the cell cannot fight, and shrink in size. This may also explain the similar behavior of the cells, which are in the same droplet.

4.5.2.6. The relationship between the fluorescence density and the cell area. Figure 4.89 shows the relation between the fluorescence density and the areas of the different cells at the same time points. For 1st and 2nd hours, the data show a reasonable agreement between the fluorescence density and the cell area (R^2=0.5415, R^2=0.5361). However, at the 3^{rd} and 6^{th} hours of temsirolimus treatment, the fluorescence density is not linearly dependent on area (R^2=0.3837, R^2=0.2255). Thus, it can be said that, for

the first two hours, area and the fluorescence density of the cells are proportionally correlated. However, this correlation is broken after 3 hours of treatment.

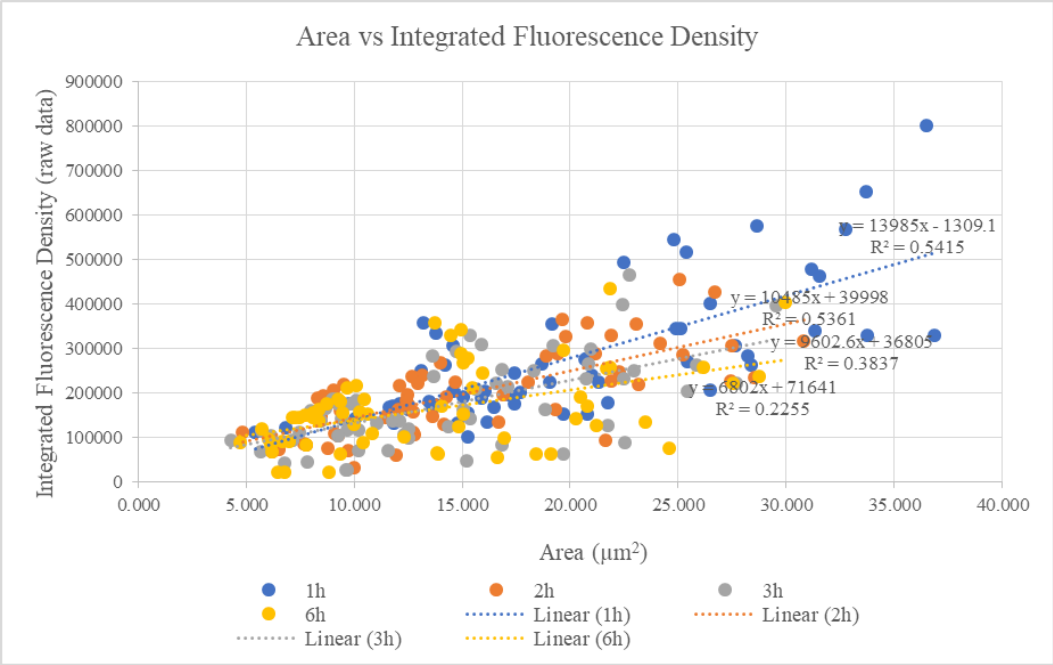

Figure 4.89. The change of fluorescence density by the cell area for each time sample.

4.5.2.7. Discussion. Temsirolimus (Toricel) inhibits the mTOR pathway and it also interferes with the proliferation, growth and survival of the tumor cells. Thus, whether tumor cell produces essential proteins needed for proliferation, growth, survival, and angiogenesis is determined by the activation of mTOR kinase protein in mammalian cells [38]. The results of the present study similarly show that temsirolimus decreases the growth and proliferation of yeast cells through inhibiting TOR kinase as well as affecting ribosome biogenesis. As a result of the decrease in growth, we speculate that the need for ribosome biogenesis and NOP56 expresison also decrease. NOP56 is a tightly regulated protein. When NOP56 levels are low, pre-rRNA biogenesis is compromised with a 3-fold increase in apoptotic cells. Conversely, when NOP56 was overexpressed for 24 hr, fewer cells in apoptosis or S-phase and an -2-fold increase in the number of cells in G2/M-phase were observed [72, 73]. Hence perturbations in NOP56 levels lead to altered ribosome biogenesis, localization, and cellular fitness.

In the Table 4.25, average areas and average area change of the cells are given. Table shows that;

- Average change of the areas under temsirolimus treatment is greater than the HU treatment.
- Average area of the cells under the temsirolimus and HU treatment decreases.
- Cells are more affected by temsirolimus treatment than they are affected by HU treatment.

Table 4.25. Average areas of the cells in different experiment.

NOP56	**CONTROL**	**TEMSIROLIMUS**	**HU**
1st (μ**m**^{2})	16.366	21.388	27.910
2nd (μ**m**^{2})	16.668	17.919	26.126
3rd (μ**m**^{2})	17.703	11.716	26.352
6th (μ**m**^{2})	18.877	10.423	24.059
18th (μ**m**^{2})	81.457		25.538
CHANGE (%)			
1 TO 2	2.661	-16.149	-5.547
1 TO 3	8.981	-42.961	-5.576
1 TO 6	14.935	-48.471	-14.843
1 TO 18	405.473		-7.796
CHANGE (%)			
1 TO 2	2.661	-16.149	-5.547
2 TO 3	6.397	-31.520	0.096
3 TO 6	5.799	-8.496	-7.491
6 TO 18	337.48		8.678

4.6. Coexpression Analysis for Rapamycin (Temsirolimus derivative) Treatment

In order to decipher the genes and their related functions, biological processes and cellular components in the cell in response to drug application a computational analysis is performed through SOM analysis. This computational analysis using gene

expression data reported in literature also help us understand what happens during the first hour of drug treatment as our experimental data in terms of cell dimension and fluorescence intensity could be obtained only from 1^{st} hour onwards.

Oliviera *et al.* studied rapamycin treatment on S. cerevisiae wild type strain YSBN6. During 120 minutes of treatment, expression data is obtained at -10^{th}, 3^{rd}, 7^{th}, 10^{th}, 14^{th}, 24^{th}, 56^{th}, and 120^{th} minutes. In the present thesis, temsirolimus, the water-soluble ester of rapamycin, is used as an inhibitor of mTOR kinase. The only difference between temsirolimus and rapamycin is that the temsirolimus molecule has an additional water-soluble group in a position unrelated to mTOR kinase activity [38,74].

4.6.1. SOM Analysis

Using the data obtained by Oliviera *et al.*, self-organizing maps are created by oposSOM package in Rstudio program. Analyses are done on these maps focusing on NOP56 and NOP58 genes. SOM analysis is expected to help understand what happens during the first hour of temsirolimus treatment, because experimental data are available after the first hour of treatment. Each tile in the SOM graph represents a metagene, which characterize the expression landscape of the gene dataset. Each metagene represents a cluster of single genes with similar, mostly highly correlated expression profiles. In this present case study, the dimension of SOM mosaics is created as 30x30, so there are 900 metagenes. In the maps, genes are always in the same metagene that they are placed. Population map in Figure 4.90 shows the population distribution among the metagenes. The results of SOM analysis are given in the following sections.

4.6.1.1. Expression Portraits. As can be seen in the expression portraits, the genes on the top right corner are underexpressed until the tenth minute of rapamycin treatment. At the same time, the genes at the bottom left corner are overexpressed. After 10 minutes rapamycin of treatment, genes at the top right start to be overexpressed while genes at the bottom left are underexpressed. Mentioned genes can be identified in the overexpressed and underexpressed spots (Figure 4.91).

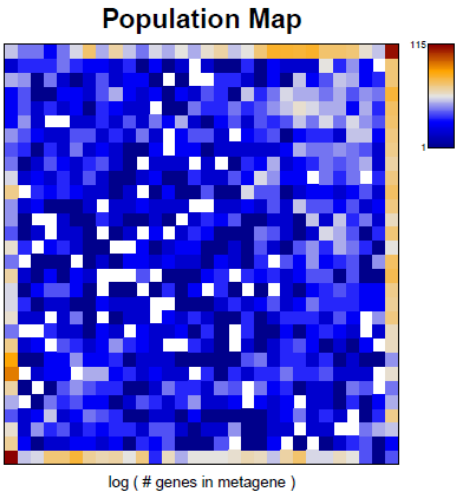

Figure 4.90. Population map.

4.6.1.2. Data Distribution. Expression data distribution can be seen in Figure C.3 in Appendix C. In general, any time during the rapamycin treatment, the genes are mainly expressed around 11.

4.6.1.3. Overexpression Spots. Following figures (Figure 4.92 and Figure 4.93) shows the overexpression summary map of three spots of strongly overexpressed metagenes at any time during the treatment. Also, the legend shows the gene enrichment of the spots, which may give idea about the biological context of the genes in the spots. In spot A, at the left bottom of the SOM graph, the genes are related to cytoplasmic translation and structural constituent of ribosome. Spot B, left bottom corner, is related to rRNA processing and ribosome biogenesis. Spot C, top right of the SOM, is related to oxidation-reduction process. NOP58 is in spot B and RPL5 is in spot A. NOP56 is close to spot B; but it is not included in spot B. The significant genes and their related functions, biological processes and cellular components in the cell in response to drug application are given in Tables C.8 to C.13 in Appendix C.

For the overexpression spots, the genes in spot A are overexpressed until the fourteenth minutes of rapamycin treatment. In this spot, there are 3 metagenes and 62 genes. When GO enrichment analysis is applied to these genes, the results show

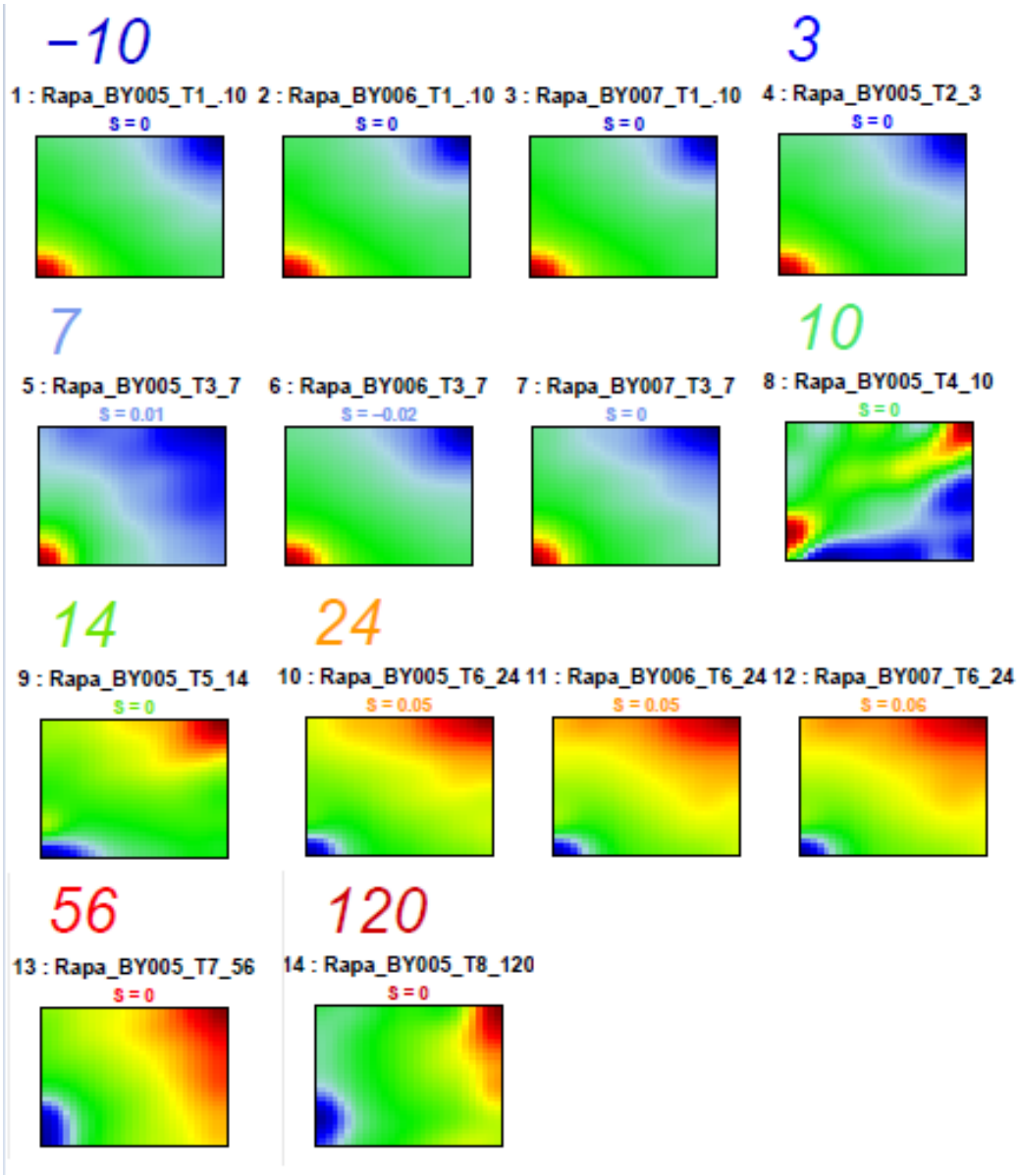

Figure 4.91. Expression portraits.

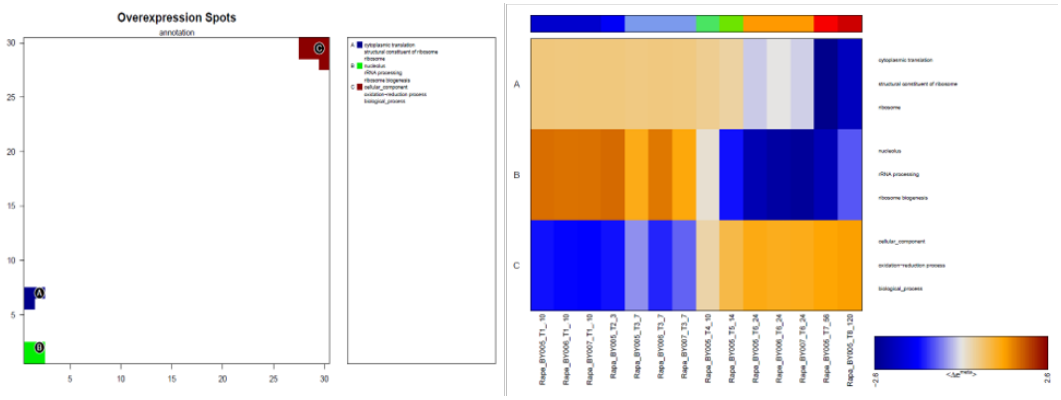

Figure 4.92. Overexpression spots and heatmap.

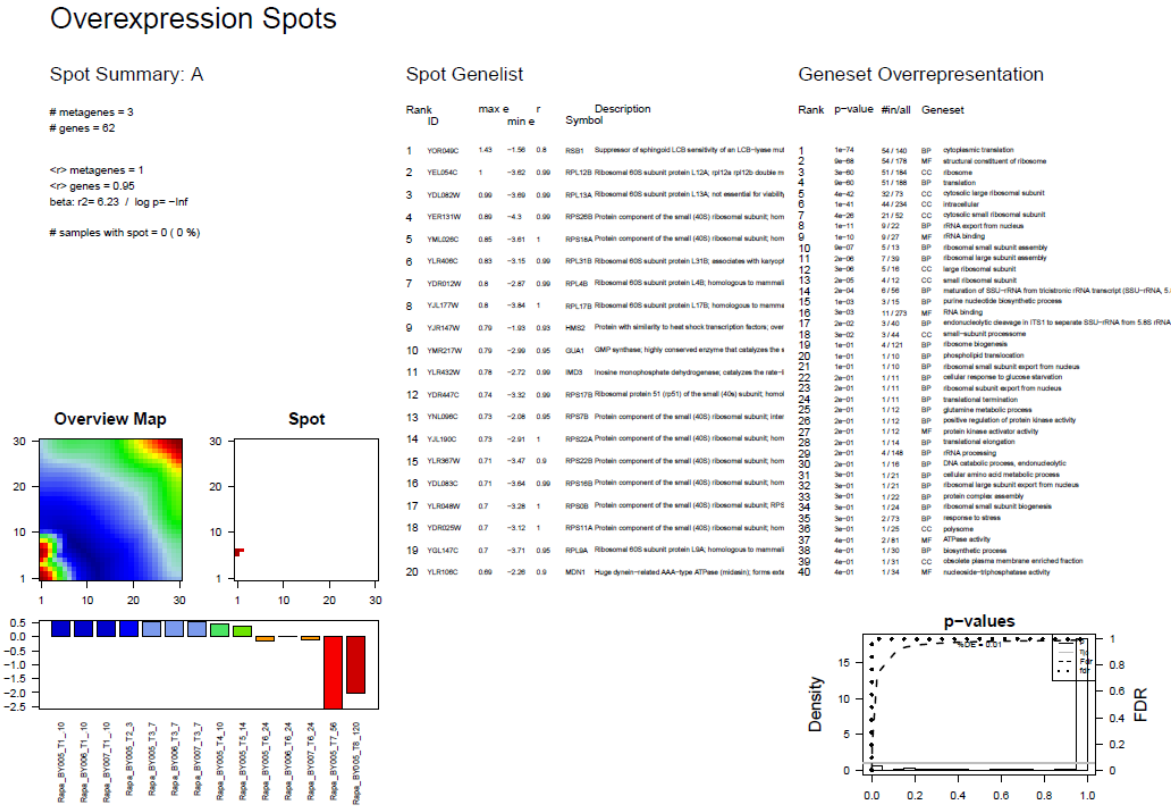

Figure 4.93. Overexpression spots report.

that they are related to cytoplasmic translation (BP), structural constituent of ribosome (MF) and ribosome (CC). Ranking is identified according to the maximum delta expression level. In spot B, there are 4 metagenes and 143 genes. The results of GO enrichment analysis of these genes show that they are related to nucleolus rRNA processing (BP) and ribosome biogenesis (BP). Genes in spot B are overexpressed especially until tenth minutes of treatment. NOP58 is available in this spot with a rank of 129. Although NOP56 is not included in any of the overexpression spots, it is so close to spot B. It may show overexpressed features of spot B. In spot C, there are 7 metagenes and 165 genes. The results of GO enrichment analysis of these genes show that they are related to cellular component and pre−autophagosomal structure (CC), oxidation reduction process (BP) and oxidoreductase activity (MF). The genes in spot C are overexpressed after the tenth minutes of treatment.

4.6.1.4. Underexpression Spots. Underexpression spots map shows the four spots that includes strongly underexpressed metagenes. Spot a, in the top right corner of SOM, is related to catalytic activity and late nucleophagy; spot b is related to mRNA cleavage and tRNA processing; spot c is related to rRNA processing and ribosome biogenesis and spot d is related to cytoplasmic translation and structural constituent of ribosome (Figure 4.94). Both NOP56 and NOP58 genes are included in spot c while RPL5 is placed in spot d. Especially 24^{th} minutes of the treatment, these genes are strongly underexpressed. Since the SOM package in RStudio does not provide the csv files of underexpressions (while running on data), NOP56 and NOP58 expression levels cannot be identified. However, from the reports generated by the software itself like Figure 4.95, the general features of spot c can be observed. In spot c, there are 8 metagenes and 172 genes. The results of GO enrichment of these genes show that they are related to nucleolus (CC), rRNA processing and ribosome biogenesis (BP). The genes in spot c are underexpressed after fourteenth minutes of treatment. The significant genes and their related functions, biological processes and cellular components in the cell in response to drug application are given in Tables C.14 and C.15 in Appendix C.

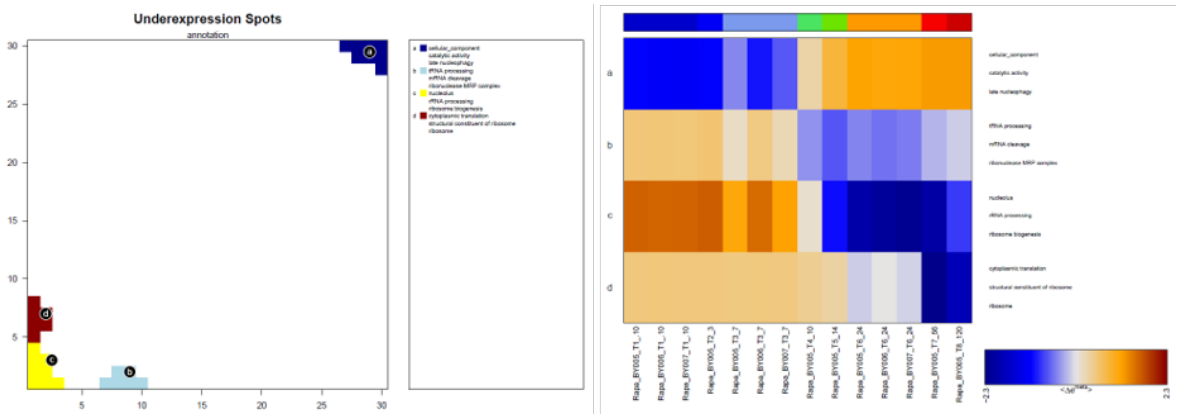

Figure 4.94. Underexpression spots and heatmap.

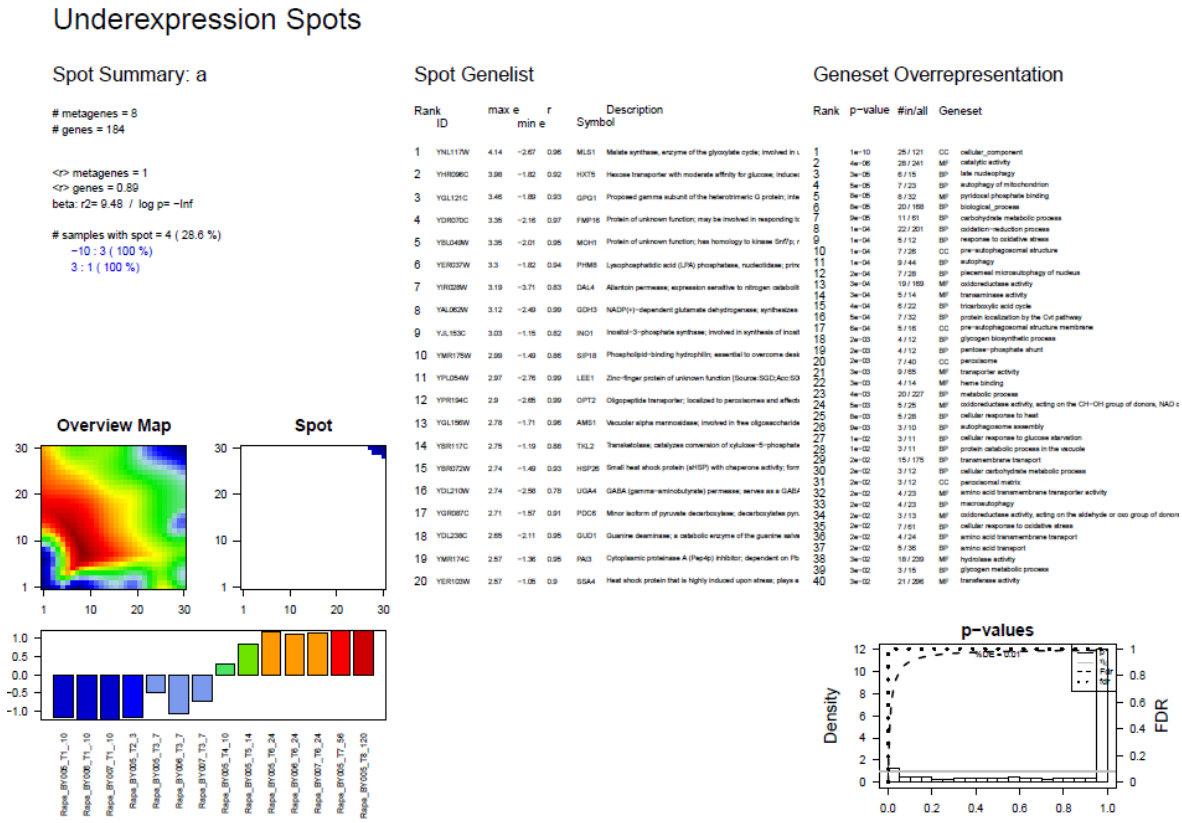

Figure 4.95. Underexpression spots report.

4.6.2. Geneset Z-score

Overrepresented gene sets are identified for each sample set (i.e. samples taken at -10 min, 7 min or 24 min). Overrepresentation of a gene set in a sample is calculated by using z-score statistics. The heatmaps are created according to biological process, molecular function and cell component. For same samples, such as -10 min, 7 min or 24 min, genesets rankings are similar and the GSZ-scores are really close to each other. The legend in the figures show the GSZ scores of the genesets.

For biological process (Figure 4.96), GSZ score of rRNA processing and ribosome biogenesis is at low levels at 24^{th} minutes of treatment, and at high levels at -10^{th} and 7^{th} minutes of treatment. Biological process of NOP56 is rRNA processing and NOP58 is endonucleolytic cleavage in 5'-ETS of tricistonic rRNA transcript. Thus, it can be said from the heatmap that both NOP56 and NOP58 have high GSZ score in the first 7 minutes of treatment.

For cellular component (Figure 4.97), GSZ score is especially low for nucleolus, but it is high for preribosome, large subunit precursor, small-subunit processome and 90s preribosome. GSZ-score of same cellular components are high at -10^{th} and 7^{th} minutes of treatment. Both NOP56 and NOP58 have the cellular component, which are nucleolus and 90S preribosome, and the heatmap also shows that the GSZ score of these cellular components are the highest scores.

For molecular function (Figure 4.98), GSZ score is especially low for RNA binding and snoRNA binding at 24^{th} min, furthermore it is low for ATP−dependent RNA helicase activity, nucleic acid binding, ATP−dependent helicase activity, DNA−directed 5'−3' RNA polymerase activity, RNA polymerase I at 24th minutes of treatment. GSZ-score of same molecular functions are high at -10^{th} and 7^{th} minutes of rapamycin treatment. Molecular function of NOP56 and NOP58 is mRNA binding and the highest GSZ score belongs to RNA binding. The top ten GSZ scores for samples are given in Tables C.16-C.18 in Appendix C.

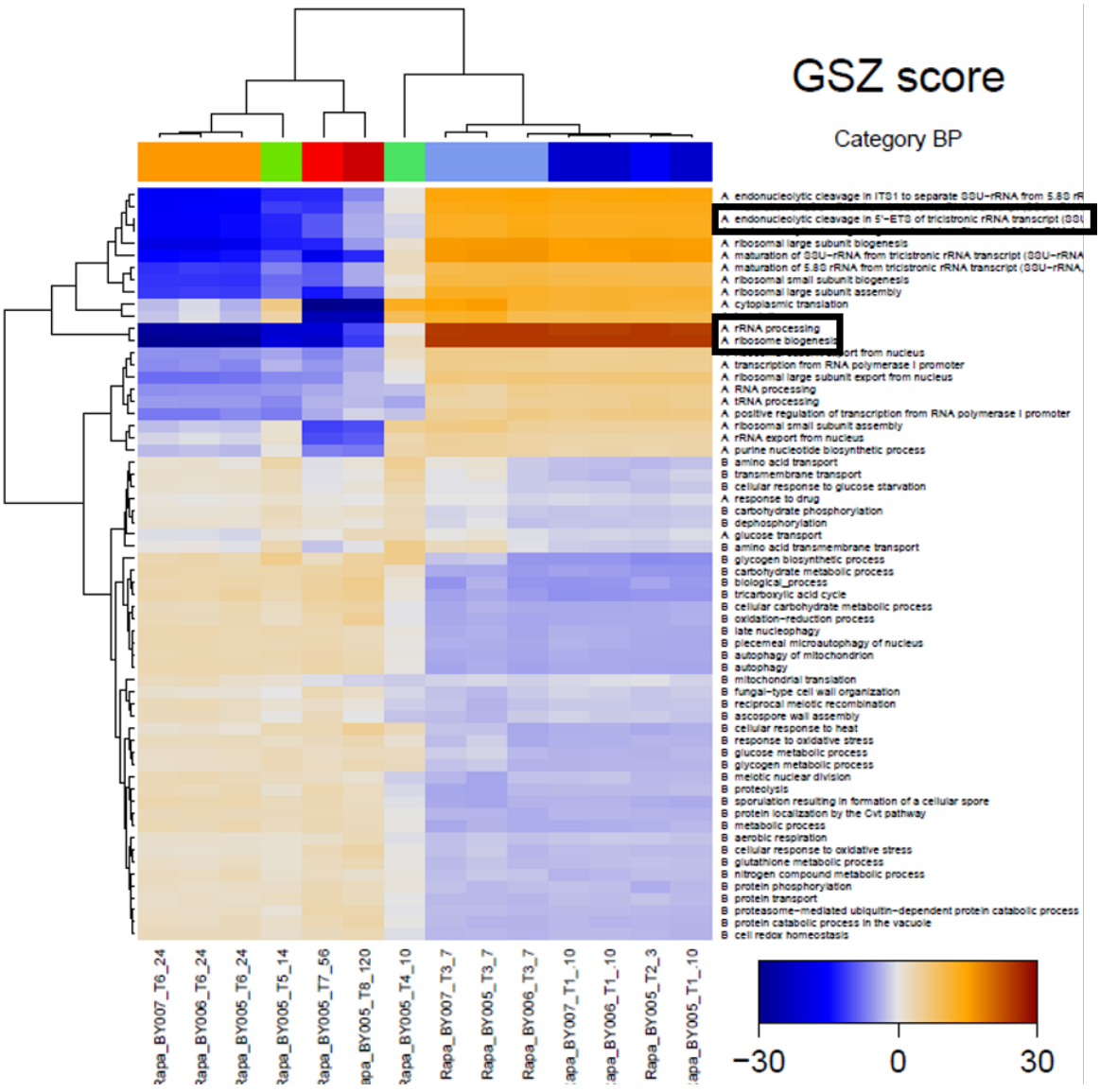

Figure 4.96. GSZ-score for biological process.

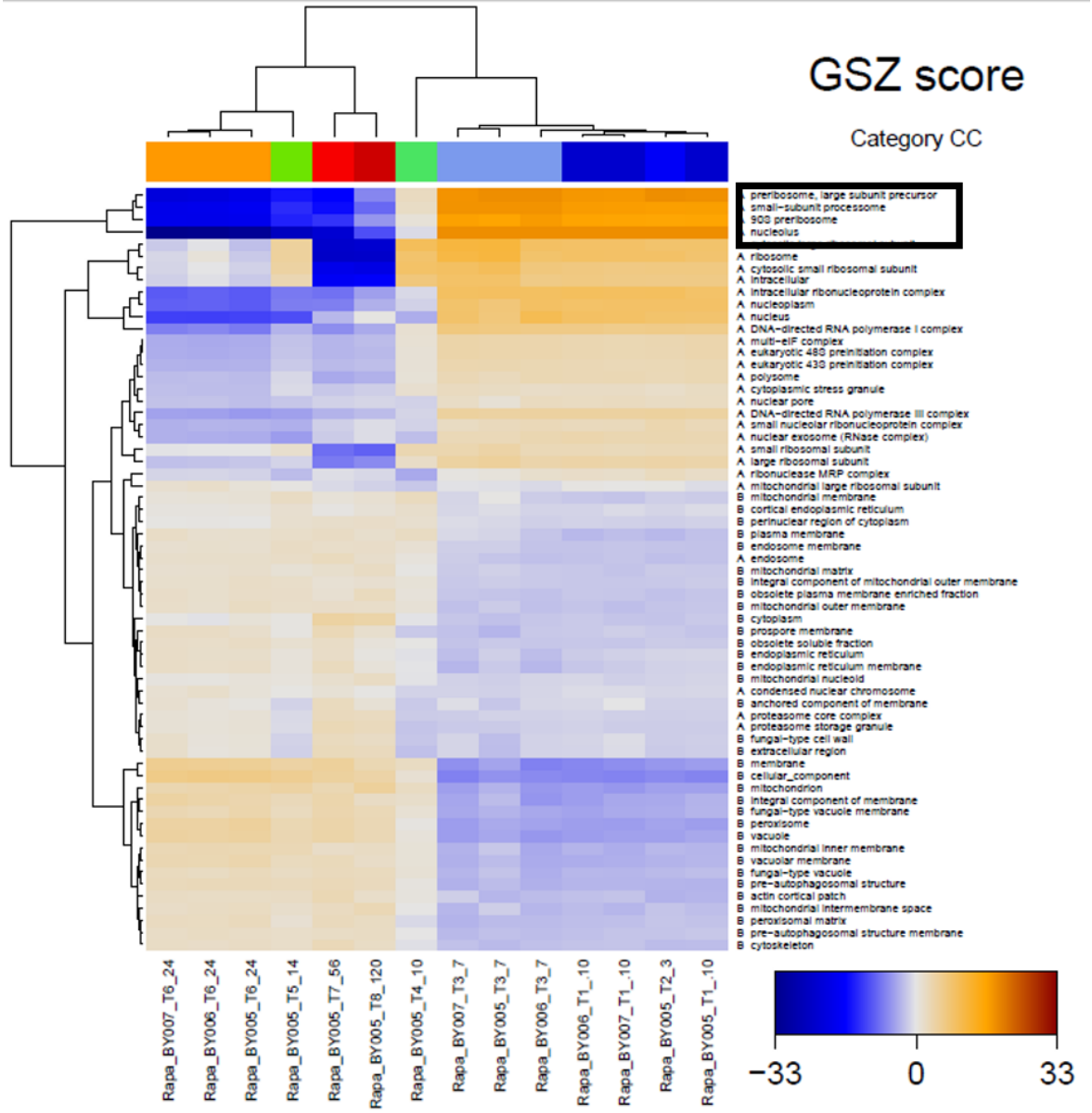

Figure 4.97. GSZ-score for cellular component.

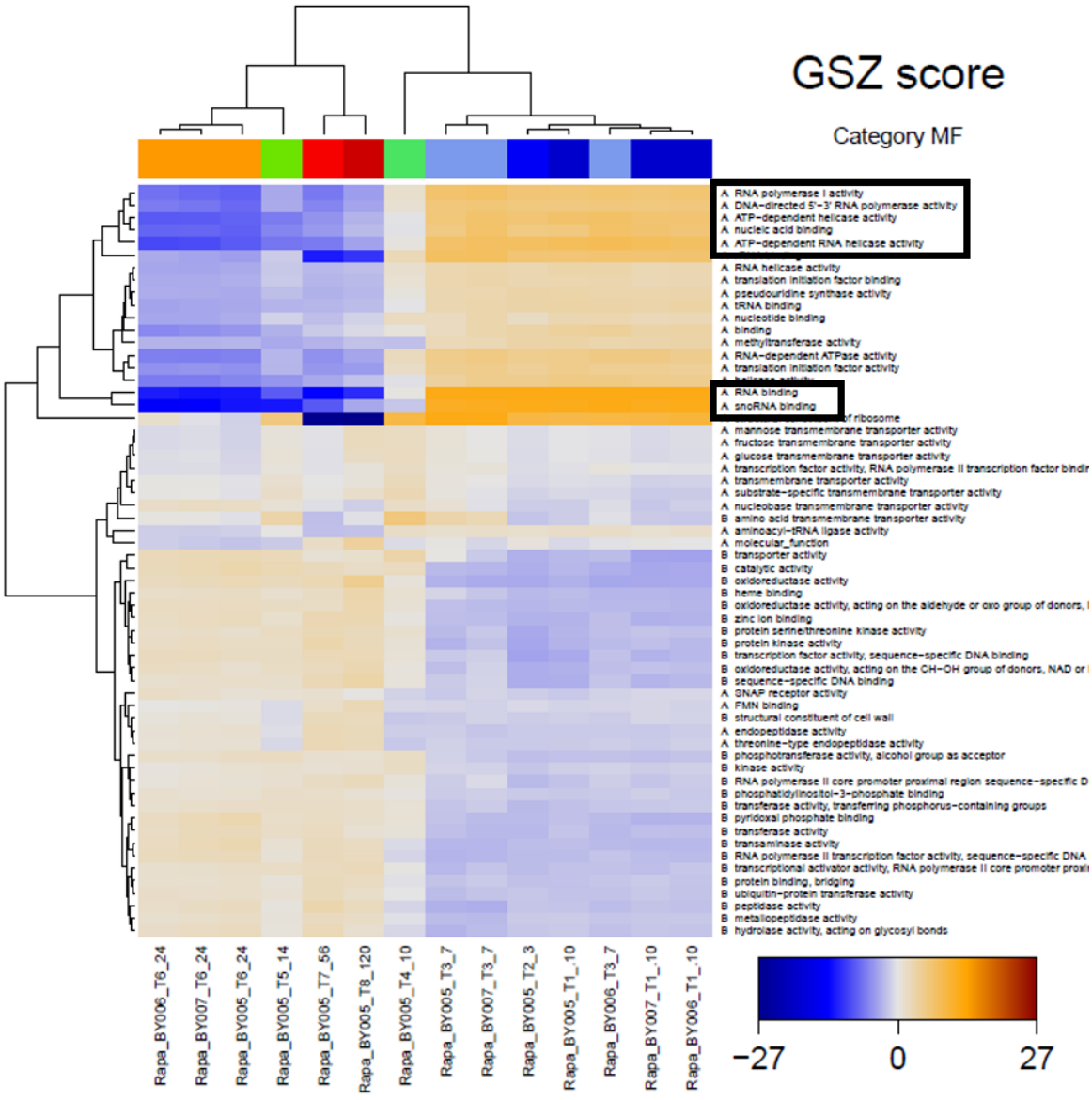

Figure 4.98. GSZ-score for molecular function.

The ribosome biogenesis under rapamycin treatment is specifically interpreted using the following graphs (Figure 4.99). After the 7^{th} minutes of rapamycin treatment, the genes, that are related to the ribosome biogenesis including NOP56 and NOP58, are affected by the drug rapamycin and are downregulated.

4.6.3. Clustering Approaches

Different clustering approaches such as D-clustering, K-clustering, Pearson clustering are used to group the gene expression data and estimate the relationship among the genes of interest and related pathways and finally the crosstalk among these pathways. Clustering methods and the related GO Terms for NOP56, NOP58 and RPL5 involved clusters are summarized in Table 4.29 at the end of the part 4.6.

4.6.3.1. D-Cluster. In cluster A, there are 282 genes and 24 metagenes. This cluster is created at the bottom left corner of the map (Figure 4.100). These genes are listed according to their max delta (final-initial exp) expression levels, and GO enrichment analysis results are given in Tables C.19-C.20 in Appendix C. Cluster A contains the underexpressed genes, and the top ten genes are given in Table C.19 in Appendix C. These genes are basically related to nucleolus (CC), ribosome biogenesis and rRNA processing (BP) and RNA binding and snoRNA binding (MF). NOP56 and NOP58 genes are in this cluster, Cluster A. However, they rank as 142 and 138, respectively. RPL5 is not involved in this cluster but it is placed close to this cluster.

Cluster B is defined at the top right of the map (Figure 4.100) and contains overexpressed genes. In this cluster, there are 20 metagenes and 299 genes. GO enrichment analysis is done to these genes and the results show that this cluster is related to cellular component, late nucleophagy and glycogen biosynthetic process (BP), and catalytic activity (MF). Top ten overexpressed genes are listed in Tables C.21-C.22 in Appendix C according to their max expression level and geneset overrepresentation.

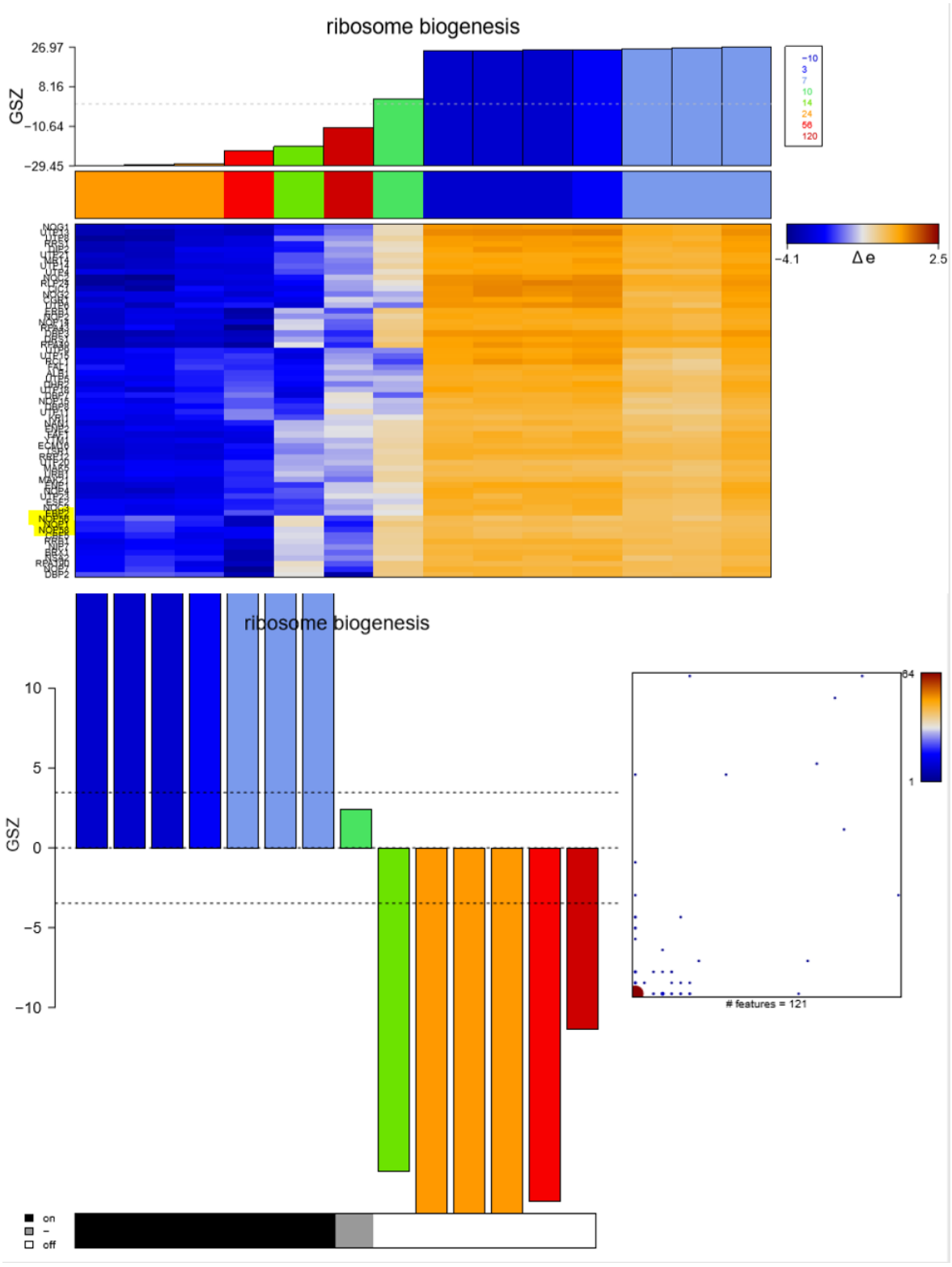

Figure 4.99. Geneset analysis-ribosome biogenesis.

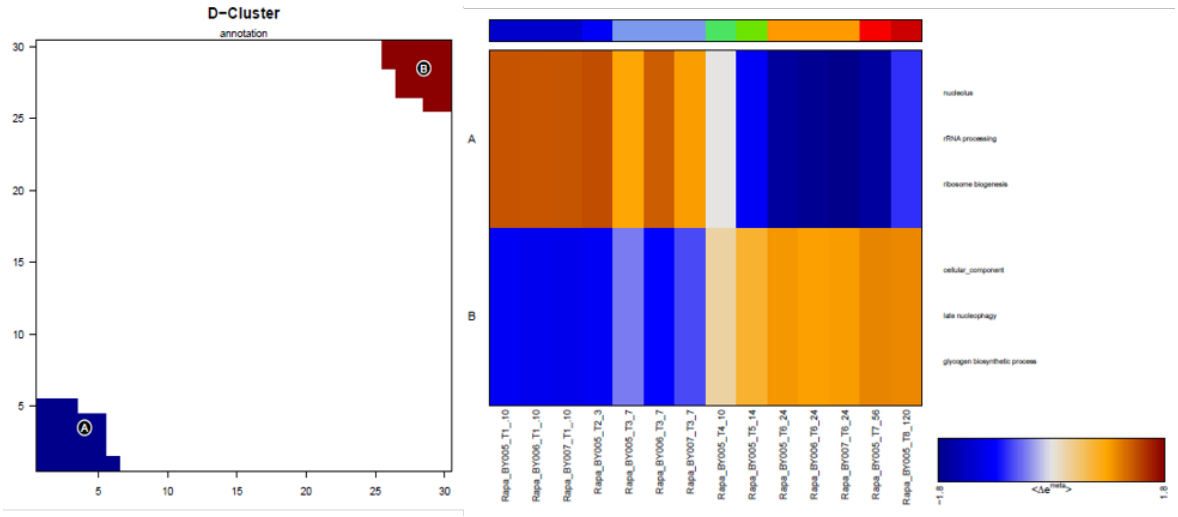

Figure 4.100. D-cluster spots and heatmap.

4.6.3.2. K-means Clustering. Alternative spots are created by using another clustering approach. K-means clustering groups genes according to their expression levels (the spot gene list is prepared according to the max expression level) and have an area-filling spot pattern. In this method, the number of clusters is set to 15, arbitrarily, to make the numbers of the metagenes in a spot close to each other. 15 random examples are initial centroids and these centroids create clusters by assigning each metagene to closest centroid. Then, 15 centroids are moved by averaging the metagenes in each cluster. Clusters are partly arranged based on the over- or under- expressions of metagenes. For example, in the overexpression map the spot B is related to ribosome biogenesis, in K-means clustering map the spot E is related to ribosome biogenesis. NOP56 and NOP58 genes are present in cluster E in K-means clustering while RPL5 is present in cluster A. When GO enrichment analysis is done on the cluster E, it can be seen that this cluster is mainly related to nucleolus, mRNA processing and ribosome biogenesis.

The top 5 genes in K-means Cluster A are given in Table C.23. The heatmap (Figure 4.101) shows the mean expression of the spots detected in all samples studied. Also, GO enrichment analyses are done for every cluster and the top three results

are given in Tables C.24 and C.26 in Appendix C. The results all of these clustering methods support each other.

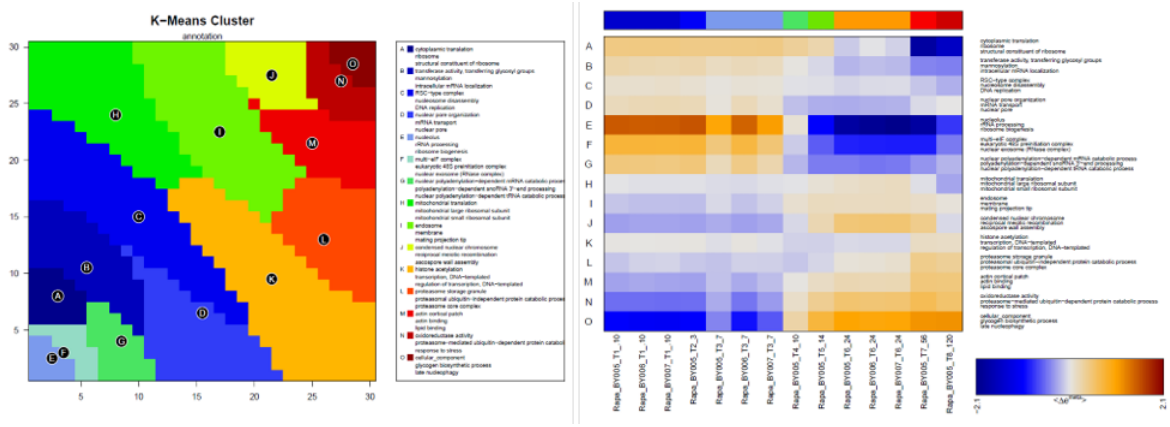

Figure 4.101. K-means clusters and heatmap.

4.6.3.3. Correlation Cluster – PCC. Acording to these clustering, clusters A to D are downregulated as the treatment time is increased. Contrarily, clusters E to J are upregulated as the time increase. OposSOM package in R studio gives the general reports but does not give the csv sheets, that includes all the genes and gene descriptions. Since the oposSOM package does not provide the csv files of correlation clusters while running on data, NOP56, NOP58 and RPL5 expression levels cannot be identified. However, from the reports, general features of spot c can be observed.

In general, correlation between the metagenes are higher than 0.9 while the correlation between the genes in the metagenes are low. Genes are placed in metagenes according to their expression profiles. It means, genes that are in different metagenes show different expression profiles. Thus, the reason of having low correlation coefficient between genes may be the different expression profile of each gene. On the other hand, mean expression level of the metagenes may be close to each other thus, their correlation coefficient is high.

NOP56, NOP58 and RPL5 genes are in **cluster A**. The metagenes in this cluster are highly correlated with each other; however, genes in this cluster are not highly

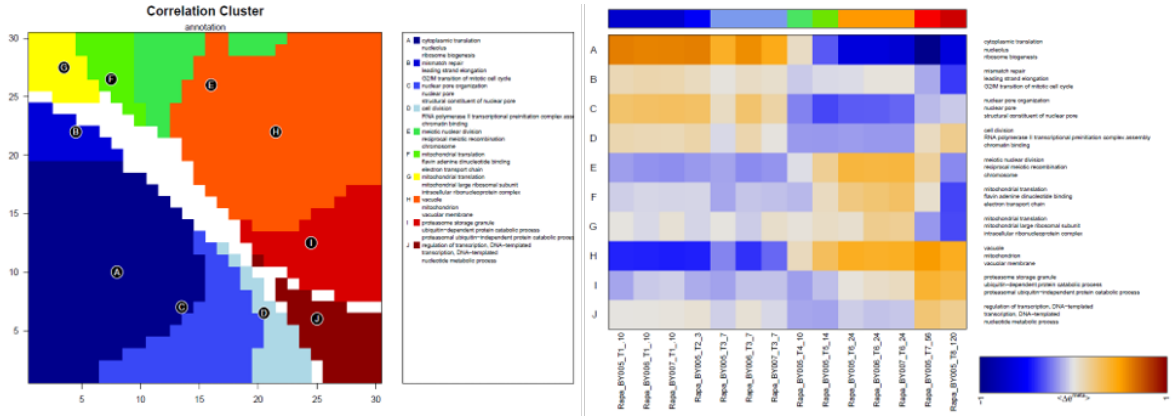

Figure 4.102. Pearson correlation clusters and heatmap.

correlated. Pearson correlation coefficient, r, is 0.94 for metagenes while it is 0.73 for genes individually. In this cluster, there are 225 metagenes and 887 genes. These genes are related to cytoplasmic translation (BP), nucleolus (CC) and structural constituent of ribosome (MF). *Cluster B* has 27 metagenes and 108 genes. The Pearson correlation coefficient of metagenes is 0.97, while that of individual genes is 0.50. *Cluster C* has 82 metagenes and 322 genes. Pearson correlation coefficient of metagenes is 0.97 while that of individual genes is 0.72. *Cluster D* has 31 metagenes and 126 genes. Pearson correlation coefficient of metagenes is 0.96 while that of genes is 0.53. This means, metagenes are highly correlated with each other in this cluster while the genes are not. According to the p-values of GO enrichment analysis, these genes are not correlated. Similarly, clusters E, F, G, H, I and J have Pearson correlation coefficient higher than 0.9 for metagenes while around 0.5 and 0.6 for individual genes. The results of GO enrichment analysis also show that the p-values of biological process, cellular component and molecular function of each cluster is low enough to say that these genes have little correlation. The significant genes and their related functions, biological processes and cellular components in the cell in response to drug application are given in Tables C.27-C.34 in Appendix C.

4.6.3.4. Genes Correlated with NOP56. There are 79 proportionally correlated genes with NOP56 which have Pearson correlation coefficient larger than 0.95 and there are 154 inversely correlated genes with NOP56 which have Pearson correlation coefficient

smaller than -0.95. Also, there are 19 highly proportionally correlated (Pearson correlation coefficient larger than 0.98) genes with NOP56 while there are 16 highly inversely correlated (Pearson correlation coefficient smaller than -0.98) genes with NOP56. The correlation is obtained from log2 expression levels of genes. Table C.35 in Appendix C shows the correlated genes with NOP56 according to their correlation order. Their related functions, biological processes and cellular components are given in Tables C.36-C.39 in Appendix C.

According to GO enrichment analysis, the genes that are correlated with NOP56 are in biological processes that are generally related to ribosome biogenesis. In SOM analysis, metagene that NOP56 is in it, also related with ribosome biogenesis. It can be concluded that, the results of both SOM analysis and correlated proteins, that are found by using Pearson Correlation Coefficient, satisfy each other.

For proportionally highly correlated genes, any significant biological process or molecular function cannot be found. However; several cellular components are specified (Table 4.26). For inversely highly correlated genes, any significant molecular function or cellular component term cannot be found. However, one biological process term (response to endoplasmic reticulum stress) is specified with a high p-value (Table 4.27).

Table 4.26. GO enrichment analysis for proportionally highly correlated genes.

Component		
GO_term	**Cluster frequency**	**p-value**
preribosome	7 out of 19 genes, 36.8%	9.83e-06
preribosome, large subunit precursor	4 out of 19 genes, 21.1%	0.00261
90S preribosome	4 out of 19 genes, 21.1%	0.00312

Two different heatmaps for highly correlated genes are created. First one (Figure 4.103) displays the expression levels of highly correlated genes. In the heatmap, samples (data taken after 3, 10, 14, ... minutes) are hierarchically clustered. Two-way clustering, which makes combined sample clustering with gene clustering, identifies the genes, that are the most important for sample clustering. According to the clustering,

Table 4.27. GO enrichment for inversely highly correlated genes.

Component		
GO_term	**Cluster frequency**	**p-value**
response to endoplasmic reticulum stress	4 out of 16 genes, 25.0%	0.00344

the data belonging to 24^{th} minutes and after, create one major cluster, and the data belonging to 14^{th} minutes and before creating another major cluster. It can be interpreted that the threshold is in between 14^{th} and 24^{th} minutes. Genes are also clustered to discover the co-regulated and functionally related genes.

Second heatmap (Figure C.3 in Appendix C) is also created according to the Pearson correlation coefficient of genes. This heatmap shows the pairwise correlation of highly correlated genes. Since these genes are highly correlated with a value higher than 0.95 or lower than -0.95, there seems to be only two colors which are red and blue, however, the colors slightly change. The diagonal has always value 1.

4.6.4. Response of Yeast Cells to Rapamycin (Temsirolimus)

In the mosaic SOMs, Nop56 is in the 1x3 metagene and NOP58 is in the 1x2 metagene. This means that these genes are on the bottom left corner of the maps. The genes in metagenes 1x2 and 1x3 are given in Table 4.28.

According to expression portraits, metagenes in the bottom left corner, which NOP56, NOP58 and RPL5 are involved in, are highly expressed until the 10^{th} minute of the rapamycin treatment. In the overexpression spots, only NOP58 gene is present in spot B and RPL5 is in spot A. In spot B, genes are overexpressed until 10^{th} minutes of treatment and in spot A genes are overexpressed until 14^{th} minutes of treatment. After that, these genes are downregulated. NOP56 gene is not in any overexpression spot, but it is in underexpressed spot c. So, it means NOP56 is strongly underexpressed after 10 minutes of rapamycin treatment.

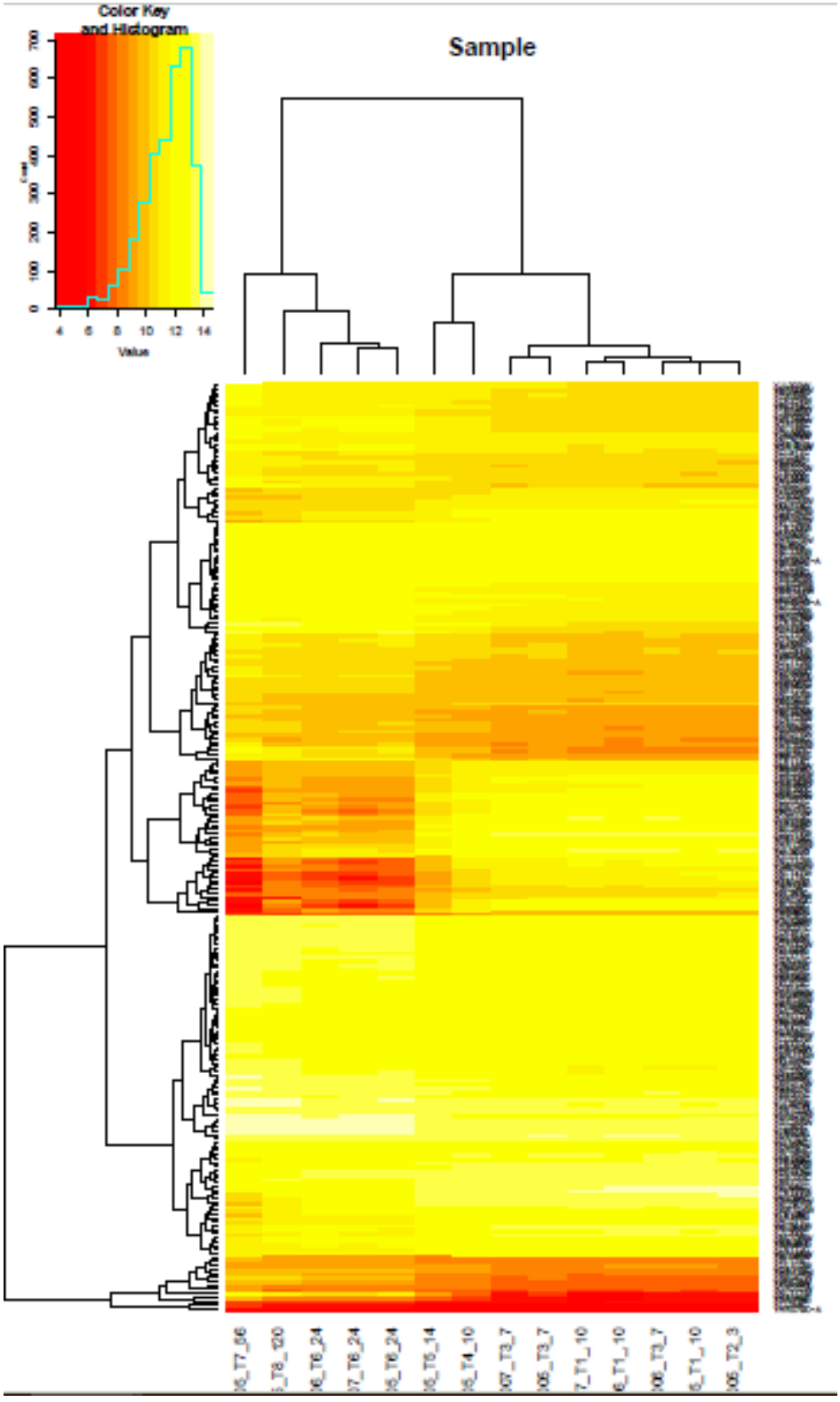

Figure 4.103. Heatmap of hierarchical clustering.

Table 4.28. Metagenes 1x2, 1x3 and 1x7.

1x2	**1x3**	**1x7**	
RRP5	BAP2	RPS11A	RPL18A
KRR1	ELP2	RPS0A	RPP1B
IMD4	DBP2	RPL34A	RPL5*
NOP1	TIF4631	RPL6B	RPL40B
FUI1	SRP40	RPL19B	RPS19A
NUG1	YVH1	RSB1	RPS22A
NOP58*	HAS1	RPL11B	RPS8A
MAE1	RPC40	RPL29	RPL22A
ATO3	UTP22	RPS3	RPL26B
GNP1	LHP1	RPL9A	RPL23A
RPS9A	NOP56*	RPL36A	RPL38
RBG1	RMT2	RPS22B	RPS17B
PPT1		SSB1	RPL21B
RKI1		RPS16B	RPS9B
SRO9		RPL17B	RPL2A
		RPS0B	RPS10A
		RPL20B	RPL34B
		RPL17A	RPL6A
		RPS18A	ADE17
		RPS11A	RPL33B
		RPL27A	RPS7A
		RPS10B	RPL16A
		RPS29A	RPL43B
		RPL2A	

When GO enrichment analysis is done on metagene 1x2, it can be seen that these genes are generally related to rRNA processing, rRNA metabolic process, maturation of SSU-rRNA from tricistronic rRNA transcript (SSU-rRNA, 5.8S rRNA, LSU-rRNA), maturation of SSU-rRNA, endonucleolytic cleavage in ITS1 to separate SSU-rRNA from 5.8S rRNA and LSU-rRNA from tricistronic rRNA transcript (SSU-rRNA, 5.8S rRNA, LSU-rRNA) and ribosome biogenesis. However, p-values and the background frequency of the terms are low; so, the result is not significant. This means, NOP58 and the other genes in the metagene might not be in similar biological process. When GO enrichment is done on metagene 1x3, it can be seen that these genes are generally related to ncRNA metabolic process, ribosome biogenesis, ncRNA processing, ribonucleoprotein complex biogenesis. However, p-values and the background frequency of the terms are high; so, the result is not significant. This means, NOP56 and the other genes in the metagene might not be in similar biological process. On the other hand, there are 47 genes that are placed in the same metagene with RPL5 gene. The common biological processes among these genes are cytoplasmic translation, peptide biosynthetic process, ribosome biogenesis and more... These genes in the metagene 1x7 are also related with the structural constituent of ribosome and rRNA binding as molecular function while they are related to cytosolic ribosome, ribosomal subunit and ribonucleoprotein complex as a cellular function. Since the p-values of the results are low enough, it can be said that the result is significant, and these genes are highly related to each other.

Pearson Correlation Coefficients are found between NOP56 and the other genes in the cluster 1x3. While calculating the correlation coefficient, the gene expression data are used. The average expression of same samples (at -10, 7, 24 min) is calculated to put a single data point for that sample. The results show that, the genes in the same metagene are highly correlated with each other. In other words, as the NOP56 is downregulated at any time point, then the remaining 11 genes strongly tend to be downregulated under any circumstances. P-values show the significance of the test.

The correlation between NOP56 and NOP58 is also found, where the Pearson correlation coefficient between them is 0.962. This means, as the NOP56 is downregulated, NOP58 also tends to be downregulated.

Pearson Correlation Coefficients are then found between NOP58 and the other genes in the cluster 1x2. The results show that, genes in the same metagene are highly correlated with each other. In other words, as the NOP58 is downregulated, remaining 14 genes strongly tend to be downregulated. Clustering methods and the related GO Terms for NOP56, NOP58 and RPL5 involved clusters are summarized in Table 4.29.

Table 4.29. Metagenes 1x2, 1x3 and 1x7.

Method	GO Biological Process	GO Cellular Component	GO Function	NOP56/ NOP58/ RPL5
Overexpressed, A	cytoplasmic translation, rRNA export from nucleus	Ribosome, cytosolic large ribosomal subunit	structural constituent of ribosome, rRNA binding	RPL5
Overexpressed, B	rRNA processing, Ribosome biogenesis	nucleolus	snoRNA binding	NOP58
Underexpressed, a	Late nucleophagy	Cellular component	Catalytic activity	-
Underexpressed, b,d	cytoplasmic translation	ribosome	Structural constituent of ribosome	RPL5
Underexpressed, c	rRNA processing, Ribosome biogenesis	nucleolus		NOP56, NOP58
D-clusters A	rRNA processing, Ribosome biogenesis	nucleolus	snoRNA binding	NOP56, NOP58
D-clusters B	late nucleophagy, glycogen biosynthetic process	pre−autophagosomal structure	catalytic activity, oxidoreductase activity	-
K-means cluster, A	Cytoplasmic translation	ribosome	Structural constituent of ribosome	RPL5
K-means cluster, E	rRNA processing, Ribosome biogenesis	nucleolus	snoRNA binding	NOP56, NOP58
Pearson Correlation clustering, A	rRNA processing, Ribosome biogenesis	nucleolus	snoRNA binding	RPL5, NOP56, NOP58

5. CONCLUSIONS AND RECOMMENDATIONS

5.1. Optimization Experiments

To obtain steady state flow and stable droplets in the microchip systems, the most important criteria are the channel size and the optimized flow rate. The channel size we used (161μm) was greater than those reported in literature (i.e. 30μm) [46]. Using small inlet size leads to generate small droplets. Generating small droplets is important since small droplets remain more stable during the experiment. Because we produced large droplets, they coalesced with each other more in our experiments. Also, the larger inlet size requires higher flow rate. To obtain smaller droplets, flow rate of oil phase must be more than the flow rate of aqueous phase. If the flow rate of oil phase was set to 600 μL/h and that of the aqueous phase was set to quarter of it, the droplet volume became more than 4 nL. To produce smaller droplets, the flow rate of oil was increased to 800 μL/h while the flow rate of aqueous phase was decreased to 40-50 μL/h (20:1 ratio). With these flow rates, the droplet volume becomes around 400 to 500 pL, i.e. decreased by 10-fold to 0.4-0.5 nL. Beyond these rates, the steady state flow was broken.

Experimental observations were investigated further by the computational study in order to understand the reasons underlying the instability and flow regime within the microfluidic bioreactor. Using COMSOL software, flow pattern and velocity profile inside the chip were identified. The COMSOL results showed that the droplet size was consistent with the droplet size generated in the experiments. COMSOL study proved that when all the three inlets are used in the experiment, the droplet diameter increases.

Because the surfactant can be toxic to the cells, surfactant concentration was optimized by examining the viability of the yeast cells in the experiments. It was seen that 3% Krytox was enough to keep the droplets stable during the 24 hours incubation and not toxic to cells. Moreover, since it is desired to be only one or at most two cells

in the droplets, yeast culture is diluted. When the culture was diluted for 'one cell per droplet' or 'ten cells per droplet', the droplets were generated yeast-free. Therefore, it was decided to dilute the yeast culture solution to a ratio of 1 to 1 with nutrient medium. However, this dilution caused an operation problem: the surface tension of such concentrated cells resulted in greater coalescence between the droplets.

Also, it is observed from the experiments that the material of the aqueous phase is important to keep the droplets stable. For example, the droplets generated with the yeast-free YPD culture solution were more stable than the yeast-free YNB culture solution.

Finally, as control experiments, yeast cell growth (without any treatment, drug-free) were conducted using diploid BY4743 strain with GFP tagged RPL5 protein and haploid EY0987 strain with RFP tagged NOP56 protein. In both experiments, the area of the cells increased, and the cells proliferated as expected. The fluorescence density, showing the amount of expression of the tagged protein, decreased until the 6^{th} hour of the incubation. This may be explained by the decrease in the amount of protein per unit area, as the area of the cells increases. After 18 hours, the intensity of fluorescence increased with the increase in the number of cells. When the cells are loaded from shake flasks to micro-aerated chambers of the microfluidic platform, they suffer from the lack of oxygen, and that caused a decrease in fluorescence intensity of GFP. However, as time passes the yeast cells adapted themselves to this micro-aerated condition and started to emit fluorescence in accordance with growth.

5.2. Drug HU Application

5.2.1. Experimental Results

Experimental studies are performed using droplet-based microfluidic chips (bioreactors) to investigate the response of single cells against HU treatment. Three experiments were conducted with two kinds of strains under drug treatment. First, 200 M drug was applied to the diploid BY4743 strain with GFP tagged RPL5 protein. Many

droplets merged with each other while they were generated. Yet, several droplets remained stable during the incubation. The response of the cells were heterogeneous. One reason may be that the droplets generated drug-free if there was an unstable flow. Another reason can be that the drug concentration may be insufficient to affect the yeast cells. 200 M HU was halved when the droplets were generated while it mixed with the yeast solution. Thus, cells faced with 100 M drug treatment.

Second, drug concentration was prepared as 400 M. In this experiment, yeast cells (RPL5:GFP tagged BY4743) were inhibited by the HU treatment, i.e. Growth of the cells were slower than the normal case. The cell cycle was monitored for 2.5 hours and it was seen that the cells did not proliferate. HU prevents the DNA replication and, this experiment supports this argument by preventing the cell proliferation.

Last, third experiment was conducted by using haploid EY0987 strain with RFP tagged NOP56 protein. As it can be seen from the decrease in the cellular area, HU generally inhibited cell proliferation. The inconsistency between the cells arise from the unsteady flow regime. Unsteady flow regime causes HU concentration to change from droplet to droplet. Also, the fluorescence intensity of the cells generally decreased under HU treatment, i.e. the expression of NOP56 decreased in the cell.

To sum up, the results of droplet-based microfluidic experiments reveal that HU clearly inhibits cell growth, decreases cell dimension and protein expression of Nop56 and RPL5, which both function in ribosome biogenesis. Nop56 directs 2'-O-methylation of pre-rRNA during its maturation and Rpl5 is required for 60S subunit assembly. Droplet based microfluidic chip system can sometime be unsteady and this breaks the homogeneity of the droplets and so, the results.

5.2.2. Computational Results

A computational SOM analysis is performed using the gene expression data reported in literature to understand the response of yeast cells to drug (HU) application and find the co-expressed genes and their functions, biological processes and cellular

components. There are 3 overexpression spots at different time points of the HU treatment. Genes in the spot A, which is overexpressed at the beginning of the treatment, are related with the cytoplasmic translation, ribosome and structural constituent of ribosome. Genes in Spot B and C are overexpressed later in the treatment and they are related to vacuole inheritance, glycolytic process, gluconeogenesis and oxidation-reduction process. There are two underexpressed spots identified. Genes in the spot a are underexpressed earlier of the treatment and they are related with the gluconeogenesis, glycolytic process and oxidation-reduction process. On contrary, genes in spot b, are underexpressed later in the treatment and they are related with the cytoplasmic translation, ribosome and structural constituent of ribosome. Both NOP56 and NOP58 as well as RPL5 are not involved in any overexpression or underexpression spots. This means that none of these genes are strongly overexpressed or underexpressed.

Other clustering approaches such as D-clustering, K-means clustering, and Pearson correlation clustering is also applied to the metagenes. According to the D-clustering approach, cluster A is overexpressed later in the treatment while cluster B is underexpressed later in the treatment. Genes in cluster A are related with gluconeogenesis, glycolytic process and cytosol. On the other hand, genes in the cluster B are related with cytoplasmic translation, ribosome and structural constituent of ribosome. None of the specified genes (NOP56, NOP58, RPL5) are placed in these clusters, however it does not mean that these genes are not affected by HU treatment. It just means that some other genes are more strongly affected than the genes of our interest by the treatment. In K-means clustering map, NOP56 is involved in spot A, in which the genes are related to ribosome, translation initiation factor activity and translational initiation. NOP58 is involved in spot C, in which the genes are related to tRNA aminoacylation for protein translation, aminoacyl tRNA ligase activity and purine nucleotide biosynthetic activity. RPL5 is involved in spot E, in which the genes are related to cytoplasmic translation, ribosome and structural constituent of ribosome. According to the Pearson correlation clustering, both NOP56, NOP58 and RPL5 are placed in cluster B. In this cluster, 1330 genes in 220 metagenes are highly related to each other and these genes are related to cytoplasmic translation, ribosome and structural constituent of ribosome.

From the GSZ score results, it can be stated that the most downregulated biological processes are translation and ribosomal small subunit assembly and the most upregulated biological processes are gluconeogenesis and glycolytic process. The most downregulated cellular components are ribosome and cytosolic small/large ribosomal subunits while the downregulated molecular function is structural constituent of ribosome. These results also support the properties of HU treatment with the ability to inhibit the ribosome biogenesis [31].

Consequently, the clusters in which NOP56, NOP58 or RPL5 are involved, are related to ribosome, cytoplasmic translation or translational initiation. The number of correlated genes in the metagenes, that involve NOP56 or RPL5, are not enough to make a gene enrichment analysis. The correlated genes in the metagene, that NOP58 is involved in, are related to RNA metabolic process, mRNA binding and ribonucleoprotein complex, and they are highly correlated to each other.

The transcription factors of the genes in Cluster B (related to ribosome biogenesis) of D-clustering approach are found in order to get an insight on the regulation of ribosome biogenesis under HU treatment. D-cluster B is selected even though it does not contain NOP56, NOP58 or RPL5 protein, since it is a statistically significant cluster and it is the most related cluster to ribosome biogenesis. Among 82 genes in D-cluster B, the transcription factors of 75 genes are found from Yeastract. A total of 158 transcription factors are identified, and it is seen that 7 of them are common in 7 genes. These are Rap1p, Yap1p, Sfp1p, Gcr1p, Cst6p, Ace2p and Swi5p, which are related with NOP56 and NOP58 indirectly. RAP1 and SFP1 genes are downregulated while GCR1, YAP1, ACE2 and SWI5 are upregulated under HU treatment.

5.3. Drug Temsirolimus (Rapamycin Derivative) Application

5.3.1. Experimental Results

Experimental studies are performed using droplet-based microfluidic chips (bioreactors) to investigate the response of single yeast cells against temsirolimus treatment. The experiments were conducted with two kinds of strains under drug treatment.

First, 0.4 μg/mL drug was applied to the diploid BY4743 strain with GFP tagged RPL5 protein, but cells faced with 0.2 μg/mL due to the mixing in the inlet. Many droplets merged with each other while they were generated. Yet, there were several droplets, which remained stable, thus, the response of the cells could be observed. The expectation was the shrinkage of the cells and the decrease in fluorescence density. Contrary to expectations, the cells in two separate experiments proliferated during temsirolimus treatment. One explanation for this situation may be that the droplets were generated drug-free. This explains the proliferation of the cells in both experiments. But this cannot explain the different fluorescence density changes between experiments. On the other hand, in the literature, it is stated that the overexpression or underexpression of ribosome biogenesis related ribosomal proteins (RPs) like RPL5, RPL11, RPS7 increase the predisposition to tumorigenesis. So, we can speculate that the increase in cell count may be explained by the tendency of cells to cancer due to the global effect of drug temsirolimus on ribosome biogenesis [73]. Although it is still unknown how perturbations or mutations in ribosomal proteins like Rpl5 result in Diamond-Blackfan anemia (DBA) and cancer, the pathological changes may result from global decline of ribosomal biogenesis owing to loss of one copy of an rp gene and subsequent reduction of translation [75, 76]. It is also speculated that some of these diseases can be explained by RPL11-mediated deregulation of c-Myc, an important player in ribosomal biogenesis [77].

Second, the experiment was conducted with haploid EY0987 strain with RFP tagged NOP56 protein, and 0.4 μg/mL drug was applied to the cells. As it can be seen from the decrease in cellular area, temsirolimus treatment slowed down the growth

and proliferation of the cells. The fluorescence intensity of the cells also decreased meaning that the expression of Nop56 decreased under temsirolimus treatment. Since it is known that temsirolimus interferes with the proliferation and the survival of the cells, this experiment satisfies the expectations.

To sum up, the results of droplet-based microfluidic experiments reveal that temsirolimus clearly inhibit EY0987 yeast cell growth, decrease cell dimension and protein expression of Nop56, which has a role in ribosome biogenesis. On the other hand, the effects on diploid BY4743 strain and RPL5 protein are unclear. Moreover, the two strains have different surface tension, as working with EY0987 strain creates more steady flow compared to the BY4743 strain, which is knocked out one copy of the protein coding gene: YAL067C (SEO1, putative permease, Suppressor of sulfoxyde EthiOnine resistance).

5.3.2. Computational Results

A computational SOM analysis is performed using the gene expression data reported in literature to understand the response of yeast cells to drug rapamycin and find the co-expressed genes and their functions, biological processes and cellular components. 3 different gene spots are identified as overexpressed at different time points of the rapamycin treatment. Of all these spots, 2 of them are overexpressed at the beginning of the treatment (Spot A and Spot B) and they are related to ribosome biogenesis, rRNA processing and cytoplasmic translation. Genes in spot C are overexpressed later in the treatment and the genes in this spot are related to oxidation-reduction process. NOP58 is in Spot B and RPL5 is in Spot A, whereas NOP56 is not in any overexpression spot. There are four spots that are underexpressed during the treatment. Genes in the spot a are underexpressed at the beginning of the treatment and they are related to catalytic activity. Genes in spot b, spot c and spot d are underexpressed later in the treatment and they are related to rRNA processing, ribosome biogenesis and cytoplasmic translation. Both NOP56 and NOP58 are involved in underexpression spot c while RPL5 is involved in spot d. From these two analyses, it can be said that,

the genes, which are related to ribosome biogenesis, and overexpressed before the drug treatment, are repressed with the rapamycin treatment.

Different clustering approaches such as D-clustering, K-clustering, Pearson clustering are used to group the gene expression data and estimate the relationship among the genes of interest and related pathways and finally the crosstalk among these pathways. Two D-clusters are identified, where cluster A involves underexpressed genes including both NOP56 and NOP58. Cluster A is related with the rRNA processing, ribosome biogenesis and nucleolus. The genes in this cluster are highly repressed after 14 minutes of treatment. Cluster B of overexpressed genes is related with the late nucleophagy and glycogen biosynthetic process. According to K-means clustering, both NOP56 and NOP58 are included in cluster E, in which the genes show underexpression after 14 minutes of treatment. The genes in this cluster are related with the ribosome biogenesis, nucleolus and rRNA processing. RPL5 is involved in K-means cluster A, in which the genes are related to cytoplasmic translation. In Pearson correlation cluster maps, both NOP56 and NOP58 as well as RPL5 are in cluster A, which contains downregulated genes and is related to cytoplasmic translation, nucleolus and ribosome biogenesis. According to expression levels, these genes are highly correlated with another 224 metagenes in cluster A.

No matter which clustering approach is used, the clusters in which NOP56, NOP58 and RPL5 are involved, are related to ribosome biogenesis, rRNA processing and nucleolus, and the genes in these clusters are suppressed after 10 to 14 minutes of rapamycin treatment. Nop56 is in a metagene together with the following genes of BAP2, ELP2, DBP2, TIF4631, SRP40, YVH1, HAS1, RPC40, UTP22, LHP1, RMT2. These genes are highly correlated (PCC) and are generally related to ncRNA metabolic process, ribosome biogenesis, ncRNA processing, ribonucleoprotein complex biogenesis. RPL5 gene is in a metagene together with the ribosomal protein (RP) genes, which have high correlation among them.

5.4. Recommendations

The aim of this study is to operate droplet based microfluidic device and have high throughput screening. The following suggestions can be applied to the constructed microfluidic platform for the future studies.

- Droplet generator and incubator chip can be fabricated by us, thus, the inlet size can be reduced to obtain smaller droplets.
- Instead of fabricating incubation chambers in the chips, straight and narrow lines can be used to incubate the droplets. Also, the traps in the chambers can be removed to prevent the coalescence of the droplets and being trapped underneath.
- A photomultiplier tube (PMT) can be used to investigate more cells by better detecting the fluorescence emitted from the cells in the droplets.
- Working with the non-sticky cells can help to maintain steady flow and ease to produce droplets of similar conditions (same drug concentration and number of yeast cells).

REFERENCES

1. Whitesides, G. M., "The origins and the future of microfluidics", *Nature*, Vol. 442, No. 7101, pp. 368–373, 2006, https://doi.org/10.1038/nature05058.

2. Zhang, C., J. Xu, W. Ma and W. Zheng, "PCR microfluidic devices for DNA amplification", *Biotechnology Advances*, Vol. 24, No. 3, pp. 243–284, 2006.

3. Andersson, H. and A. Van den Berg, "Microfluidic devices for cellomics: A review", *Sensors and Actuators, B: Chemical*, Vol. 92, No. 3, pp. 315–325, 2003.

4. Alex McMillan, G. V. C., *Elveflow Plug & Microfluidics*, https://www.elveflow.com/microfluidic-tutorials/microfluidic-reviews-and-tutorials/microreactors-and-microfluidics-in-chemistry- a-review/, accessed in January 2018.

5. Dressler, O. J., R. M. Maceiczyk, S. I. Chang and A. J. Demello, "Droplet-based microfluidics: Enabling impact on drug discovery", *Journal of Biomolecular Screening*, Vol. 19, No. 4, pp. 483–496, 2014.

6. Yamashita, H., M. Morita, H. Sugiura, K. Fujiwara, H. Onoe and M. Takinoue, "Generation of monodisperse cell-sized microdroplets using a centrifuge-based axisymmetric co-flowing microfluidic device", *Journal of Bioscience and Bioengineering*, Vol. 119, No. 4, pp. 492–495, 2015, http://dx.doi.org/10.1016/j.jbiosc.2014.09.018.

7. Baret, J. C., O. J. Miller, V. Taly, M. Ryckelynck, A. El-Harrak, L. Frenz, C. Rick, M. L. Samuels, J. B. Hutchison, J. J. Agresti, D. R. Link, D. A. Weitz and A. D. Griffiths, "Fluorescence-activated droplet sorting (FADS): Efficient microfluidic cell sorting based on enzymatic activity", *Lab on a Chip*, Vol. 9, No. 13, pp. 1850–1858, 2009.

8. Mazutis, L., J. Gilbert, W. L. Ung, D. A. Weitz, A. D. Griffiths and J. A. Heyman, "Single-cell analysis and sorting using droplet-based microfluidics.", *Nature protocols*, Vol. 8, No. 5, pp. 870–91, 2013.

9. Beneyton, T., I. P. M. Wijaya, P. Postros, M. Najah, P. Leblond, A. Couvent, E. Mayot, A. D. Griffiths and A. Drevelle, "High-throughput screening of filamentous fungi using nanoliter-range droplet-based microfluidics", *Scientific Reports*, Vol. 6, pp. 1–10, 2016.

10. Abate, A. R., T. Hung, P. Mary, J. J. Agresti and D. A. Weitz, "High-throughput injection with microfluidics using picoinjectors", *Proceedings of the National Academy of Sciences*, Vol. 107, No. 45, pp. 19163–19166, 2010.

11. Fallah-Araghi, A., J. C. Baret, M. Ryckelynck and A. D. Griffiths, "A completely in vitro ultrahigh-throughput droplet-based microfluidic screening system for protein engineering and directed evolution", *Lab on a Chip*, Vol. 12, No. 5, pp. 882–891, 2012.

12. Joensson, H. N., M. Uhlén and H. A. Svahn, "Droplet size based separation by deterministic lateral displacement- separating droplets by cell-induced shrinking", *Lab on a Chip*, Vol. 11, No. 7, pp. 1305–1310, 2011.

13. Huh, D., J. H. Bahng, Y. Ling, H.-h. Wei, O. D. Kripfgans, J. B. Fowlkes, J. B. Grotberg and S. Takayama, "Gravity-Driven Microfluidic Particle Sorting Device with Hydrodynamic Separation Amplification that can perform size profiling and continuous mass-", *Analytical*, Vol. 79, No. 4, pp. 1369–1376, 2007.

14. Lyu, F., M. Xu, Y. Cheng, J. Xie, J. Rao and S. K. Tang, "Quantitative detection of cells expressing BlaC using droplet-based microfluidics for use in the diagnosis of tuberculosis", *Biomicrofluidics*, Vol. 9, No. 4, 2015.

15. Wu, N., Y. Zhu, S. Brown, J. Oakeshott, T. S. Peat, R. Surjadi, C. Easton, P. W. Leech and B. A. Sexton, "A PMMA microfluidic droplet platform for in vitro

protein expression using crude E. coli S30 extract", *Lab on a Chip*, Vol. 9, No. 23, pp. 3391–3398, 2009.

16. Chou, W. L., P. Y. Lee, C. L. Yang, W. Y. Huang and Y. S. Lin, "Recent advances in applications of droplet microfluidics", *Micromachines*, Vol. 6, No. 9, pp. 1249–1271, 2015.

17. Srinivasan, V., V. K. Pamula and R. B. Fair, "Droplet-based microfluidic lab-on-a-chip for glucose detection", *Analytica Chimica Acta*, Vol. 507, No. 1, pp. 145–150, 2004.

18. Baroud, C. N., F. Gallaire and R. Dangla, "Dynamics of microfluidic droplets", *Lab on a Chip*, Vol. 10, No. 16, pp. 2032–2045, 2010.

19. Gai, Y., J. W. Khor and S. K. Tang, "Confinement and viscosity ratio effect on droplet break-up in a concentrated emulsion flowing through a narrow constriction", *Lab on a Chip*, Vol. 16, No. 16, pp. 3058–3064, 2016, `http://dx.doi.org/10.1039/C6LC00478D`.

20. Casadevall I Solvas, X. and A. Demello, "Droplet microfluidics: Recent developments and future applications", *Chemical Communications*, Vol. 47, No. 7, pp. 1936–1942, 2011.

21. Sjostrom, S. L., Y. Bai, M. Huang, J. Nielsen, H. N. Joensson and H. A. Svahn, "Droplet Based Directed Evolution of Yeast Cell", Vol. 17, No. 10, pp. 1270–1272, 2013.

22. Lombardi, D. and P. S. Dittrich, "Advances in microfluidics for drug discovery", *Expert Opinion on Drug Discovery*, Vol. 5, No. 11, pp. 1081–1094, 2010.

23. Joensson, H. N. and H. Andersson-Svahn, "Droplet microfluidics—a tool for protein engineering and analysis", *Lab on a Chip*, Vol. 11, No. 24, p. 4144, 2011.

24. Woolford, J. L. and S. J. Baserga, "Ribosome biogenesis in the yeast Saccharomyces cerevisiae", *Genetics*, Vol. 195, No. 3, pp. 643–681, 2013.

25. Armistead, J. and B. Triggs-Raine, "Diverse diseases from a ubiquitous process: The ribosomopathy paradox", *FEBS Letters*, Vol. 588, No. 9, pp. 1491–1500, 2014, http://dx.doi.org/10.1016/j.febslet.2014.03.024.

26. Teng, T., G. Thomas and C. A. Mercer, "Growth control and ribosomopathies", *Current Opinion in Genetics and Development*, Vol. 23, No. 1, pp. 63–71, 2013, http://dx.doi.org/10.1016/j.gde.2013.02.001.

27. Vincent, N. G., J. M. Charette and S. J. Baserga, "The SSU processome interactome in Saccharomyces cerevisiae reveals potential new protein subcomplexes.", *RNA (New York, N.Y.)*, p. rna.062927.117, 2017, http://www.ncbi.nlm.nih.gov/pubmed/29054886.

28. Stepanov, G. A., J. A. Filippova, A. B. Komissarov, E. V. Kuligina, V. A. Richter and D. V. Semenov, "Regulatory Role of Small Nucleolar RNAs in Human Diseases", *BioMed Research International*, Vol. 2015, pp. 1–10, 2015.

29. Lykke-Andersen, S., B. K. Ardal, A. K. Hollensen, C. K. Damgaard and T. H. Jensen, "Box C/D snoRNP Autoregulation by a cis-Acting snoRNA in the NOP56 Pre-mRNA", *Molecular Cell*, Vol. 72, No. 1, pp. 99 – 111.e5, 2018, http://www.sciencedirect.com/science/article/pii/S1097276518306774.

30. Lo Monaco, P., V. Marcel, J. J. Diaz and F. Catez, "2′-O-methylation of ribosomal RNA: Towards an epitranscriptomic control of translation?", *Biomolecules*, Vol. 8, No. 4, pp. 1–13, 2018.

31. Brighenti, E., D. Treré and M. Derenzini, "Targeted cancer therapy with ribosome biogenesis inhibitors: a real possibility?", *Oncotarget*, Vol. 6, No. 36, 2015.

32. Ikeda, Y., Y. Ohta, H. Kobayashi, M. Okamoto, K. Takamatsu, T. Ota, Y. Manabe, K. Okamoto, A. Koizumi and K. Abe, "Clinical features of SCA36", *Neurology*, Vol. 79, No. 4, pp. 333–341, 2012, https://n.neurology.org/content/79/4/333.

33. García-Murias, M., B. Quintáns, M. Arias, A. I. Seixas, P. Cacheiro, R. Tarrío, J. Pardo, M. J. Millán, S. Arias-Rivas, P. Blanco-Arias, D. Dapena, R. Moreira, F. Rodríguez-Trelles, J. Sequeiros, Á. Carracedo, I. Silveira and M. J. Sobrido, "'Costa da Morte' ataxia is spinocerebellar ataxia 36: clinical and genetic characterization", *Brain*, Vol. 135, No. 5, pp. 1423–1435, 2012, https://doi.org/10.1093/brain/aws069.

34. Kobayashi, H., K. Abe, T. Matsuura, Y. Ikeda, T. Hitomi, Y. Akechi, T. Habu, W. Liu, H. Okuda and A. Koizumi, "Expansion of intronic GGCCTG hexanucleotide repeat in NOP56 causes SCA36, a type of spinocerebellar ataxia accompanied by motor neuron involvement", *American Journal of Human Genetics*, Vol. 89, No. 1, pp. 121–130, 2011, http://dx.doi.org/10.1016/j.ajhg.2011.05.015.

35. DeJournette, C. J., J. Kim, H. Medlen, X. Li, L. J. Vincent and C. J. Easley, "Creating Biocompatible Oil–Water Interfaces without Synthesis: Direct Interactions between Primary Amines and Carboxylated Perfluorocarbon Surfactants", *Analytical Chemistry*, Vol. 85, No. 21, pp. 10556–10564, 2013, https://doi.org/10.1021/ac4026048.

36. Dimensions, M., *Molecular Dimensions*, https://www.moleculardimensions.com/products/4538-50-vv-Jeffamine-ED-900-pH-70/, accessed in May 2018.

37. Alvino, G. M., D. Collingwood, J. M. Murphy, J. Delrow, B. J. Brewer and M. K. Raghuraman, "Replication in Hydroxyurea: It's a Matter of Time", *Molecular and Cellular Biology*, Vol. 27, No. 18, pp. 6396–6406, 2007.

38. Fagone, P., M. Donia, K. Mangano, C. Quattrocchi, S. Mammana, M. Coco, M. Libra, J. A. Mccubrey and F. Nicoletti, "Comparative Study of Rapamycin and Temsirolimus Demonstrates Superimposable Anti-Tumour Potency on Prostate Cancer

Cells", *Basic and Clinical Pharmacology and Toxicology*, Vol. 112, No. 1, pp. 63–69, 2013.

39. Powers, T. and P. Walter, "Regulation of Ribosome Biogenesis by the Rapamycin-sensitive TOR-signaling Pathway in Saccharomyces cerevisiae", *Molecular Biology of the Cell*, Vol. 10, No. 4, pp. 987–1000, 2013.

40. Oliveira, A. P., S. Dimopoulos, A. G. Busetto, S. Christen, R. Dechant, L. Falter, M. Haghir Chehreghani, S. Jozefczuk, C. Ludwig, F. Rudroff, J. C. Schulz, A. Gonzalez, A. Soulard, D. Stracka, R. Aebersold, J. M. Buhmann, M. N. Hall, M. Peter, U. Sauer and J. Stelling, "Inferring causal metabolic signals that regulate the dynamic TORC1-dependent transcriptome", *Molecular Systems Biology*, Vol. 11, No. 4, pp. 802–802, 2015.

41. Hardwick, J. S., F. G. Kuruvilla, J. K. Tong, A. F. Shamji and S. L. Schreiber, "Rapamycin-modulated transcription defines the subset of nutrient-sensitive signaling pathways directly controlled by the Tor proteins", *Proceedings of the National Academy of Sciences*, Vol. 96, No. 26, pp. 14866–14870, 2002.

42. Löffler-Wirth, H., M. Kalcher and H. Binder, "oposSOM: R-package for high-dimensional portraying of genome-wide expression landscapes on bioconductor", *Bioinformatics*, Vol. 31, No. 19, pp. 3225–3227, 2015, `https://doi.org/10.1093/bioinformatics/btv342`.

43. Project, S., *Saccharomyces Cerevisiae Genome Database*, `https://downloads.yeastgenome.org/expression/microarray/Oliveira_2015_PMID_25888284/`, accessed in April 2018.

44. National Center for Biotechnology Information, N., *GEO Accession viewer, GSE54852*, `https://www.ncbi.nlm.nih.gov/geo/`, accessed in April 2018.

45. Loll-Krippleber, R. and G. W. Brown, "P-body proteins regulate transcriptional rewiring to promote DNA replication stress resistance", *Nature Communications*, Vol. 8, No. 1, p. 558, 2017, https://doi.org/10.1038/s41467-017-00632-2.

46. Beneyton, T., S. Thomas, A. D. Griffiths, J. M. Nicaud, A. Drevelle and T. Rossignol, "Droplet-based microfluidic high-throughput screening of heterologous enzymes secreted by the yeast Yarrowia lipolytica", *Microbial Cell Factories*, Vol. 16, No. 1, pp. 1–14, 2017.

47. Peters, F. and D. Arabali, "Interfacial tension between oil and water measured with a modified contour method", *Colloids and Surfaces A: Physicochemical and Engineering Aspects*, Vol. 426, pp. 1–5, 2013, http://www.sciencedirect.com/science/article/pii/S0927775713001994.

48. Lopes, M., C. Cotta-Ramusino, A. Pellicioli, G. Liberi, P. Plevani, M. Muzi-Falconi, C. S. Newlon and M. Foiani, "The DNA replication checkpoint response stabilizes stalled replication forks", *Nature*, Vol. 412, No. 6846, pp. 557–561, 2001, https://doi.org/10.1038/35087613.

49. Koç, A., L. J. Wheeler, C. K. Mathews and G. F. Merrill, "Hydroxyurea Arrests DNA Replication by a Mechanism that Preserves Basal dNTP Pools", *Journal of Biological Chemistry*, Vol. 279, No. 1, pp. 223–230, 2004.

50. Madaan, K., D. Kaushik and T. Verma, "Hydroxyurea: a key player in cancer chemotherapy", *Expert Review of Anticancer Therapy*, Vol. 12, No. 1, pp. 19–29, 2012, https://doi.org/10.1586/era.11.175.

51. Çakır, M. V., H. Binder and H. Wirth, "Profiling of Genetic Switches using Boolean Implications in Expression Data", *Journal of Integrative Bioinformatics*, Vol. 11, No. 1, 2017.

52. Wirth, H., M. Löffler, M. von Bergen and H. Binder, "Expression cartography of human tissues using self organizing maps", *BMC Bioinformatics*, Vol. 12, pp. 1–24, 2011.

53. Zhang, J. and H. Fang, "Using Self-Organizing Maps to Visualize, Filter and Cluster Multidimensional Bio-Omics Data", M. Johnsson (Editor), *Applications of Self-Organizing Maps*, chap. 9, IntechOpen, Rijeka, 2012, https://doi.org/10.5772/51702.

54. Rodgers, J. L. and W. A. Nicewander, "Thirteen Ways to Look at the Correlation Coefficient", *The American Statistician*, Vol. 42, No. 1, pp. 59–66, 1988, http://www.jstor.org/stable/2685263.

55. Wikipedia, *Pearson Correlation Coefficient*, https://en.wikipedia.org/wiki/Pearson_correlati- on_coefficient, accessed in September 2018.

56. Pang, C. N. I., A. Goel, S. S. Li and M. R. Wilkins, "A Multidimensional Matrix for Systems Biology Research and Its Application to Interaction Networks", *Journal of Proteome Research*, Vol. 11, No. 11, pp. 5204–5220, 2012, https://doi.org/10.1021/pr300405y.

57. Hahn, S., S. Buratowski, P. A. Sharp and L. Guarente, "Isolation of the gene encoding the yeast TATA binding protein TFIID: A gene identical to the SPT15 suppressor of Ty element insertions", *Cell*, Vol. 58, No. 6, pp. 1173–1181, 1989, http://www.sciencedirect.com/science/article/pii/0092867489905151.

58. Tora, L., "A unified nomenclature for TATA box binding protein (TBP)-associated factors (TAFs) involved in RNA polymerase II transcription", *Genes & Development*, Vol. 16, No. 6, pp. 673–675, mar 2002, http://genesdev.cshlp.org/content/16/6/673.short.

59. Martina, M., D. Bonetti, M. Villa, G. Lucchini and M. P. Longhese, "Saccharomyces cerevisiae Rif1 cooperates with MRX-Sae2 in promoting

DNA-end resection", *EMBO reports*, Vol. 15, No. 6, pp. 695–704, 2014, http://embor.embopress.org/content/15/6/695.

60. Holland, M. J., T. Yokoi, J. P. Holland, K. Myambo and M. A. Innis, "The GCR1 gene encodes a positive transcriptional regulator of the enolase and glyceraldehyde-3-phosphate dehydrogenase gene families in Saccharomyces cerevisiae.", *Molecular and Cellular Biology*, Vol. 7, No. 2, pp. 813–820, 1987, https://mcb.asm.org/content/7/2/813.

61. Uemura, H. and Y. Jigami, "Role of GCR2 in transcriptional activation of yeast glycolytic genes.", *Molecular and Cellular Biology*, Vol. 12, No. 9, pp. 3834–3842, 1992, https://mcb.asm.org/content/12/9/3834.

62. Witkin, K. L., J. M. Friederichs, O. Cohen-Fix and S. L. Jaspersen, "Changes in the Nuclear Envelope Environment Affect Spindle Pole Body Duplication in Saccharomyces cerevisiae", *Genetics*, Vol. 186, No. 3, pp. 867–883, 2010, https://www.genetics.org/content/186/3/867.

63. Rout, M. P., J. D. Aitchison, A. Suprapto, K. Hjertaas, Y. Zhao and B. T. Chait, "The Yeast Nuclear Pore Complex", *The Journal of Cell Biology*, Vol. 148, No. 4, pp. 635–652, 2000, http://jcb.rupress.org/content/148/4/635.

64. Wozniak, R. W., G. Blobel and M. P. Rout, "POM152 is an integral protein of the pore membrane domain of the yeast nuclear envelope.", *The Journal of Cell Biology*, Vol. 125, No. 1, pp. 31–42, 1994, http://jcb.rupress.org/content/125/1/31.

65. Okazaki, S., T. Tachibana, A. Naganuma, N. Mano and S. Kuge, "Multistep Disulfide Bond Formation in Yap1 Is Required for Sensing and Transduction of H2O2 Stress Signal", *Molecular Cell*, Vol. 27, No. 4, pp. 675–688, 2007, http://www.sciencedirect.com/science/article/pii/S1097276507004479.

66. Ptak, C., A. M. Anderson, R. J. Scott, D. de Vosse, R. S. Rogers, Y. Sydorskyy, J. D. Aitchison and R. W. Wozniak, "A Role for the Karyopherin Kap123p in Microtubule Stability", *Traffic*, Vol. 10, No. 11, pp. 1619–1634, 2009.

67. Johnson, A. W., E. Lund and J. Dahlberg, "Nuclear export of ribosomal subunits", *Trends in Biochemical Sciences*, Vol. 27, No. 11, pp. 580–585, 2002, http://www.sciencedirect.com/science/article/pii/S0968000402022089.

68. Mendenhall, M. D. and A. E. Hodge, "Regulation of Cdc28 Cyclin-Dependent Protein Kinase Activity during the Cell Cycle of the Yeast Saccharomyces cerevisiae", *Microbiology and Molecular Biology Reviews*, Vol. 62, No. 4, pp. 1191–1243, 1998, https://mmbr.asm.org/content/62/4/1191.

69. Chen-Wu, J. L., R. Padmanabha and C. V. Glover, "Isolation, sequencing, and disruption of the CKA1 gene encoding the alpha subunit of yeast casein kinase II.", *Molecular and Cellular Biology*, Vol. 8, No. 11, pp. 4981–4990, 1988, https://mcb.asm.org/content/8/11/4981.

70. Gautier, T., T. Bergès, D. Tollervey and E. Hurt, "Nucleolar KKE/D repeat proteins Nop56p and Nop58p interact with Nop1p and are required for ribosome biogenesis.", *Molecular and Cellular Biology*, Vol. 17, No. 12, pp. 7088–7098, 1997, https://mcb.asm.org/content/17/12/7088.

71. Dragon, F., J. E. G. Gallagher, P. A. Compagnone-Post, B. M. Mitchell, K. A. Porwancher, K. A. Wehner, S. Wormsley, R. E. Settlage, J. Shabanowitz, Y. Osheim, A. L. Beyer, D. F. Hunt and S. J. Baserga, "A large nucleolar U3 ribonucleoprotein required for 18S ribosomal RNA biogenesis", *Nature*, Vol. 417, No. 6892, pp. 967–970, 2002, https://doi.org/10.1038/nature00769.

72. Mills, E. W. and R. Green, "Ribosomopathies: There{\textquoteright}s strength in numbers", *Science*, Vol. 358, No. 6363, 2017, https://science.sciencemag.org/content/358/6363/eaan2755.

73. Zhang, Y. and H. Lu, "Signaling to p53: Ribosomal Proteins Find Their Way", *Cancer Cell*, Vol. 16, No. 5, pp. 369–377, 2009, http://dx.doi.org/10.1016/j.ccr.2009.09.024.

74. Hartford, C. M. and M. J. Ratain, "Rapamycin: Something old, something new, sometimes borrowed and now renewed", *Clinical Pharmacology and Therapeutics*, Vol. 82, No. 4, pp. 381–388, 2007.

75. Ellis, S. R. and J. M. Lipton, "Chapter 8 Diamond Blackfan Anemia: A Disorder of Red Blood Cell Development", *Red Cell Development*, Vol. 82 of *Current Topics in Developmental Biology*, pp. 217–241, Academic Press, 2008, http://www.sciencedirect.com/science/article/pii/S0070215307000087.

76. Liu, J. M. and S. R. Ellis, "Ribosomes and marrow failure: coincidental association or molecular paradigm?", *Blood*, Vol. 107, No. 12, pp. 4583–4588, 2006, http://www.bloodjournal.org/content/107/12/4583.

77. Dai, M.-S., H. Arnold, X.-X. Sun, R. Sears and H. Lu, "Inhibition of c-Myc activity by ribosomal protein L11", *The EMBO Journal*, Vol. 26, No. 14, pp. 3332–3345, 2007, http://emboj.embopress.org/content/26/14/3332.

APPENDIX A: RESULTS FOR OPTIMIZATION EXPERIMENTS

The content is given in the CD.

APPENDIX B: RESULTS FOR HU TREATMENT

The content is given in the CD.

APPENDIX C: RESULTS FOR TEMSIROLIMUS TREATMENT

The content is given in the CD.